Optoelectronic Properties of InAs/GaAs Columnar Quantum Dot Laser Diodes

Meletios Mexis

A thesis submitted for the degree of doctor of philosophy

Department of Physics and Astronomy

Cardiff University

August 2009

ProQuest LLC
789 East Eisenhower Parkway
P.O. Box 1346
Ann Arbor, MI 48106-1346

DECLARATION

This work has not previously been accepted in substance for any degree and is not concurrently submitted in candidature for any degree.

Signed ..... (candidate) Date 06/04/2009

.....

STATEMENT 1

This thesis is being submitted in partial fulfillment of the requirements for the degree of Doctor of Philosophy.

Signed ..... (candidate) Date

..... 06/04/2009

STATEMENT 2

This thesis is the result of my own independent work/investigation, except where otherwise stated. Other sources are acknowledged by explicit references.

Signed ..... (candidate) Date

.....

06/04/2009

STATEMENT 3

I hereby give consent for my thesis, if accepted, to be available for photocopying and for inter-library loan, and for the title and summary to be made available to outside organisations.

Signed ..... (candidate) Date

.....

06/04/2009

STATEMENT 4: PREVIOUSLY APPROVED BAR ON ACCESS

I hereby give consent for my thesis, if accepted, to be available for photocopying and for inter-library loans after expiry of a bar on access previously approved by the Graduate Development Committee.

Signed ... Not applicable (candidate) Date

.....

Abstract

In this thesis results are described with the aim of examining the optoelectronic properties of InAs/GaAs columnar quantum-dots and comparing them with those of more conventional self-assembled quantum-dots.

The polarisation properties of a set of columnar quantum-dot samples -of varied aspect ratio and *In* compositional contrast between the rod-shaped dot and the surrounding 2-D layer- are studied. For this investigation a new method to obtain the ratio of the fundamental TE/TM optical response using edge photo-absorption spectroscopy is proposed, which corrects for the polarisation-dependent features of the experimental set-up. The method is verified by application to compressive and tensile strained InGaP quantum well structures, where the results are in agreement with known ratios of the band-edge matrix elements. When applied to columnar quantum-dot samples it is shown that the TE/TM optical response depends on the dot aspect ratio and the *In* compositional contrast. A polarisation-independent photo-absorption is illustrated for a columnar quantum-dot of an aspect ratio (dot's height over diameter) 3.51:1, which is desired for use in semiconductor optical amplifiers. For the columnar dot of an extremely high aspect ratio, 7.5:1, a room temperature TM-dominant polarisation lasing emission is observed.

By studying the Quantum-Confined Stark Effect, a dramatic enhancement of the Stark shift amplitude is shown for columnar quantum-dot samples of an increased dot aspect ratio from 0.63:1 up to 1.12:1, which may have application in optical modulation/switching. For a higher aspect ratio columnar quantum-dot the shift of the band edge of the photo-absorption spectra is reduced dramatically and this has been attributed to an overall effect where the observable shift becomes the result of higher energy transitions, where their oscillator strength change very rapidly within the studied range of field. For the highest aspect ratio dot, i.e of aspect ratio 10:1, there is no any observable shift.

Acknowledgements

I would like first to thank my PhD supervisors Prof. Peter Blood and Prof. Peter Smowton. Without their continuous support and encouragement it wouldn't be possible to complete this work. I would like to give my special thanks to Peter Blood for his willingness and effort to provide me with a detailed and complete scientific insight into the basic and advanced laser physics in his weekly lectures and the personal meetings we had. He put a lot of effort and helped me establish my first steps in research. The input of Peter Smowton in this work deserves particular praise as well. His effort and knowledge during this project were endless. I would also like to give credit and my thanks to our collaborators Prof. Andrea Fiore, Dr. Liahne Li and Philipp Ridha of EPFL in Lausanne, for their excellent and very fruitful collaboration. This made the project interesting and at the same time very enjoyable. Particular, I would like to thank Andrea Fiore for his very stimulating remarks and Philipp Ridha who was very keen to provide me with all the necessary information.

In addition, I would like to thank my colleagues within the group for making my experience in the group very enjoyable. Special thanks to Deepal with whom I had a constructive scientific interference. I am glad that we collaborated together in his project and that I contributed to the theoretical investigation of the work which relied on his excellent fabrication skills. Apart from that I should thank him, Mohammed and James for giving me very pleasant company while I was working. For the hours I was away from my lab duties I have to give many and special thanks to Leonidas, Monika, Giannis, Naveen, Nathalie, Grigoris, Eleni, Danilo and Oscar for providing me a great company and gave me the opportunity to interact and became a great fan of the university's multi-cultural environment.

Last but not least, the most of my thanks should go to my mother Zinovia and my sister Maria for their endless support during these many years of my studies away from my hometown. Without believing on me nothing would be possible.

To my father Vasilleio

"As you set out for Ithaka
hope your road is a long one,
full of adventure, full of discovery

.....

Keep Ithaka always in your mind.
Arriving there is what you're destined for.
But don't hurry the journey at all.
Better if it lasts for years,
so you're old by the time you reach the island,
wealthy with all you've gained on the way,
not expecting Ithaka to make you rich.

Ithaka gave you the marvelous journey.
Without her you wouldn't have set out.
She has nothing left to give you now.

And if you find her poor, Ithaka won't have fooled you.
Wise as you will have become, so full of experience,
you'll have understood by then what these Ithakas mean".

Constantine P. Cavafy (1911)

"Optoelectronic Properties of InAs/GaAs Columnar Quantum Dot Laser Diodes"

Contents

Chapter 1-Introduction and theoretical background

1.1 Project aims and motivation

The principal aim of the work presented here is to investigate the optoelectronic properties of InAs/GaAs columnar-Quantum Dot materials grown by a new approach. The project work involves a close collaboration with the Quantum Device Group in Swiss Federal Institute of Technology in Lausanne (EPFL), where the material structures were grown and processed. The main work objectives form two basic points: first, to explore the optical polarisation properties of these structures in order to understand the effect that strain, composition and size of dot have on polarisation-selective emission and absorption characteristics and second, to provide information about the electronic properties of columnar-Quantum Dots, i.e behaviour of carriers' wave-functions inside the dot under the presence of an external applied field.

Quantum Dot (QD) systems have attracted great interest for laser diodes due to the expectation for low-threshold current, weak temperature insensitivity and broadband gain spectra [Bimberg 1999]. In recent years there has been a lot of research effort for optimisation of InAs/GaAs QD laser diodes in order to operate sufficiently at wavelengths of 1.3 and 1.55 μm, where is the minima of loss and dispersion in optical fibres used for optical communication [Hecht 1999]. Because of the great potential of QD systems, there is a growing interest in using these materials as emitters, detectors, optical amplifiers and optical modulators in communication systems. However, it is necessary to resolve issues such as polarisation sensitivity that QD systems show in light amplification by fabricating novel QD structures, in which control over the polarisation can be achieved [Kita 2002]. At the same time the last few years' research is moving towards fabricating novel columnar-QD systems in order to engineer the wave-functions inside the dot in such a way to optimise laser operation or to use them for a wide range of applications as mentioned above.

1.2 Thesis Structure

The remainder of **chapter 1** describes the basic semiconductor physics in order to provide all the necessary understanding on the work carried out in the next chapters. Towards the end of the chapter a brief historical evolution of the quantum dot laser diodes give an introduction to the study of novel columnar-QD laser structures.

Chapter 2 describes the experimental apparatus and techniques used through the next chapters in order to extract the required information from the studied samples. This includes measurements on different types of strained QW materials, previously studied, in order to explain and verify a suggested novel method in **chapter 3** with a purpose to identify the polarisation response of columnar-QD materials using photo-current spectroscopy. In the last section of the latter chapter the escape mechanisms of photo-generated carriers in a dot are described by obtaining low-temperature measurements.

The suggested method is then applied in **chapter 4** in order to identify the polarisation properties of a set of columnar-QDs samples and compare it with that of standard aspect ratio QD material. In the later section, field-dependent photo-absorption spectroscopic measurements are taken in order to investigate the Quantum-Confined Stark Effect in columnar-QD with a varied aspect ratio. Then, the dual polarisation property of laser emission of an extremely high aspect ratio columnar-QD is presented and explained in the final section.

Chapter 5 gives a summary of the main points of the experimental results analysis obtained in chapters 3 and 4 and proposes possible ways to further explore and develop the work suggested in this thesis.

1.3 Introduction to semiconductor lasers

1.3.1 Basic semiconductor theory

The basics of the semiconductor theory are described in detail in many textbooks on solid state physics [Hook 1991]; here a brief anaphora to the main points is given. Within a solid-state semiconductor, atoms combine together to form a crystal structure and the periodic arrangement of atoms in the crystal is called lattice. Electrons occupy discrete atomic energy levels, but when arranged in a crystal structure they form energy bands separated by a region of forbidden energy called the band-gap [Kittel 1996]. The potential function of a single crystal material is periodic. Due to the periodicity of the crystal the whole structure can be described by a repeated basic lattice, called Bravais lattice, which is generated by the unit vectors, $\vec{a}_1$, $\vec{a}_2$ and $\vec{a}_3$ and a set of integers k, l and m so that each lattice point can be obtained from the vector $\vec{R} = k\vec{a}_1 + l\vec{a}_2 + m\vec{a}_3$ [Zeghbroeck 2007]. In order to solve Schrödinger's wave equation it is consider that the electrons are standing in a periodic potential U($\vec{r}$), with the periodicity of Bravais lattice. Thus,

$$U(\vec{r} + \vec{R}) = U(\vec{r}) .$$

Equation 1.3.1

Within a crystal a reciprocal lattice can also been defined where the central cell of it, called 1st Brillouin zone, is of special physical importance. This zone is defined for a wave-vector $\vec{k}$ (k has units of reciprocal length) with value ranging between -π/α and +π/α, where α is the lattice constant representing the spacing between the periodically arranged atoms. Values of $\vec{k}$ outside the Brillouin zone reproduce lattice motions described by values within the limit ± π/α. Through Schrondinger's equation the solutions can be described in terms of a plane wave and a periodic function $u(\vec{k}, r)$ consisting the periodicity of the crystal, i.e

$$u(\vec{k}, \vec{r} + \vec{R}) = u(\vec{k}, \vec{r}),$$

Equation 1.3.2

The solution is called Bloch's function and it has the form

$$\psi = e^{i\vec{k}r}u(\vec{k},r)\,.$$

Equation 1.3.3

It follows that if the wave-vector of the Bloch wave function lies outside the first Brillouin zone it can always be brought within it by choice of a suitable lattice vector. The wave function then remains unchanged and all the energy bands can be represented lying within the 1st Brillouin zone [Davies 1978]. An energy band structure of a direct-band gap III-V semiconductor in the center of the 1st Brillouin zone is shown in figure 1.3.1. For small values of $\vec{k}$, the shape of the bands can often be approximated to that of a parabola, which is described by equation

$$E = \frac{\hbar^2\vec{k}^2}{2m^*},$$

Equation 1.3.4

which relates the energy with the particle momentum, given by the equation $\vec{p} = \hbar\vec{k}$, for a particle of an effective mass m^*. The effective mass is a theoretical concept which allows treating the carrier, standing under the presence of the lattice electric field, as a free particle.

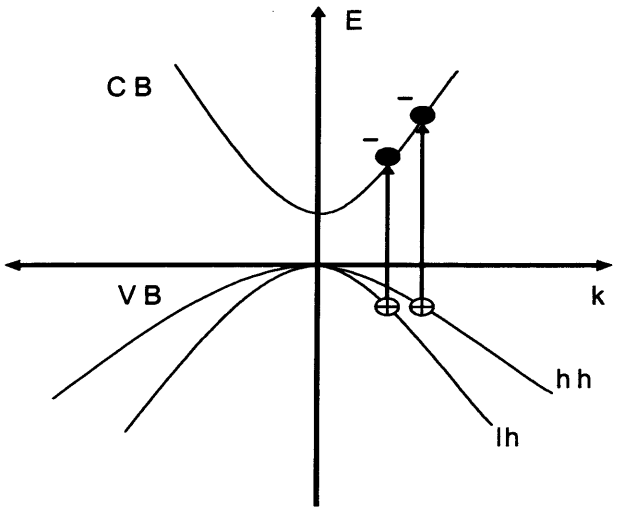

Figure 1.3.1 An idealised energy band diagram of a III-V semiconductor at the centre of the Brillouin zone. Arrows show the transitions of electrons from the VB to the CB leaving a positive charged hole. The split-off hole valence band is not included in the diagram.

In the simplest case the conduction band (CB) is empty of electrons, whereas the valence band (VB) is fully occupied with electrons. When electrons obtain the necessary energy, greater than the band gap energy which is determined by the energy separation of CB and VB at k=0, the electron is elevated into the CB and leaves a vacant position of electron, which is considered as a positive charged hole. The curvature of the 3-bands displayed in figure 1.3.1 is determined by the effective masses of electron and hole. Thus, from the diagram in figure 1.3.1 there are two different values of effective masses of holes, where the hole of heavier effective mass is called heavy-hole (hh) and the one with the lighter is called light-hole (lh).

1.3.2 Crystal structure of GaAs

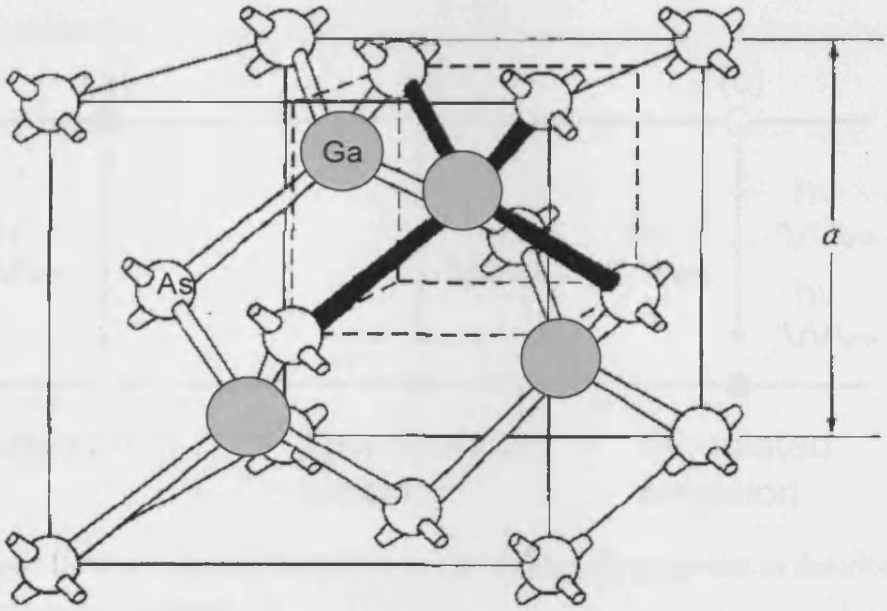

Figure 1.3.2 The zincblende lattice of GaAs as appears in ref. [Neaman 1997]

A gallium arsenide (GaAs) forms a periodic structure called zincblende and differs from the diamond structure -in which atoms are of the same species, such as silicon- only in that there are two different types of atoms in the lattice. The important feature of GaAs structure is that the atoms are joined together in tetrahedron formation in that way in order each Ga (or As) atom has four nearest As (or Ga) neighbours. A schematic diagram of a zinc blende lattice of

GaAs is shown in figure 1.3.2, where the lattice constant α represents the length of each side between two face-centered cubic (FCC) lattices.

1.3.3 Optical absorption and radiative recombination

All possible optical transitions that can occur between two energy states are analytically described by Einstein's relations [Einstein 1917]. The possible optical transitions, which are illustrated graphically in figure 1.3.3, are absorption, spontaneous emission and stimulated emission. However, it should be noted that the transitions processes presented above can be described by Einstein theory in a semi-classical phenomenological way and can only be justified by using quantum-mechanical treatment of the radiation field [Loudon 1983].

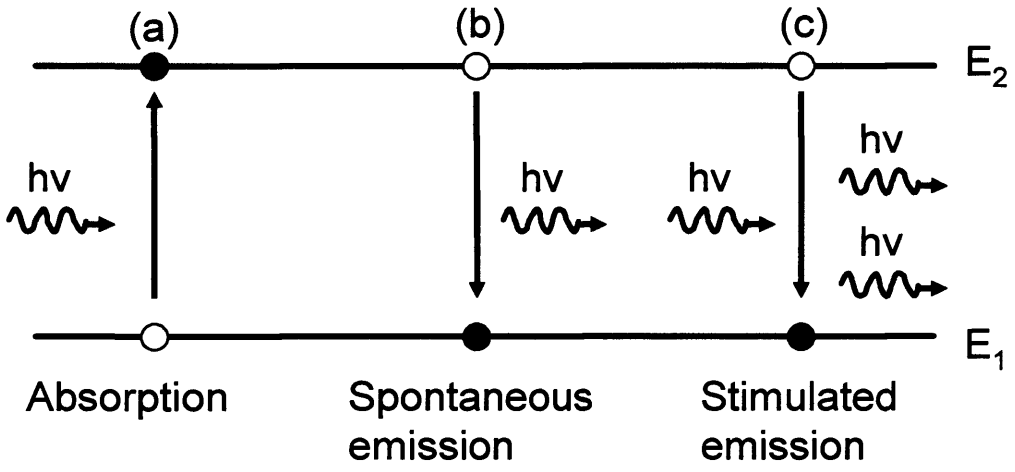

Figure 1.3.3 All optical transitions in a two-energy level system as described by the Einstein equations.

The above optical processes are described in terms of Fermi functions f_1 and f_2 defining the probabilities of occupancy of the states 1 and 2 respectively. In general, the carriers obey the Pauli Exclusion Principle and the occupancy probability can be described by a Fermi-Dirac distribution in thermal equilibrium [Reif 1965]

$$f = \frac{1}{e^{\frac{E-E_f}{kT}}+1},$$

Equation 1.3.5

where f is the probability for occupancy at energy E, E_f is the Fermi level, k the Boltzmann's constant and T temperature. The Fermi level is defined as the level where the Fermi function is equal to half.

1.3.4 Laser diode

In order to achieve laser action from a semiconductor medium, where the coherent (stimulated) emission compared to other processes (absorption and spontaneous emission) is dominant, the first basic requirement is the laser medium to be under non-equilibrium state [Casey 1978]. Thus population inversion, where the electron population of the upper state exceeds the population of ground state, should be obtained by electrically pumping the laser medium, therefore injecting carriers into the upper state of a semiconductor junction. The second requirement is that the semiconductor gain medium, which amplifies the generated light power, should be enclosed in a cavity with the two ends of the cavity to consist partially reflected mirrors in order to provide optical feedback [Siegman 1986]. In the simplest case the value of the mirrors reflectivity is defined from the refractive index difference of the semiconductor/air interfaces. Lasing threshold is reached when the round trip gain, within an optical mode, is sufficient to overcome the light optical scattering and the mirror losses within and at both ends of cavity respectively, which is described by the equation [Agrawal 1993]

$$G_{th} = a_i + \frac{1}{L_c} ln\left(\frac{1}{R}\right).$$

Equation 1.3.6

G_{th} is the threshold modal gain, L_C is the length of the cavity, a_i is the optical scattering losses and R is the mirror reflectivity.

The first stimulated emission was demonstrated in the region of microwave radiation by Charles Townes in the mid-50s (the history of laser is given for example in ref. [Berlotti 2004]). This device -called MASER- is the precursor of LASER developed in the early 60s [Maiman 1960]. The first semiconductor lasers were p-n homojunction diodes, where the doping (p or n) takes place at the same material, and were characterised by very high values of threshold current [Hall 1962]. Moreover, an improvement of laser performance was achieved gradually with the creation of a p-i-n double heterostructure (DH) laser [Alferov 1970]. This structure involves an undoped GaAs being sandwiched by higher band gap p and n-type AlGaAs regions. Both carriers and optical field are confined in a DH due to the potential barriers around GaAs and to the refractive index difference between AlGaAs barriers and the GaAs gain medium respectively. The difference in the refractive index supports the wave guiding of the optical field in the core of the DH, within the gain generation region.

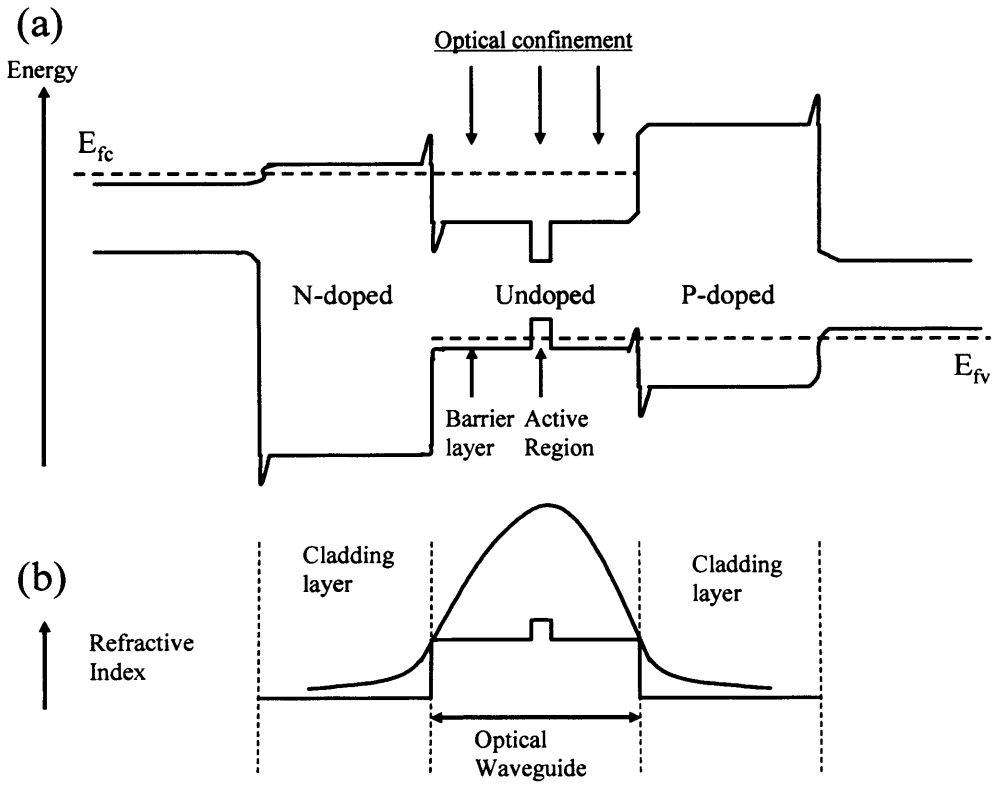

Figure 1.3.4 Simple diagram of a SCH QW p-i-n junctions under forward bias showing (a) the energy bands and (b) the refractive index profile of the constitute materials.

Improvements in the growth techniques of DH led to the design of the active layer, being 100 to 200nm thick in the early 70s, to about an order of magnitude thinner in the early 80s. When the active region thins down to 10nm, the quantum confinement of carriers takes place in the growth direction (see figure 1.3.4), defining a Quantum Well (QW) region. The first experimental observation of a QW was published in 1974 [Dingle 1974]. Because of the thin QW active region of lasers, in order to retain the optical confinement of the early DH a Separate Confinement Heterostructure (SCH) (details are given ref. [Coldren 1995]) was designed, illustrated in figure 1.3.4. In a SCH the electrical confinement is improved by the inclusion of barriers on either side of the QW and the optical confinement can be independently controlled by altering the width of the barrier material.

1.4 P-n junction theory

In the work presented in next chapters the photo-absorption spectrum of a wave guided laser diode is obtained by light incident onto the edge of the diode. A photo-current or photo-voltage signal is then measured by the detection of the photo-generated carriers. In this paragraph the basic physics in the simplest case of a p-n junction are described and the process of photo-absorption and signal detection is discussed in detail. The equations quoted here for the simple case of a p-n junction are still valid for the QW p-i-n hetero-junctions – studied in the next chapters- as it appears to have similar rectifying characteristics [Wilson 1998].

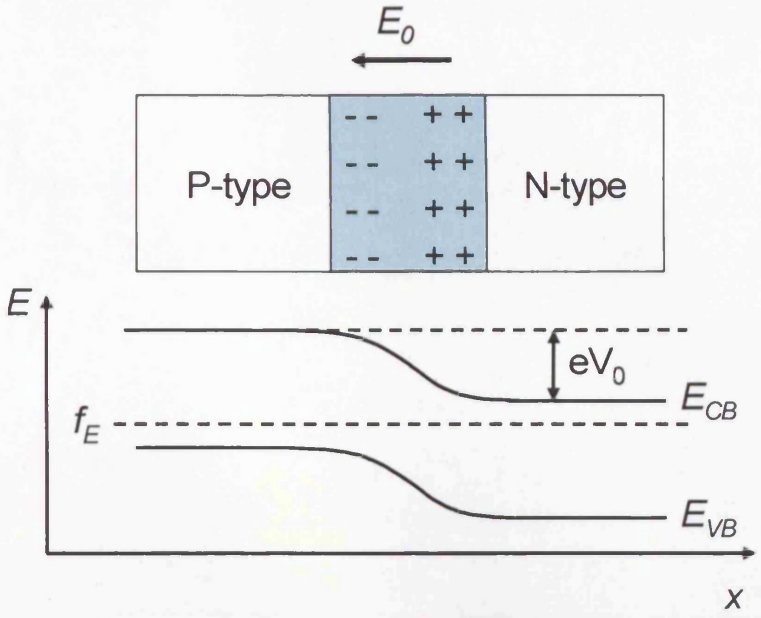

Figure 1.4.1 Schematic representation of a p-n junction.

In a p-n junction, shown in figure 1.4.1 -under equilibrium condition- a "built-in" field E_0 is present, corresponding to a "built-in" voltage value V_0, in a region depleted of carriers, therefore called "depletion region". In thermal equilibrium the rate at which electrons are created by thermal excitation, leaving an equivalent number of holes in VB, described by a generation rate G_0, which is equal to the rate of recombination of e^--h^+ pairs. With applied voltage and in the case of steady state the addition of electron and hole currents result to a total current, called steady-state dark current I_{dark}, given by the equation [Neaman 1997]

$$I_{dark} = I_0\left(e^{\frac{qV}{kT}} - 1\right),$$

Equation 1.4.1

where I_0 is the reverse saturation current of equation

$$I_0 = q\left(\frac{N_P D_e}{L_e} + \frac{P_N D_h}{L_h}\right).$$

Equation 1.4.2

D_e, D_h are diffusion coefficients and L_e, L_h diffusion lengths of electron and hole respectively. N_P and P_N are the electrons and holes densities in a p and n region respectively.

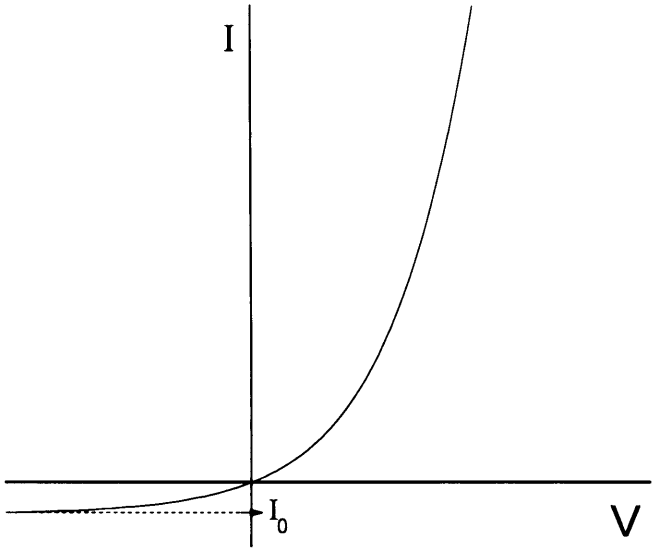

Figure 1.4.2 I-V characteristic of a p-n junction diode.

The term "dark" of the total current is given because of the absence of a photo-generated current along the junction. The current-voltage characteristic of a p-n junction diode in the absence of light is presented in figure 1.4.2.

The p-n junction's built-in potential V_0 is given by the equation

$$V_0 = \frac{kT}{q} ln\left(\frac{N_A N_D}{n_i^2}\right),$$

Equation 1.4.3

where n_i, N_A and N_D is the intrinsic, acceptor and donor carrier density respectively.

1.4.1 Reverse biased p-n junction

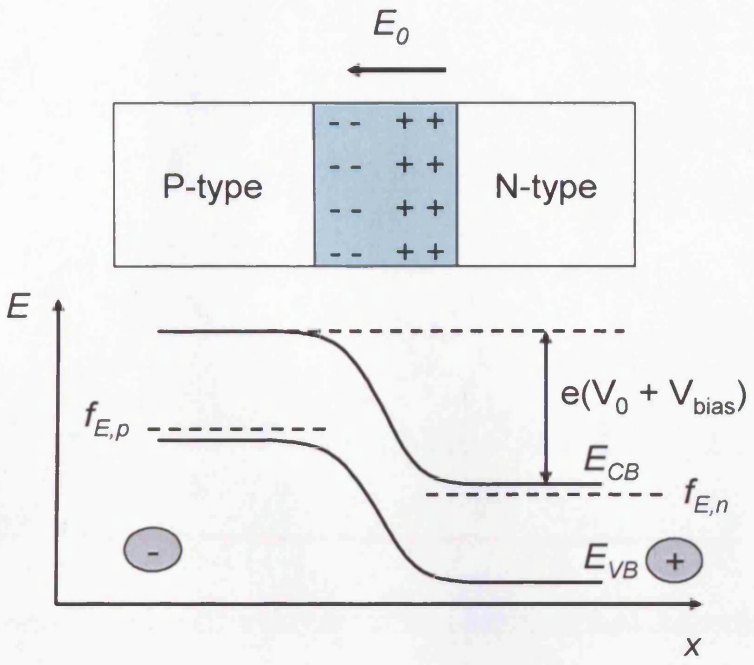

Figure 1.4.3 P-n junction under reverse bias.

Figure 1.4.3 shows the p-n junction under reverse bias, where the external applied voltage is in the growth direction, running from n- to p-type region of the junction. This has an effect on the voltage of depletion region, getting increased by a factor V_{bias} corresponding to the external applied bias value. Thus, in this case the carriers are extracted from the junction, due to the induced field, and the current across the junction saturated to a value I_0 according to the I-V diagram of figure 1.4.2.

1.4.2 Light illumination of p-n junction

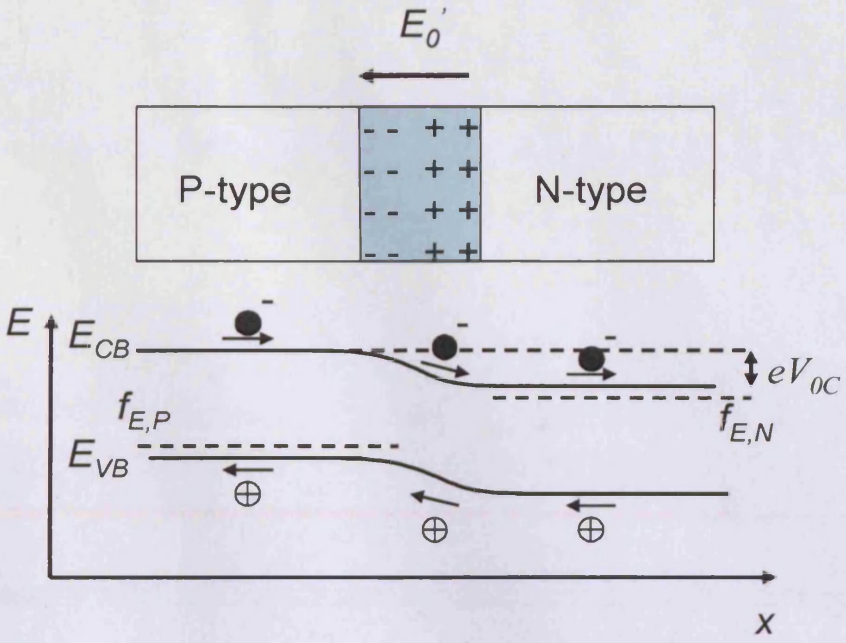

Figure 1.4.4 P-n junction under photo-generated current.

The illumination of the p-n junction with light of photon energy higher than the bandgap energy of the p-n junction material $h\nu > E_g$, will create electrons and holes which will be swept away by the built-in electric field of the depletion region. The photocurrent I_P, created by the distribution of the excess photo-generated carriers inside the p-n junction, will eventually affect the juction's potential. The depletion region is reduced and a forward junction current I_j -counter to I_P- is created. The additional generated carriers due to light illumination are described by an optical generation rate G [Orton 1990]. The total generated carriers are given by the sum of the optical and the thermal generation rate, $G + G_0$. The total current I_{tot} across the junction becomes zero when a steady state condition is reached again, given by equation 1.4.4

$$I_{tot} = I_j - I_P = I_0\left(e^{\frac{qV}{kT}} - 1\right) - I_P.$$

Equation 1.4.4

The characteristic I-V curve is summarised in figure 1.4.5, where the curve has been shifted downwards compared to that without light illumination and the intercept of the I-V curve to I axis is equal to the photo-generated current I_P.

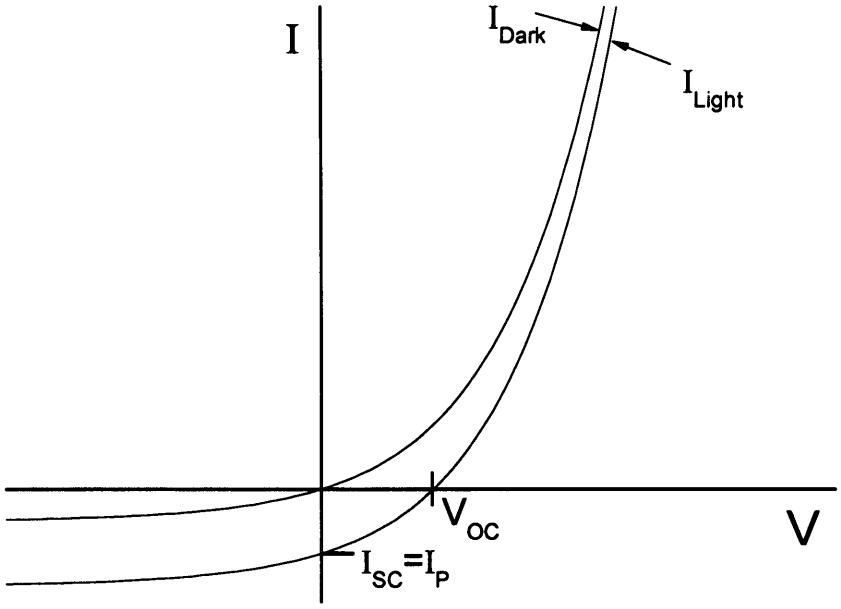

Figure 1.4.5 IV characteristic of a p-n junction diode under light illumination. The I_{Light} on the plot corresponds to the total current I_{tot} in the equation (1.4.4).

From figure 1.4.5 two critical values can be extracted which are involved in the operation of the photodiode. The one is the potential value V_{OC}, which is reduced relative to that of the unbiased built in potential V_O of the junction. V_{OC} refers to open-circuit condition, when the total current along the p-n junction is zero. In this case, equation 1.4.4 is written in the form

$$V_{OC} = \frac{kT}{q} ln\left(1 + \frac{I_P}{I_0}\right).$$

Equation 1.4.5

The other critical value is the short-circuit current value, I_{SC} which is equal to the photo-generated current I_P, given by

$$I_P = I_0\left(e^{\frac{qV_{OC}}{kT}} - 1\right).$$

$$I_P = I_0\left(e^{\frac{qV_{OC}}{kT}} - 1\right).$$

Equation 1.4.6

The current I_P generated by light absorption is proportional to the incident light irradiance I_{IR} and is given by the equation [Wilson 1998]

$$I_{SC} = \frac{\eta I_{IR} A q \lambda_0}{hc},$$

Equation 1.4.7

where η -called quantum efficiency- is the fraction of the incident radiation which contribute to the current flow along the p-n junction, as a few e^--h^+ pairs created far from the depletion region of the junction recombine before reaching the depletion region. A is the illuminated area and λ_0 the wavelength of the incident light.

1.5 Applied electric field in a p-i-n junction

In the previous section, the p-n junction characteristics under reverse bias were discussed. By the application of only a few volts across the junction very high values of field are generated, e.g 10^5 V/cm. In this section the effects of such high field values are discussed for the simple case of a p-i-n junction, where the formed intrinsic region consists of a bulk material and a QW.

1.5.1 Franz-Keldysh Effect

In a bulk material the energy band in the presence of an electric field changes shape, as is illustrated in figure 1.5.1, and this has an effect on the absorption edge studied independently by W. Franz and L.V. Keldysh [Keldysh 1958] (e.g in ref [Fox 2001]). In an optical absorption experiment the energy gap, under the presence of an electric field perpendicular to the epitaxial layers of the structure, is reduced since below band gap the incident photons can get absorbed via interband transitions by spatial tunnelling of electrons. The red-shift of the

band gap energy due to reduction of band gap is the basis of electro-optical modulators that have the advantage that they can be integrated with semiconductor lasers on the same chip [Miller 2004].

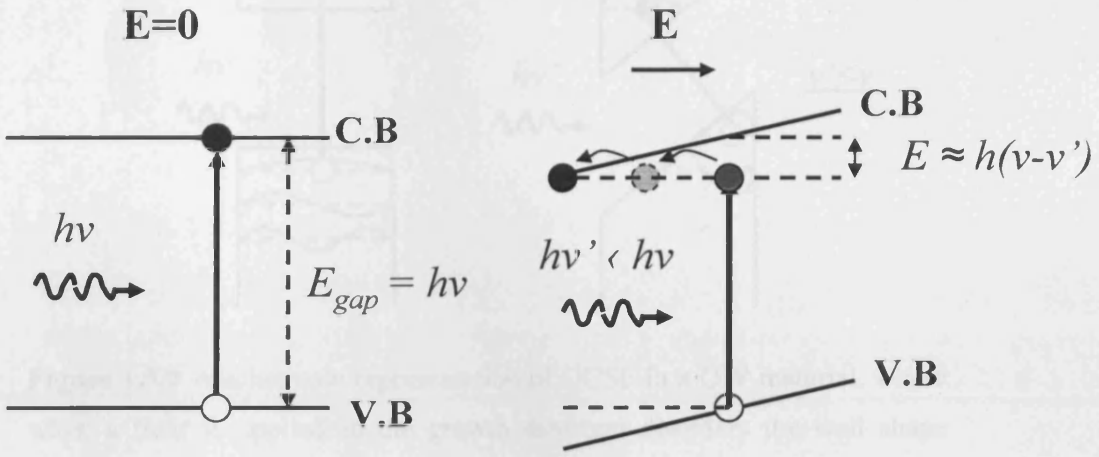

Figure 1.5.1 Schematic diagram showing the Franz-Keldysh effect due to the presence of electric field.

1.5.2 Quantum-Confined Stark Effect

Until now, the application of an electric field only in a bulk material has been discussed. When the field is applied in a material structure were the carriers can be quantum-confined in a very narrow region then the resultant shift in the energy transitions is described by the Quantum-Confined Stark Effect (QCSE) [Miller 1984a] and shows unique characteristics compared to Franz-Keldysh effect. This effect is studied in detail in chapter 4 with an application of a field in columnar-QD materials. However, the basic physical principal for a QW under an applied field are given here.

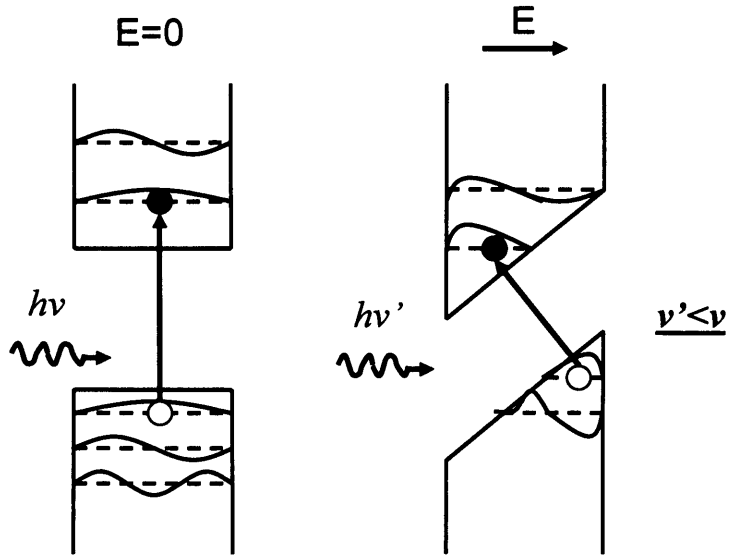

Figure 1.5.2 A schematic representation of QCSE in a QW material, where when a field is applied in the growth direction disorders the well shape causing a reduction in the transition energies.

The application of an electric field perpendicular to a QW has a different effect compared to that in a bulk material. Within an applied field the well shape is distorted and the energy states between the CB and VB energy states are coming closer together. This reduces the energy of the transitions and the effect in a photo-absorption experiment is observed by a red-shift of the absorption spectra with increased value of applied field. In addition, the electrons and holes are pulled apart towards different directions by the presence of the field. In the case of a QW this electron-hole separation is limited by the well barriers therefore, the presence of strong photon absorption is even apparent for very high values of applied field, whereas in the Franz-Keldysh effect there is a broadening of band-edge absorption even for small values of applied field. Moreover, there is another effect that counteracts the energy red-shift but has less effect in the overall energy shift. The bending of the energy bands with applied field narrows the well width at the edges causing a shift of the electron and hole energy bands upwards and downwards respectively, which causes a blue-shift in the energy transitions. The effect of an applied field parallel to the well is similar to that applied in a bulk material since carriers are not confined in this direction, therefore the shift of the absorption edge, in that case, can be described by the Franz-Keldysh effect.

The electro-absorption effect in a multiple QW structure is approximately 50 times larger than that in bulk materials [Wood 1988]. Thus, QW materials have been attractive for application in optical modulation [Wood 1984] [Temkin 1987] and optical switching [Miller 1984b].

1.6 Transition Matrix Element

The strength of the transition of an electron from the VB to the CB, due to the presence of an electromagnetic field, is described by the transition matrix element M_T. The square of the transition matrix element refers to the probability of a transition to occur as appears in formula [Zory 1993]

$$|M_T|^2 = |\langle u_v|\hat{e}\cdot p|u_c\rangle|^2|\langle F_h|F_e\rangle|^2,$$

Equation 1.6.1

where F_h, F_e are the envelope and u_v, u_c are the Bloch's functions of holes and electrons in the VB and CB respectively. The product of the envelope function F and the Bloch's function u gives the overall wave-function Ψ of an electron and a hole. The factor $\langle u_v|\hat{e}\cdot p|u_c\rangle$ is an optical perturbation term depending on the light polarisation $\hat{e}$ and is described by the Hamiltonian factor $\hat{e}\cdot p$. When the wave functions are perfectly spatially overlapping the factor $\langle F_h|F_e\rangle$ is unity and the transition of an electron from the VB to CB is likely to occur under the perturbation of an electromagnetic field. In the case where there is no spatial overlapping of the wave functions, the transition matrix element reduces to a value close to zero and the transition is highly unlikely to occur.

In a QW due to the confinement in one direction the degeneracy of light and heavy hole at $k=0$, shown in early figure (figure 1.3.1), is removed. The transition strength of electrons from the lh- or hh-VB to CB depends on the polarisation of the incident light. The $|M_T|^2$ resultant equations [Zory 1993] for transverse magnetic (TM) and transverse electric (TE) polarisations of the induced optical field are:

$$\textit{TM polarisation } (\hat{e} \,//\, z)\text{: } |M_T|^2 = |M|^2 \left[\frac{2}{3}\langle F_{lh}|F_e\rangle^2\right] \text{ (a)}$$

and

$$\textit{TE polarisation } (\hat{e} \perp z)\ |M_T|^2 = |M|^2 \left[|\langle F_{hh}|F_e\rangle|^2 + \frac{1}{3}\langle F_{lh}|F_e\rangle^2\right] \text{ (b)},$$

Equation 1.6.2

where y is the quantisation direction of the QW (see figure 1.6.1) and $|M|^2$ is a momentum matrix element, constant for a given material. A further analysis of $|M|^2$ factor is out of the scope of this thesis as in the following chapters only the ratio of the two polarisation TE over TM is used, therefore the factor $|M|^2$ cancels out, being the same for both polarisations. Equations 1.6.2 are valid only close to the band edge energy at k≈0. Away from the band-edge and for non-zero values of wave vector due to band-mixing effects an alteration in the shape of hh- and lh- energy bands occurs, causing a change in the transition strength.

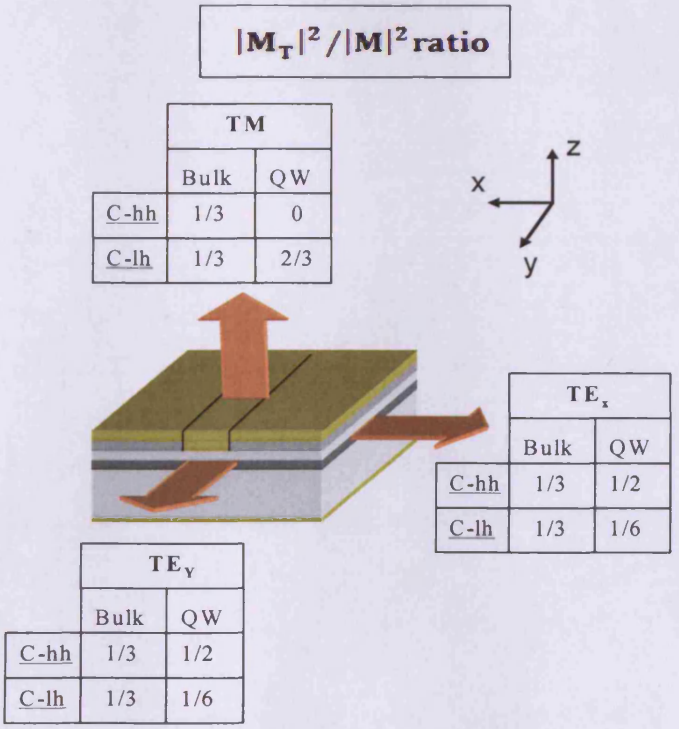

Figure 1.6.1 $|M_T|^2/|M|^2$ ratio for different transition and light polarisation relative to the bulk material and to the plane of the QW as appears in ref [Lewis 2002a].

By assuming a perfect spatial overlap of the envelope functions, i.e $\langle F_{lh}|F_e\rangle = 1$ and $\langle F_{hh}|F_e\rangle = 1$, within tables of figure 1.6.1, values of ratio $|M_T|^2/|M|^2$ are summarised with respect to TE and TM polarisation for hh- and lh-VB to CB transitions according to equation 1.6.2. The TE and TM polarisation are illustrated with respect to the device geometry, where the z-axis defines the direction of epitaxial growth.

The values of $|M_T|^2/|M|^2$ in the case of bulk material show that the transition strength of c-hh and c-lh transitions are the same under TM and TE polarised light contrary to the QW material, where the relative magnitude $|M_T|^2/|M|^2$ depends upon TE and TM polarisation. In the case where light of TM polarisation illuminates the QW the strength of the transition is zero and the transition matrix element is given by the equation $|M_T|^2 = \frac{2}{3}|M|^2$. For TE polarised light there is both a contribution of e1-lh1 and e1-hh1 energy transitions. However, the e1-hh1 transition is stronger than that of e1-lh1 by a factor of 4.

It should be noted that the above calculations for the transition matrix element are not absolute and there is always a small deviation from the true values of wave function overlap integrals, having values less than unity. This is due to the different shape of electron and hole wave functions because of their different effective masses. Thus, the overlap cannot be perfect and an integral value $\langle F_h|F_e\rangle$ between 0.90 and 1 is given [Coldren 1995]. Therefore, the ratio $|M_T|^2/|M|^2$ values given in figure 1.6.1 are approximately valid as well.

1.7 Quantum Well strain layers

Strain is induced in a semiconductor when is formed by materials where their crystal structure are of different native lattice constant. The induction of biaxial strain within a QW material structure has the effect of splitting the lh and hh sub-bands as is illustrated in figure 1.7.1. When the lattice constant of the well material is larger than that of the barrier material the strain is compressive, whereas in the opposite case is tensile. In strained QW the coupling between the lh and hh bands results in highly non-parabolic sub-band dispersion [Bastard

1988]. The effect that has the strain on the band structure has been found to be beneficial for the fabrication of more efficient laser sources [Yablonovitch 1986] [Adams 1986].

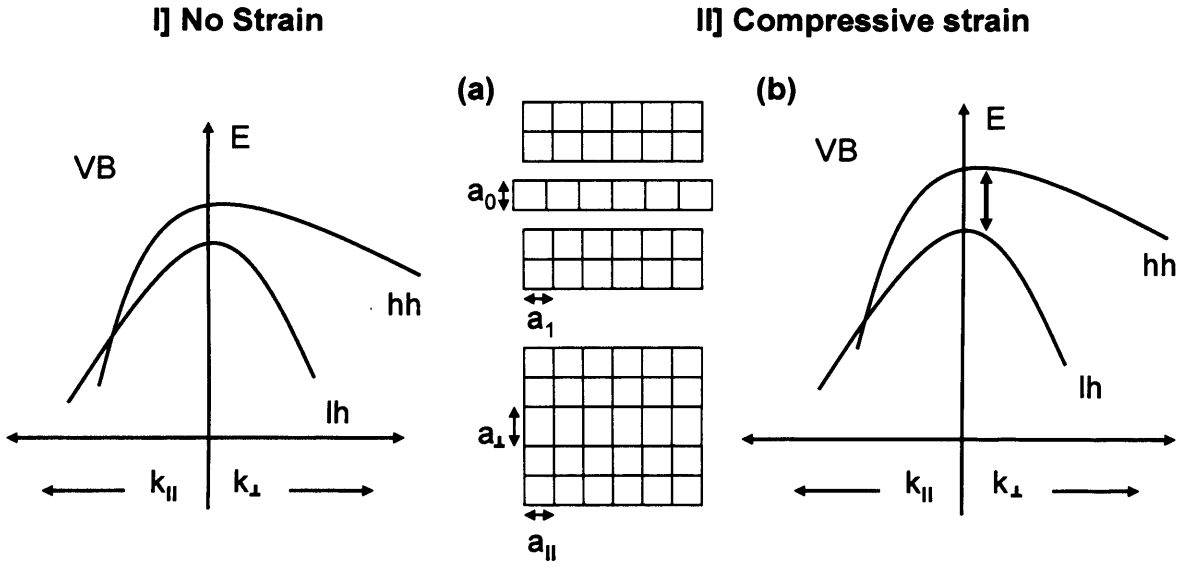

Figure 1.7.1 VB energy diagram of I] an unstrained QW and II] under strain QW. Diagram (a) shows the crystal deformation caused by the growth of material with a lattice constant a_0 between the layers of a material with a smaller lattice constant a_1, which causes a shift of the hh energy band with respect to that of the lh as illustrated in diagram (b).

In the case of tensile strain an upward shift of conduction band and a downward shift of the average valence band in the energy diagram is observed, while the valence band hh- and lh- energy bands are pushed towards each other. For a compressive strained QW, there is an upward shift of the hh-band against the lh-band (figure 1.7.1), and the energy bandgap of a hh transition is less than that of the lh ($Eg(lh) > Eg(hh)$). In the case of tensile strain the hh- and lh- bands are moved towards each other, with the degree of the strain to determine whether the band edge energy is of hh-type, i.e $Eg(lh) > Eg(hh)$ or lh-type, i.e $Eg(hh) > Eg(lh)$.

1.8 Self-assembled InAs/GaAs Quantum Dot materials

1.8.1 Quantum dots: A brief introduction

As has been already mentioned, the fabrication of QW structures (section 1.3) and the introduction of strain into the crystal lattice (section 1.7) have improved the laser performance through the 1980s. However, the idea of reducing the confinement dimensions from a 2-dimensional (2-D) system to 1-D (Quantum Wires) [Kapon 1989] and finally to 0-D (Quantum Dots), with confinement in all three-dimensions, can be beneficial to improve the laser characteristics such as reduced threshold current density, temperature insensitivity, and narrow spectral emission [Bimberg 1999]. The first QD laser was proposed in 1976 [Dingle 1976] and then evolved by Y. Arakawa and H. Sakaki [Arakawa 1982]. The theoretical predicted improvements of QD laser performance compared to Quantum Well or Quantum Wire laser is due to 3-dimensional confinement of carriers, where bands of energy states are substituted by discrete energy levels in an individual dot. Thus, this 0-D system is called an "artificial atom" because the discrete energy levels are similar to the energy levels within an atom. However, because of the non-uniformity in the size, shape and composition of the formed self-assembled dots a dominant inhomogeneous broadening mechanism is responsible for the deviation of QD laser devices performance with respect to the theoretical expected. Also, contrary to theoretical predictions, QD laser devices show temperature-sensitive characteristics. This is due to the thermal escape of carriers, at elevated temperatures [Matthews 2002], which deteriorate the laser performance. However, since the theoretical prediction in the early 90s for advanced performance of QD laser compared to QW, the QD system have been developed in a great extent to include different materials emitting from visible [Micic 1996] [Damilano 1999] to near infrared up to 1.55μm [Sopanen 2000]. Ground state lasing emission at room temperature has been reported for InAs/GaAs QD lasers [Huffaker 1998] [Ledentsov 2002], with values of threshold current density being lower compared to that of QWs [Grundmann 2000]. Several approaches have been investigated in order to reduce the leakage current due to thermal escape of carriers by using tunneling injection structures [Asryan 2001] or enhancing the emission properties of the dots by stacking layers of dots on top of each other [Yu 1999]. Even issues such as the dot's size non-

uniformity, which is responsible for the broadening of emission spectrum, can treated by using a new growth technique [Verma 2008] growing dots of almost identical shape, with low density of defect states. Performance improvement has been reported as well by the growth of dots in a QW (dot-in well or DWELL) [Lester 1999], [Mukai 1999]. In the DWELL structures the dots are grown on a thin InGaAs layer and then are capped by a thin layer of the same composition material. The dot sample which is used in the experiments described in this thesis is a DWELL structure and more information about the properties of this type of structure can be found in ref [Sandall 2006].

There are two epitaxial techniques widely used for the fabrication of QD systems; Metal Organic Chemical Vapor Deposition [Ludowise 1985] and Molecular Beam Epitaxy (MBE) [Cho 1971]. The latter one is used for the growth of the structures studied in this thesis. MBE can produce high quality layers, in atomic level, with a good control of thickness, doping and composition [Ustinov 2003]. The most predominant method for growing QD materials is through the self-assembled Stranski-Krastanow (SK) growth mode. The formation of dots takes place by depositing a thin film of e.g InAs, of a few monolayers, on an e.g GaAs substrate [Ustinov 2003]. Due to lattice mismatch of about 7 percent between the InAs and GaAs layers there is a large strain energy which relaxes by the formation of In(Ga)As islands on top of the GaAs substrate. Beneath the mixed In-Ga composition islands, forming the QDs, there is a InAs layer -few monolayers in thickness- relaxing partially by the formation of dots. Under current injection, carriers are relaxed into the QDs through this layer, which is called the wetting layer (WL).

1.8.2 Quantum Dots for optical amplification/modulation/switching

In this chapter, an introduction has been made about the benefits of quantum confinement towards the improvement of laser diodes performance. However, the unique properties that quantum-confined semiconductor shows can be also utilized to replace commercial erbium-doped fiber amplifier or other suggested rare-earth doped fiber amplifiers [Ohishi 1991] [Yamada 1998] with Semiconductor Optical Amplifiers (SOA). Bulk semiconductor

amplifiers can fill the gap of wavelength bands not commercially covered by rare-earth doped fiber amplifiers, but provide large noise figure (NF) coming from the Amplified Spontaneous Emission (ASE) [Akiyama 2005]. By replacing the active material of a SOA with QW or QD the NF can be improved. Moreover, it has been reported that the use of QDs is advantageous compared to QW in SOA due to their high output power [Berg 2003] [Grundmann 2000], low noise figure [Komori 1991] [Berg 2003] and broad gain bandwidth with ultrafast gain response [Akiyama 2005]. The low-noise figure is due to reduced spontaneous to stimulated emission rate and the small waveguide loss that QD materials are exhibit. The fast gain recovery and high saturation output power is due to the fast carrier dynamics [Borri 2000] and to a combination of low ground state differential gain of QDs -where the differential gain is defined as the derivative of gain over the carrier density- and large energy separation between the ground, excited and WL states [Berg 2003] respectively.

However, for practical applications of quantum confined systems in SOAs an important issue is to have a control over the polarisation with aim to achieve a polarisation-insensitive light amplification. It follows that the control should be achieved over the polarisation of optical gain, which is determined by the band-edge of the quantum-confined material (see section 1.6). For QW and QD structures parameters such as the composition and strain are important to control the band edge. Polarisation-insensitive QW SOA has already been reported [Magari 1991] [Joma 1992] [Koonath 2002] by introducing tensile strain in the QW, therefore moving the hh- and lh- bands towards each other, as it is already mentioned in section 1.7. In the case of QD material the TE polarised light is strongly absorbed by the dot compared to TM due to the shape and the biaxial strain induced in these structures. This is discussed and explained in more detail in section 3.3.1 of chapter 3. Nevertheless, by the growth of repeated close-spaced dot layers on top of each other, fabricating columnar quantum dots, the dot size and the biaxial strain distribution can be altered, so as either to provide polarisation-insensitive QDs as first proposed by Takashi Kita and his co-workers [Kita 2002] and recently demonstrated for 1.5-μm wavelength bands [Yasuoka 2008a], or QDs showing even a TM-dominant gain [Yasuoka 2008b].

In QDs, the reduction of the dimensional confinement from 2-D to 0-D enhances further the electro-optic effects [Aizawa 1991]. Thus, the use of QDs in a new type of devices such as ultra-high speed optical switches [Nakamura 2002] and small low-energy consumption modulators [Qassaimeh 1998] [Tatebayashi 2007] [Moreau 2007] have been already proposed with aim to replace the bulk or QW active region of these devices. Moreover, in columnar-QD systems giant electron-hole dipole moment values are observed here and also have been reported in ref. [Krenner 2008]. An increase of the dipole moment value can cause a dramatic change in the refractive index variation with applied field [Yamamoto 1985], which is desired for applications in optical modulation/switching.

1.8.3 From Quantum Dots to Columnar-Quantum Dots

A) Closely-stacked Quantum Dot

Having introduced earlier, the idea of enhancing the laser performance by stacking multiple layers of QDs [Yu 1999] a great deal has been moved towards this direction. It has been found that when the intermediate layer between formed dot layers is reduced from 20 to 10 nm the self-assembled QDs aligned in the growth direction [Sugawara 1999a]. This has been explained in terms of the strain fields induced by the islands formation of the first grown QD layer which results in a preferred direction of *In* migration in the upper layers [Xie 1995]. Therefore, In(Ga)As islands on the top layers are formed at the same spatial position as in the layers below. By reducing even further the intermediate layer, to the order of 2 or 3 nm, the close-spaced QD layers form a columnar-shaped structure [Solomon 1996a] [Ledentsov 1996a] which was first defined by Yoshiaki Nakata as closely-stacked InAs islands [Nakata 1997]. The height of the dot can be controlled through the intermediate layer thickness and by changing the growth conditions. At the same time the shape uniformity of the self-assembled dots is experimentally evidenced by the narrower width of luminescence emission (electroluminescence [Solomon 1996b] or photoluminescence [Ledentsov 1996b]) compared to that of one-layer QD materials. The emission is red-shifted with increasing number of closely-stacked QD layers and this is due to the quantum-mechanical vertical coupling of the QDs which occurs for vertical intra-dot space of less than 4nm according to ref [Fonseca 1998]. In the case of coupling the wave functions of the vertical aligned dots are overlapping

and the whole columnar-shaped structure can be considered as one QD. The above characteristics of stacked In(Ga)As QD are responsible for improvement in QD laser devices performance [Heinrichsdorff 1997] [Shoji 1997].

B) Columnar-Quantum Dot

However, closely-stacked QDs exhibit degradation in their emission efficiency due to the presence of many defect states formed during the growth process. This issue can be overcome by growing an intermediate layer of thickness less than the height of the self-assembled InAs islands. Thus, the dots of the upper layers are in physical contact with the dots of layers below, therefore forming a columnar-QD [Sugawara 1999a]. In this case, the thickness of the intermediate layer is less than 1nm (3 monolayers of GaAs). The columnar-QDs exhibit an improvement in the photoluminescence emission efficiency and at the same time show similar characteristics with those of closely-stacked QDs, such as high uniformity of dot shape and narrow photoluminescence emission spectrum. In addition, control over the dot height is possible via the number of cycles of the thin InAs/GaAs superlattice [Nakata 2000] [He 2007] [Li 2007]. Low threshold current and high output power lasing emission from columnar-QD laser diodes has been reported [Mukai 1998].

1.9 Summary

In this chapter, I have outlined the background theory relevant to the understanding of the work illustrated in the following chapters. I began in first section by giving an insight into the aims and the motivation, which lies behind this thesis work. Then, in section 1.2 I described the basic thesis structure. The following sections from 1.3 to 1.7 form an introduction to the basic laser theory. This includes an analytical description of well known values of transition matrix elements for QW systems and a brief introduction to strained layer QW structures. In the last section 1.8 I reviewed the historical development of QD lasers and I discussed issues related to the performance of these structures. Finally, in the last section, a brief introduction to closely-stacked and columnar-QD materials has been given.

Chapter 2-Device characterisation techniques

2.1 Introduction

In this chapter details about the methods and the experimental apparatus used to characterise the set of InAs/GaAs columnar-QD materials, are described. Most of the experimental apparatus used were pre-existing. However, improvements and alterations are mentioned with the present chapter to describe how the data was obtained and processed so as to reveal the required information about the materials studied.

I begin, in the first section 2.2, by introducing the type of laser diode structures used for obtaining experimental data. Then, I describe techniques used to validate and acquire data associated with current-voltage-light diode characteristics.

In section 2.3, I review the main characterisation experiment used in this thesis that measures light absorption by the laser diode with respect to the photon energy. The chapter concentrates on the information that can be extracted by using polarisation-selective edge photo-absorption spectroscopy in comparison with other experimental approaches. This is shown by measurements on compressive and tensile strained GaInP/AlGaInP QW materials which are further used to briefly discuss the polarisation-dependent response of the experimental set-up. The expected behaviour of these materials is known and they are used in order to verify a suggested method in chapter 3 so as to remove the relative system polarisation response from the measurements in order to study the fundamental light interaction with columnar-QD materials in chapter 4.

2.2 Device preparation and Current-Voltage-Light (IVL) measurements

2.2.1 Device processing and preparation

The materials studied in this work form two groups of structures:

1. GaInP/AlGaInP QW structures with a 50μm wide oxide-isolated contact stripe, emitting at 633nm, are used to establish the new technique. This type of laser structure is sketched in figure 2.2.1. In the middle of the top contact a 50 μm wide area of insulating oxide layer, sketched graphically beneath the p-metal contact, is removed prior to metallisation. Therefore, the area formed by the stripe defines the path in which carriers are injected into the active region. The laser diodes are cleaved typically into a square 300 x 300 μm chip. Also, oxide-isolated stripe structures of high-performance InAs/GaAs QD emitting at 1.3μm-grown in Sheffield's ESPRC National Centre for III-V Technologies- were used in this thesis.

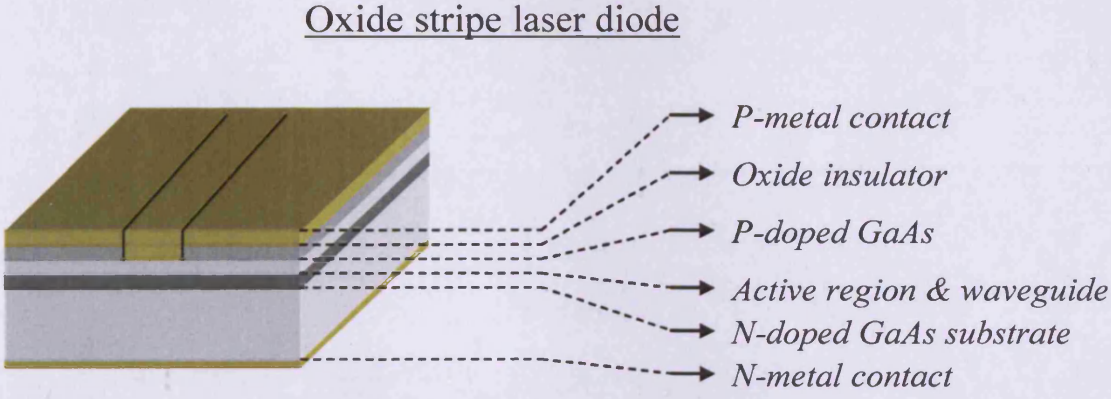

Figure 2.2.1: Schematic diagram of an oxide-isolated stripe laser diode.

2. Ridge-waveguide (RW) InAs/GaAs columnar-QD structures are illustrated in figure 2.2.2. The ridge provides one additional dimension of wave-guiding compared to that of oxide stripe laser diode. The wave-guiding is applied not only in the growth direction but also in the growth plane and parallel to the laser's facet due to the effective index change in this direction. For very narrow ridge widths in the order of only a few microns the RW laser diode can support a single lateral wave-guided optical mode.

The RW structures studied in this thesis were grown and processed by Dr. Liahne Li and Philipp Ridha respectively at the Swiss Federal Institute of Technology Lausanne (EPFL). The ridge width was varied from 10 to 120μm and was formed by etching the p-side of the material into the waveguide area (p-doped AlGaAs) to 200nm above the active region [Ridha 2008a], which consist the GaAs barrier material and the quantum-confined area. The P-metal contact is deposited only at the top of the ridge waveguide and the remaining area is covered by a dielectric polymer, benzocyclobutene (BCB), to ensure electrical insulation and to provide a desired refractive index difference in the lateral direction for improving the properties of the wave-guiding. The devices used for edge photo-current measurements were 2 mm long and for laser measurements 3 mm and 4 mm long.

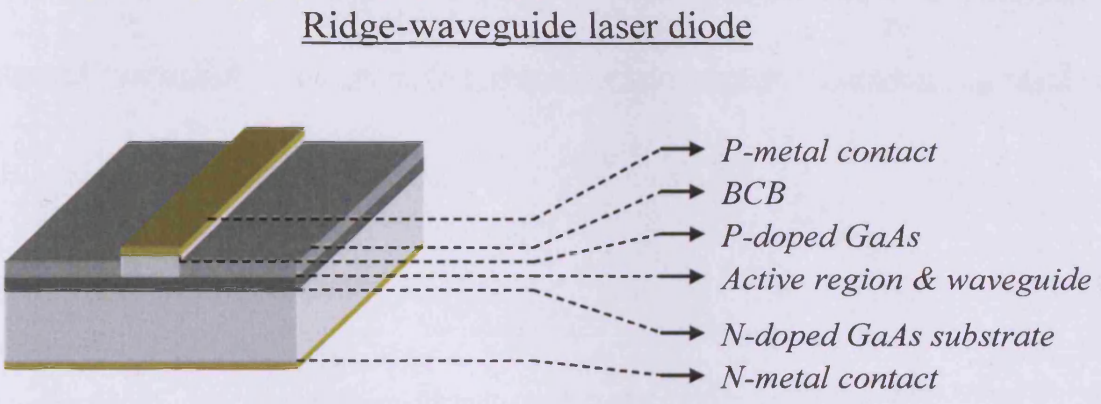

Figure 2.2.2: Schematic diagram of a RW laser diode.

All the structures were grown on an n-type substrate and the active region is lying close to the p-contact. The devices are mounted onto a copper heat sink attached to a T0-39 transistor header by using silver epoxy. Before gold wires are attached to the top contact of laser chips for electrical current injection the devices are examined in the microscope for any visible mirror or general structural imperfection which can increase the optical losses, and therefore the laser threshold current density. The device characteristics are always measured pulsed in low duty cycle regime to avoid self-heating effects which can affect the laser performance. The pulse width used in every measurement is 500 ns and the pulse frequency is 1 kHz, giving a duty cycle of 0.05%.

2.2.2 Current-Voltage (I-V) characteristics

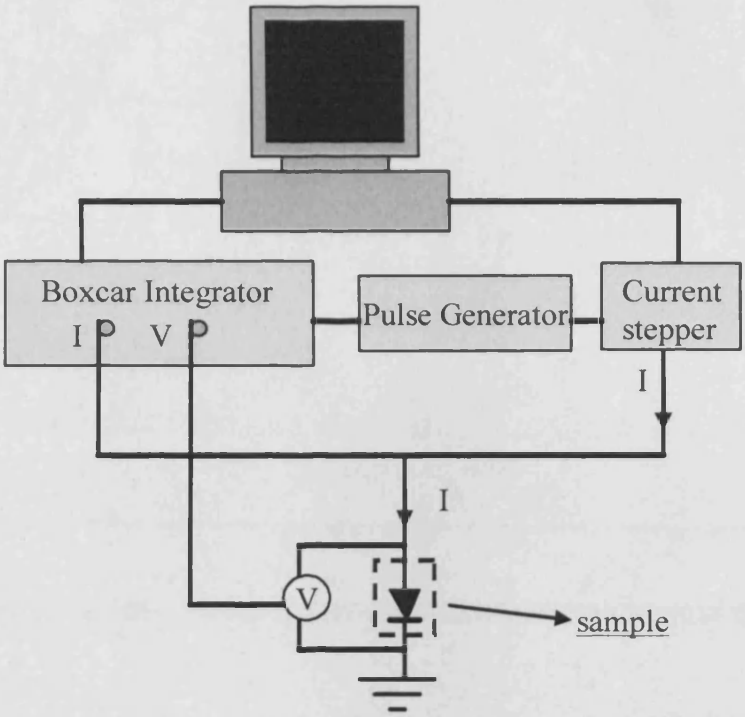

Figure 2.2.3: Experimental set-up for measuring IV characteristics.

The apparatus -sketched in figure 2.2.3- is used to measure the Current-Voltage (IV) characteristics of the devices and is pre-existing together with a suitable computer program. A pulse current is injected into the tested sample through a current stepper controlled by the computer. The PC monitors the current and the voltage amplitude through the boxcar integrator. The boxcar is used to obtain sample in time readings of the voltage and current pulses using gates, where the width of the gates defines the time over which the readings are taken. The signal is averaged over many gates so as to obtain low signal to noise ratio measurements. Then the output signal is sent to the PC, where the readings are saved in a file.

An example of the IV characteristic of a columnar-QD device is illustrated graphically in figure 2.2.4, where by inversing the diode direction of figure 2.2.3 (earth the p-type instead of n-type region) reverse bias current values were obtained as well. The minimum current measured value is 0.1mA. The computer program is adjusted to stop increasing the reverse bias value for values of current higher than 0.3mA for the case of reverse (negative) bias

measurements. Therefore, current measurements with respect to negative voltage values are obtained before the breakdown voltage point [Neamen 1997] is reached. After this point the current amplitude will increase rapidly.

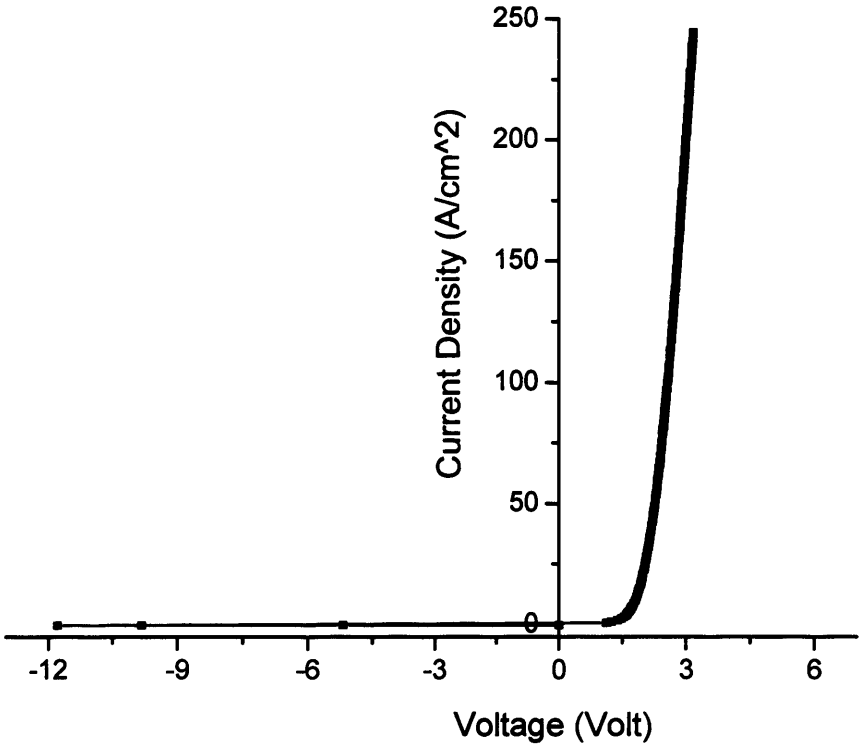

Figure 2.2.4: Reverse and forward bias IV characteristic of CQD sample.

Apart from, the importance of forward bias IV characteristic measurements which indicates any electrical contact problem, -i.e Ohmic- instead of diode-like curve- caused during the device processing or the device mounting, it is important as well to know if there is any current leakage path for devices under reverse bias. If this is the case then the samples are unsuitable to be used for the Quantum-Confined Stark Effect (QCSE) measurements of chapter 4. All the columnar-QD tested samples had good rectifying properties with reverse current amplitude less than 0.3mA for voltage values up to -10 or -12 V. Photo-current measurements were obtained only for reverse bias values corresponding to a current less than 0.3 mA according to the I-V characteristic. For the standard QD sample this limit was reached for a value of -9 V.

2.2.3 Current-Light (I-L) characteristics

The apparatus in paragraph 2.2.2, with an addition of a photodiode, has also been set-up for measuring light characteristics of laser diodes. However, because of the dual-polarisation nature of light emission from the extremely high aspect ratio columnar-QD (studied in chapter 4) the use of a polariser is required and this is not possible with the experimental set-up shown in figure 2.2.3. Also, with the experimental set-up which is described in the following text the near field emission and the light spectrum can be recorded by any data readings taken during the experiment. The experimental set-up was initially designed by Dr. Craig Walker and since then it has undergone improvements of the optics, electronics, the computer's matlab code and the translation stage which is specially designed by Deepal Naidu for a precise device alignment allowing six independent degrees of freedom. The sample is housed within a cryostat allowing measurements to be taken down to 200K. The cryostat is mounted on the translation stage and the light emitted by the sample is coupled into the slits of a spectrometer through a micro-lenses array which collimates and focuses the light. Before light reaches the spectrometer's input slit a polariser is used to select between the two orthogonal polarisations, TE or TM. From the spectrometer's output slit the light is collected by a Xenics XEVA-126 camera consisting a 2-D 256x320 InGaAs array of pixels which allow the near field and light spectrum to be recorded simultaneously, as shown in figure 2.2.5.

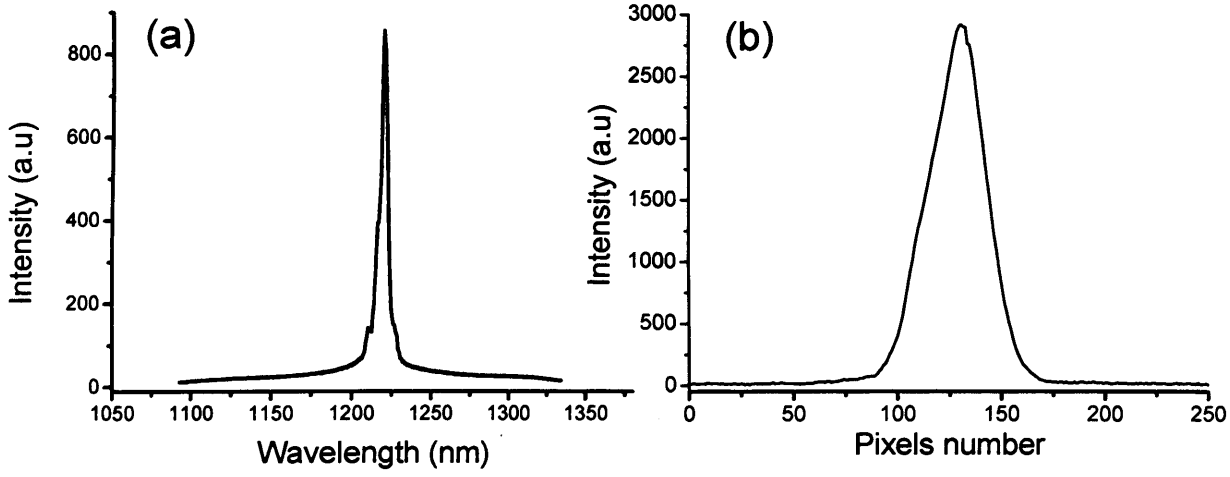

Figure 2.2.5: (a) Light spectrum and (b) near field emission -along the x-axis- from a lasing InAs/GaAs QD device (see diagram 1.6.1 in page 21, where the xyz-axes are defined).

The threshold current density is obtained from measurements of light output versus current (LI) (figure 2.2.6(a)). Figure 2.2.6(b) demonstrates a light spectrum at threshold; at the point where the spontaneous emission is clamped (definition as appears in ref. [Coldren 1995]) and stimulated emission starts to take over rapidly, increasing when this point is passed. A light-current curve is reproduced in figure 2.2.6(a) where the point of threshold is determined by extrapolating the LI curve back to the zero light axes. However, the determination of threshold by monitoring the light spectrum when manually increasing the current pulse amplitude is also considered to be fairly accurate and agrees well (within an error of $\pm 1.5 A/cm^2$) with the value extrapolated from the LI curve. An example of the light spectrum at threshold, is illustrated in figure 2.2.6(b) and shows the point where an ultra-narrow emission peak appears within the broad spontaneous emission spectra, increasing further rapidly with even a small increase in current amplitude, corresponding to stimulated emission. The error in the estimation of threshold current density is considered to be approximately $\pm 1.5 A/cm^2$, including the accuracy in which the current amplitude and the length/width of the laser diode can be determined.

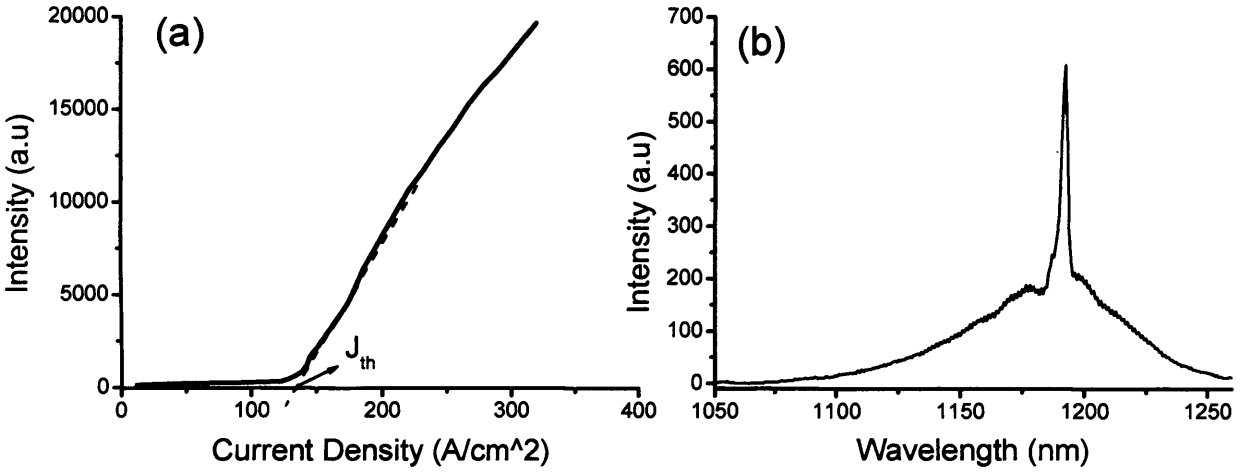

Figure 2.2.6: A graphical example of threshold current density estimation by either (a) plotting the LI curve or (b) retrieving the light spectrum at threshold for an InAs/GaAs quantum rod laser diode at 200K.

A second experimental set-up is used to measure the light intensity in mW (power), at room temperature. The device is mounted in a translation stage having 4 degrees of freedom; one rotational and other three in X, Y and Z-axes. The emitted light passes through a polariser

and is focused by a x40 micro-lens into the entrance of an integrated sphere calibrated to measure low-power emitting laser diodes. The light emission is converted in mW by using as a reference measurement the light emission when the device is set direct into the integrated sphere (i.e without using lens or polariser).

2.3 Edge photo-absorption spectroscopy

2.3.1 *Introduction*

In this section, photo-absorption spectroscopy is used to identify electronic transitions associated with the component materials of the studied semiconductor laser diodes. In general, edge photo-voltage or photo-current spectroscopy can be applied in any waveguide P-N hetero-junction laser diode where the photo-generated electron-hole pairs are separated by the junction field, inducing external photo-current amplitude. Thus, the experiment described in this section should have general applicability. By performing polarisation-selective edge photo-voltage spectroscopy, information about the magnitude and the type of strain -induced in the structure- can be extracted [Mogensen 1997a], which is not trivial to obtain with normal-incident photo-voltage spectroscopy, where the light incidents at the top of the device at the growth direction of the semiconductor. Then, follows an extended introduction on edge photo-voltage spectroscopy applied on compressive- and tensile-strained GaInP/AlGaInP QW materials, with a well known behaviour, so as to use them to verify a method which is suggested in chapter 3 in order to remove any polarisation-dependent feature of the experimental set-up from the actual measurements. Then this method is used in chapter 4, where the polarisation properties of an InAs/GaAs standard QD and for a set of columnar-QD materials –grown by a new approach- are studied.

2.3.2 *Experimental set-up*

The experimental set-up outlined in figure 2.3.1 is implemented for both Edge Photo-Voltage Spectroscopy (E-PVS) and Edge Photo-Current Spectroscopy (E-PCS) depending on the impedance of external circuit set-up. The apparatus was pre-existing and it was constructed by Paul Mogensen [Mogensen 1997b]; however, a few changes in the computer code improved significantly the Signal to Noise Ratio (SNR) enabling data to be taken for cases where the signal is extremely low. Also changes of the monochromator set-up, which are mentioned in appendix A, allow using the experiment efficiently for measurements in a wide range of wavelengths.

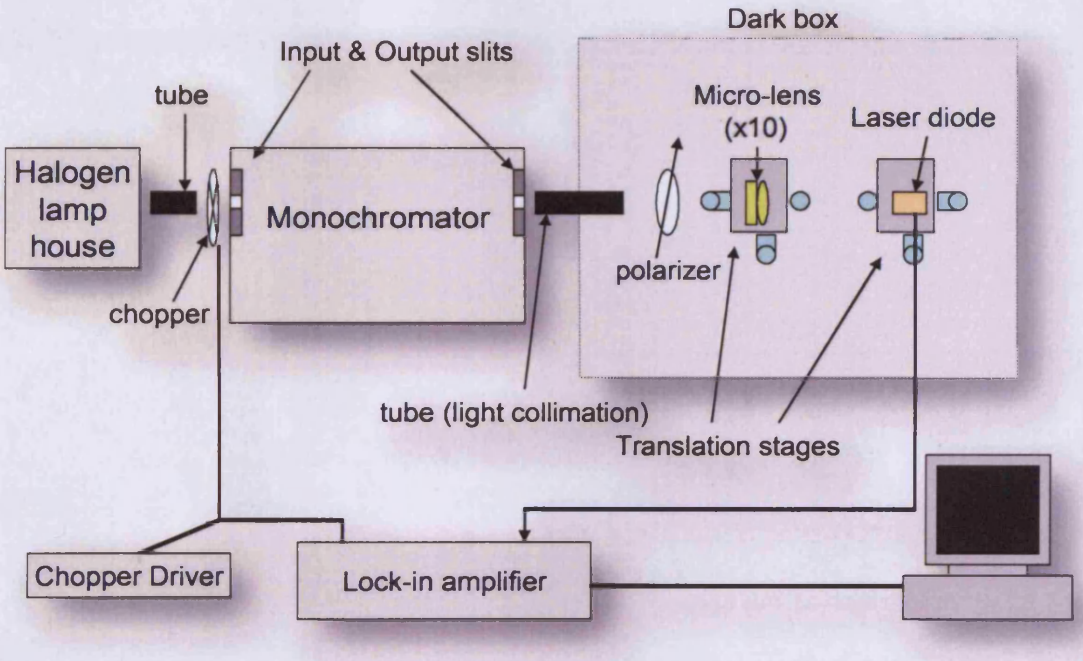

Figure 2.3.1: Experimental set-up for photo- absorption measurements.

The light source of configuration in figure 2.3.1 configuration is a 150Watt Halogen lamp operating at 24 V. The characteristic emission of the Halogen lamp contains all the wavelengths of light spectrum from visible to near-infrared (higher than 10% of the peak irradiance value for a wavelength range of 400nm to 2450nm) with peak irradiance at 880nm.

The lamp is followed by an optical chopper which modulates the light at a tunable and controllable frequency being 139Hz for all the measurements described here. The chopper is connected with a lock-in amplifier (phase-sensitive detector) and the frequency of the optical chopper is used as a reference in the detection of the photo-generated signal.

A monochromator and a polariser, following the chopper, are used to select light of specific wavelength and polarisation respectively. An array of two optical lenses collimates the output monochromatic light before reaching the polariser. The polariser is used to select either Transverse Electric (TE) or Transverse Magnetic (TM) for light polarised parallel or perpendicular to the growth plane of the semiconductor respectively. The polarised light rays reach the edge of the photodiode sample, after being focused by a x10 micro-lens, and get wave-guided inside the sample. Both the lens and sample are mounted on two Cartesian xyz-translation stages with the one holding the sample, to have three additional rotational degrees of freedom through all three axes allowing the waveguide device to align directly with the incident light. In the above experimental configuration the light is guided through closed tubes connecting all the parts of the apparatus, and the illumination of the sample takes place inside a dark box so as the whole system to stay unperturbed of any ambient light. A computer controlled stepper motor rotates the angle of the monochromator grating to select the output wavelength. The computer is also connected with the lock-in amplifier so as to record the signal data output by using a suitable computer program.

The output signal of the lock-in amplifier (LIA) is either the measured value of the voltage drop across the photodiode (sample) -applying E-PVS- by assuming that the external circuit impedance is high enough to ensure that the junction is operating under open-circuit conditions ($I_{tot} \approx 0$-see section 1.4.2), or is related to the amplitude of current flows external to the photodiode under short-circuit conditions ($V \approx 0$), therefore E-PCS is applied. A schematic representation of both set-ups is shown in figure 2.3.2. For photo-voltage measurements the signal is detected from measurement of voltage drop across the diode (sample) by connecting the sample with the high-impedance input of LIA. The LIA has also a built-in amplifier, which effectively has zero input impedance and hence by connecting the sample with this input no voltage is generated across the device as a result of the photo-current. Therefore, the

latter LIA output is used for photo-current measurements, where in this case a field across the diode can be applied externally in order to obtain field-dependent photo-current measurements.

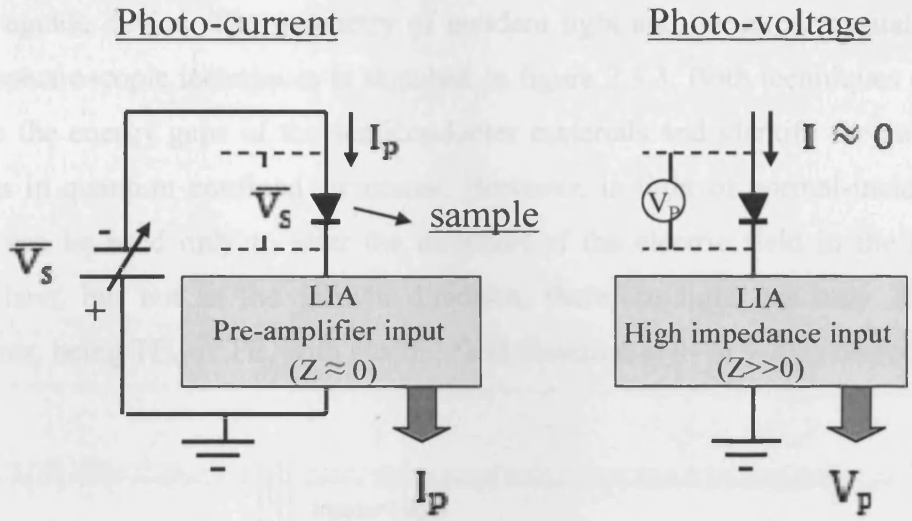

Figure 2.3.2: Circuit diagrams illustrating the set-up under which the photo-induced signal is corresponding to photo-current or photo-voltage. In the case of photo-current circuit set up an adjustable field $\overline{V_S}$ can be applied across the laser diode.

For low-temperature photo-current measurements described in chapter 3 the above apparatus is adjusted. The sample is housed within a cryostat which allows measurements to be taken down to 120K. For this reason a different translation stage used to hold the cryostat – designed and kindly provided to me by Stella Elliot- having the same degrees of freedom with those of the stage used in room temperature experimental set-up. Instead of using the dark box the whole apparatus is placed within a dark room to ensure isolation from any light signal interference.

2.3.3 *Edge and normal-incident spectroscopy*

PVS in semiconductor devices can be obtained by light of normal incidence [Blood 1985] or by light incident on the edge (E-PVS) [Mogensen 1997a] [Smowton 1996] [Liang 2002] of a laser waveguide device. The geometry of incident light and the experimental configuration for both spectroscopic techniques is sketched in figure 2.3.3. Both techniques can be used to determine the energy gaps of the semiconductor materials and identify the sub-band energy transitions in quantum confined structures. However, in light of normal-incidence PVS the polariser can be used only to alter the direction of the electric field in the semiconductor growth plane, but not in the growth direction, therefore light has only TE polarisation components, being TE_x or TE_y with electric field direction at x- or y-axis respectively.

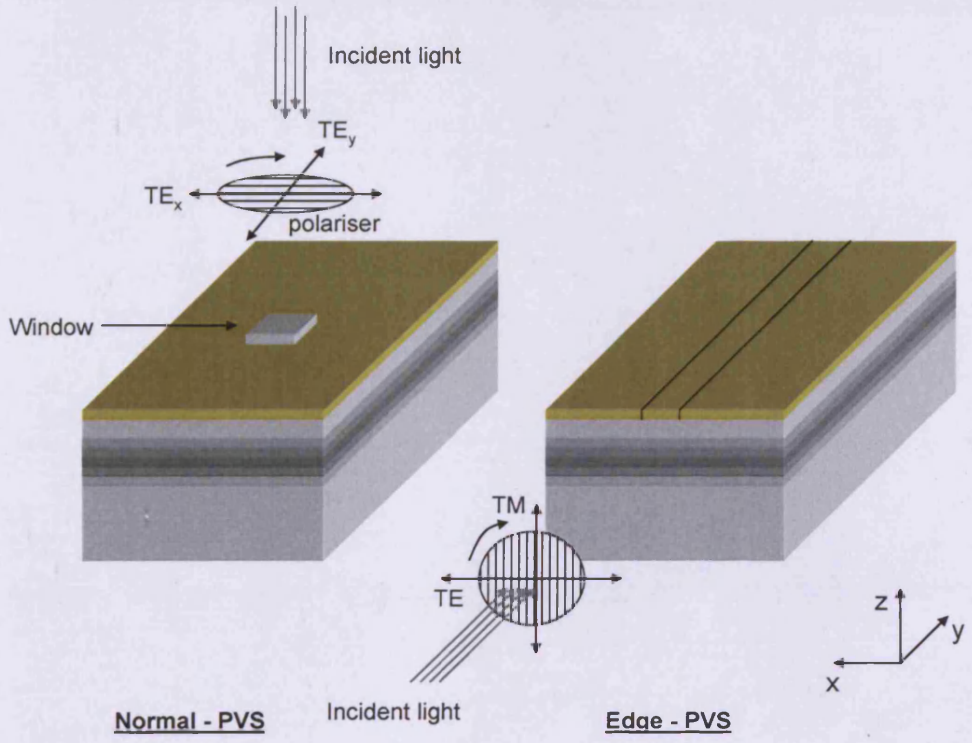

Figure 2.3.3 Configuration for edge- and normal- light incident PVS showing possible orientations of light electric field for both techniques. The active region is the dark sketched area of a typical waveguide laser diode, with the dark colour scale to show the refractive contrast between the different layers. The darker in the middle has the higher refractive index to support light wave-guiding.

In E-PVS by altering the polariser angle both TE and TM polarisations are obtained. Therefore, the advantage of E-PVS compared to normal- incidence PVS is that the first can be used to distinguish heavy-hole (hh) from light-hole (lh) type energy transitions [Smowton 1996] due to selection rules associated with the coupling of different light polarisation to these transitions in a QW material (see section 1.6). Light polarised in the growth plane of a semiconductor (TE-polarisation) interacts both with lh and hh transitions having though stronger interaction in the latter case. TM polarised light can only interact with lh transitions.

2.3.4 *Measurements on compressive and tensile strained InGaP Quantum Well systems*

The electronic and optical properties in two different types of strained GaInP QW structures operating at 633 nm have been thoroughly analysed by Smowton *et al.* [Smowton 1996]. The material structure of the investigated laser diodes is shown in figure 2.3.4. By altering the *In* composition of the $Ga_xIn_{1-x}P$ layer it is possible to control the lattice constant of the QW material. Thus, the lattice constant can be smaller or larger than that of the surrounding material $(Al_{0.6}Ga_{0.4})_{0.5}In_{0.5}P$ inducing tensile or compressive strain in the QW layer respectively. However, by both varying the *In* composition and the width of the QW layer the energy sub-bands in the QW are tailored properly to design different type of strained GaInP QW emitting at similar wavelengths [Smowton 1996]. Following an early discussion (section 1.7) the lh–hh energy sub-bands position and ordering depends upon strain. Therefore, a difference in the optical properties of these laser diodes is also expected. Polarisation-selective E-PVS is a suitable technique for investigation of such properties.

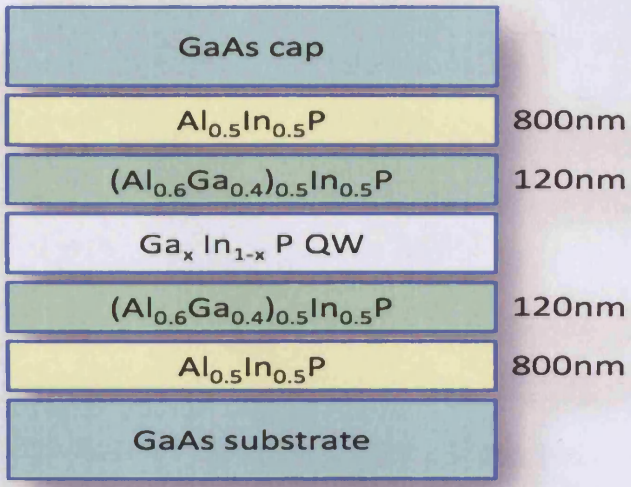

Figure 2.3.4 Material structure of InGaP QW where the degree and the type of strain (compressive or tensile) is determined by the well *In* composition.

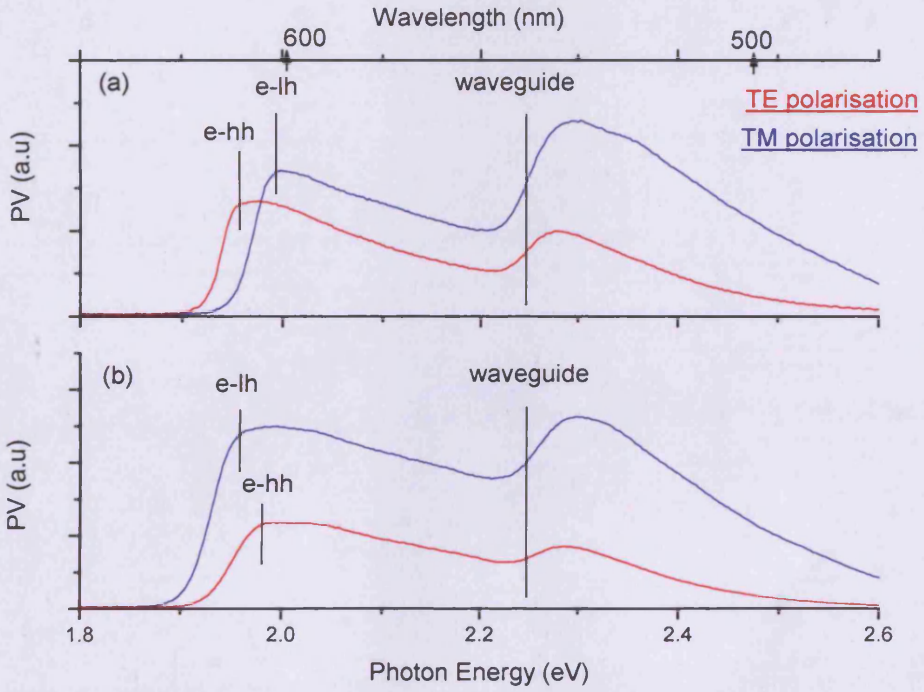

Figure 2.3.5 TE and TM polarisation edge photo-voltage spectra for (a) compressive and (b) tensile strained GaInP QW laser structure.

The measured photo-voltage spectra for TE and TM light, obtained by rotating the polariser, are shown in figure 2.3.5. At the sub-band edge of a QW TM polarised light only interacts with the lh-subband, whereas the TE polarised light interacts with both lh and hh sub-bands. So, in the case of the compressive strained InGaP QW sample (figure 2.3.5(a)) the lowest energy absorption feature of the TE spectrum is associated with the electron-hh (e^--hh^+) transition and the lowest energy TM absorption edge with e^--lh^+ transition. The latter also makes a small contribution to the TE response. In figure 2.3.5(b) the lh- and hh- sub-bands of the tensile strain QW are indicated with different order than that of figure 2.3.5(a). The lowest absorption feature is associated with e^--lh^+ transition because it appears for TM polarised light. The absorption feature at higher energy (2.25 eV) for both samples occurs at the same energy for both TE and TM polarisation and this is associated with the bulk waveguide core material where the light- and heavy-hole valence bands are degenerate.

However, the magnitude of the interaction of light with bulk material does not depend upon the polarisation and the difference in the TE and TM response from the waveguide core is a consequence of the experimental arrangement due to polarisation dependence of the output to the monochromator. It follows that the relative TE and TM photo-voltage response of the QW is not a direct measure of the relative strength of the interaction of lh and hh transitions with polarised light. In the next chapter, a method to calibrate the relative polarisation response is described and verified by application to these compressive and tensile strained GaInP QWs, where the polarisation response is well known. Then in order to identify the not well known fundamental interaction of light with electronic states of varied aspect ratio and *In* composition InAs/GaAs quantum dots, described by the transition matrix element, the particular method is applied.

2.3.5 *Photo-current, photo-voltage and photon flux linearity*

In this paragraph, both edge photo-current & photo-voltage measurements are taken at the same time to show proportionality between the two spectra. Therefore, the suggested technique which is explained in detail in chapter 3 can be applied to either photo-current or photo-voltage measurements.

The induced photo-current signal amplitude is proportional to the incident light irradiance (photon flux) (see eq. 1.4.7-page 16) and is related to the photo-voltage signal via the exponential term qV_{OC}/kT as appears in equation 1.4.6, $I_P = I_0(e^{\frac{qV_{OC}}{kT}} - 1)$, in where the short-circuit photo-current amplitude I_P is associated to the open-circuit photo-voltage amplitude V_{OC}. However, for low photo-voltage amplitudes [Blood 1985] where $qV_{OC} \ll KT$, the current-voltage relation is taken to be linear which in turn determines a linear relation between the photo-voltage amplitude and photon flux.

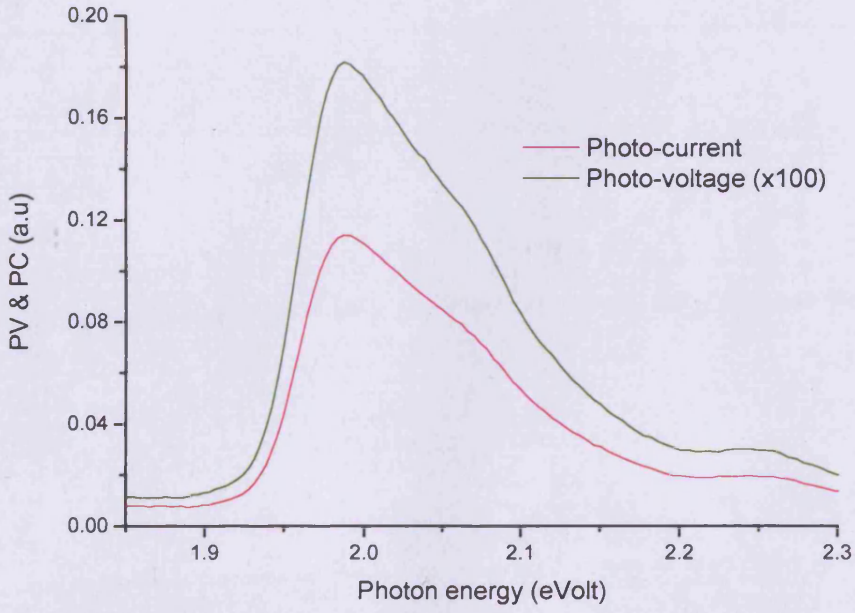

Figure 2.3.6 Photo-current (purple line) and photo-voltage (deep green) spectra of compressively strained GaInP QW.

To indentify the relation between the two photo-induced quantities together E-PVS and E-PCS are applied for the compressive strained GaInP QW and the results are shown in figure 2.3.6, where for clarity the two spectra are normalized in similar signal amplitude. The ratio of the two photo-induced spectra is displayed in figure 2.3.7, where it is found to have a constant value of 65, being deviated from this value by 5.6% for the whole photon energy range. This small deviation is considered to be in the level of noise of the obtained data.

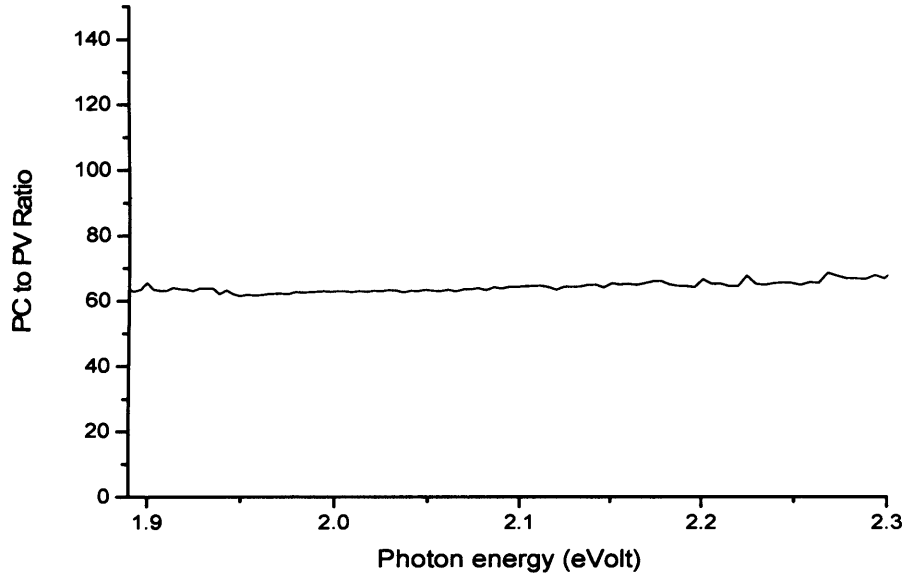

Figure 2.3.7 Ratio of photo-current to photo-voltage spectra.

2.4 Summary

In this chapter, I have described in detail the experimental methods together with improvements and alterations undergone in order to use them for characterisation of the InAs/GaAs columnar-QD materials.

I began in section 2.2 by describing the two different types of laser structures used in this thesis; an oxide-isolated 50μm wide contact stripe device of either a compressive or tensile strained GaInP QW material and a RW-geometry laser diode of InAs/GaAs columnar-QD material. I have described the experimental set-up used to test the samples, before using them

in any other experiment, by obtaining a full range of reverse and forward bias I-V characteristics. Then, I introduced the experimental procedure in which the near field emission, the light spectrum, and the threshold current density are obtained in order to identify the emission properties of extremely high aspect ratio columnar-QD device with respect to temperature. Room temperature threshold current measurements where the light output measured in mW are also obtained by an experimental set-up assembled by myself. All the above experiments are performed in pulsed mode and at a low duty cycle.

In section 2.3 I described in detail the apparatus used to perform edge photo-absorption spectroscopy. The advantage of polarisation-selective edge light incidence photo-absorption spectroscopy over that of normal light incidence was analysed. Then, I described how information about the different type of e-h transitions is obtained, by applying E-PVS in two compressive and tensile strained GaInP QW structures, in order to identify the type of strain induced in these structures. Next, I analysed briefly the polarisation-dependent response of the experimental set-up which affects the polarisation-selective photo-absorption measurements.

Chapter 3-Polarisation properties and characteristics of Quantum Dots

3.1 Introduction

In this chapter a new method is suggested to directly measure the polarisation dependence of the light-matter interaction using edge photo-absorption spectroscopy by correcting for polarisation-dependent features of the experimental system.

I begin, in the first section, 3.2, by illustrating the polarisation-dependent response of the edge photo-absorption spectroscopy experimental set-up by introducing a new experimental configuration. I then describe a technique which calibrates the relative polarisation response in order to obtain the ratio of the fundamental TE/TM optical response of a quantum-confined system from the measurement of the polarisation dependence of the edge photo-absorption spectrum. This is followed by a validation of the method described here by application to compressive and tensile strained InGaP QW structures in order then to apply it to a set of columnar-QD materials, of varied aspect ratio and *In* composition, with aim to study the effect that dot shape and *In* composition have on the polarisation properties.

In section 3.3, I use the method of section 3.2 to derive the relative TE over TM optical response of an InAs/GaAs QD DWELL material. At the end of this section temperature and field-dependent photo-current spectroscopic measurements are performed for the standard QD, which is used as a reference sample to study the CQSE of columnar-QD materials in chapter 4. Then, I discuss the escape mechanisms under which the photo-generated carriers contribute to the overall electrical signal and useful conclusions about the nature of the photo-current signal are drawn.

3.2 Polarisation response of quantum-confined structures

3.2.1 *Edge Photo-Voltage Spectroscopy: Polarisation-dependent system response*

The polarisation dependent system response of edge photo-absorption set-up is illustrated further, with respect to paragraph 2.3.4 of chapter 2, by introducing a new experimental configuration in figure 3.2.1 where the orientation of the device-polariser relative to the monochromator's output slit is changed by 90^0.

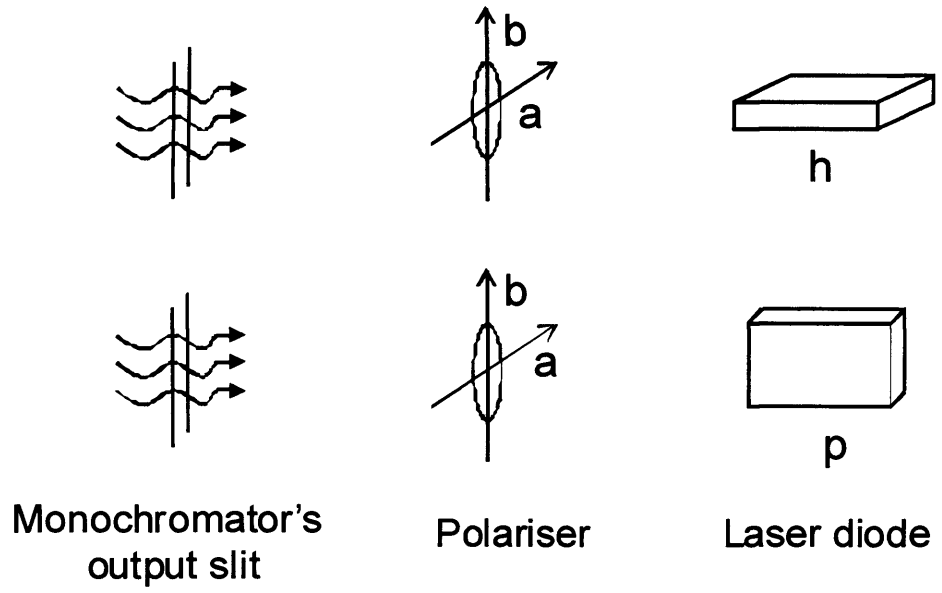

Polariser: a or b

Sample: h or p

Polarisation	*I*	*II*
TE	*a+h*	*b+p*
TM	*b+h*	*a+p*

Figure 3.2.1 Schematic diagram of the experimental system illustrating relative orthogonal orientations of the slit of the monochromator, the electric field vector of light transmitted by the polarizer (*a* and *b*) and the plane of the waveguide and QW of the device (*h* and *p*). The relative position of the device (*p*:perpendicular and *h*:horizontal) and polariser position (*a* and *b*) determines the TE or TM polarisation.

Light emerges from the vertical slit of the monochromator onto the polariser which may be oriented such that the electric field vector is horizontal or vertical relative to the slit (denoted by *a* and *b* respectively). The sample is effectively a 50 μm wide waveguide which collects light from a width of about 0.5 mm and it may be oriented with the plane of the waveguide and well in a horizontal or perpendicular vertical alignment relative to the slits (denoted by *h* and *p* respectively). The interaction of light with the well system is defined by the polarisation relative to the plane of the QW, and the TE and TM configurations for horizontal and perpendicular sample orientations are shown in figure 3.2.1. The TM polarisation measurements according to figure 3.2.1 were obtained by setting the polariser at position ***b*** or ***a*** for a horizontal or perpendicular device orientation. In a similar way the TE polarisation measurements were taken by setting the polariser at position ***a*** when the device is horizontal or by rotating both the device and polariser by 90^0 (polariser position ***b*** – device orientation perpendicular).

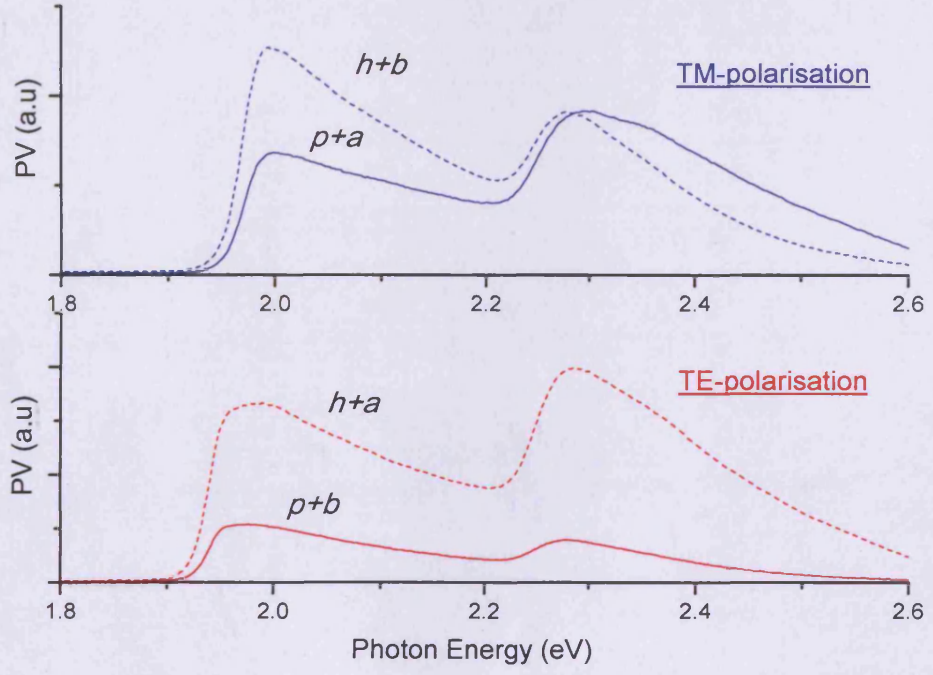

Figure 3.2.2 TE (red-colour) and TM (blue-colour) polarisation edge photo-voltage spectra of the compressive strain GaInP QW obtained with different orientations of the sample and the polariser relative to the monochromator. The dashed line refers to horizontal device position and the solid line to perpendicular.

The spectra of figure 3.2.2 which are obtained by taking all four possible combinations of polariser and sample orientation with respect to monochromator-light source show that the photo-voltage signal response is different for spectra corresponding to the same TE or TM polarisation but different sample orientation (h&p). As was mentioned above this is an artefact of the experiment resulting from two contributions to the overall polarisation behavior of the system. When the polariser is rotated, the spectrum of light incident on the sample edge changes due to the partial polarisation of light by the grating of the monochromator. In the case of sample rotation, keeping the polariser in a fixed angle, the coupling of light into the waveguide is changed by the geometrical orientation of the narrow monochromator slit and the flat waveguide. Both of these effects are eliminated by taking measurements for all four combinations of polariser and sample orientation. In paragraph 3.2.3 a new method is described for characterising the interaction of light with the electronic structure of the quantum-confined system itself by removing any of these experimental artifacts.

3.2.2 Calibration technique

Considering the proportionality of the photo-voltage amplitude to the incident photon flux (section 2.3.5) an equation for the obtained signal is derived by adding a few terms which contribute to the overall photo-voltage signal. These terms are defined as follows:

The factor $S(\lambda, \alpha \; or \; \beta)$ represents the dependence of the photon flux, incident on the sample, on the orientation of the polariser relative to the slits and incorporates the spectral output of the lamp and the monochromator system; therefore it is wavelength dependent. The terms α and β refers to the position of the polariser as is shown in figure 3.2.1. The next factor $C(p \; or \; h)$ represents the geometrical coupling of light into the QW and waveguide and depends on the orientation of the sample with relation to slits. This may be weakly dependent on wavelength, but wavelength dependence of the ratio of this factor for the two different device orientations does not affect the outcome of the analysis below. The rate of the photo-generation of carriers is expressed by the term $G(TE \; or \; TM)$ and depends on the relative

orientation of the electric field vector and the sample. This quantity is fundamental and therefore important as in the analysis below it is considered to be proportional to the transition matrix element (M_T), which denotes how strongly the light interacts with matter. Subsequently, an effort to explore the term $G(TE\ or\ TM)$ or the ratio of the two generation rates $G(TE)$ and $G(TM)$ allows finding the true response of the semiconductor device for the whole photon energy range. In addition, a fraction of light incident on the semiconductor is not waveguided inside the device because it is reflected and this is denoted by a reflectance factor $r(\lambda)$, which is assumed to be in some extent polarisation-independent. Thus, a term $1 - r(\lambda)$ should be added in the equation defining the photo-voltage amplitude and represents the light that is transmitted inside the waveguide.

Considering all these contributed factors the E-PVS spectra obtained for all possible orthogonal combinations of the position of the device and the polariser can be represented by a set of four equations

$$\begin{cases} \text{polariser rotation} \begin{cases} V_h(\lambda, TE) \simeq \big(1 - r(\lambda)\big)C(h)S(\lambda,\alpha)G(TE)I_{IN}(\lambda) & \textbf{(a)} \\ \text{sample rotation} \begin{cases} V_h(\lambda, TM) \simeq \big(1 - r(\lambda)\big)C(h)S(\lambda,\beta)G(TM)I_{IN}(\lambda) & \textbf{(b)} \\ \text{polariser rotation} \begin{cases} V_p(\lambda, TM) \simeq \big(1 - r(\lambda)\big)C(p)S(\lambda,\alpha)G(TM)I_{IN}(\lambda) & \textbf{(c)} \\ V_p(\lambda, TE) \simeq \big(1 - r(\lambda)\big)C(p)S(\lambda,\beta)G(TE)I_{IN}(\lambda) & \textbf{(d)} \end{cases} \end{cases} \end{cases}$$

Equation 3.2.2

where the indices p and h refer to the device position relative to the slits and I_{IN} represents the magnitude of the incident photon flux on the polariser. From these equations the ratios of the polarisation sensitivity factors $S(\alpha)/S(\beta)$ and geometry factors $C(p)/C(h)$ at a given wavelength are given by

$$\frac{S(\alpha)}{S(\beta)} = \left(\frac{V_p(TM)}{V_h(TM)}\ x\ \frac{V_h(TE)}{V_p(TE)}\right)^{1/2}$$

Equation 3.2.3

and

$$\frac{C(p)}{C(h)} = \left(\frac{V_p(TE)}{V_h(TE)} \, x \, \frac{V_p(TM)}{V_h(TM)}\right)^{1/2}.$$

Equation 3.2.4

By dividing equations 3.2.2(a) and (b), the relationship between the TE and TM E-PVS signals for the same sample orientation is

$$V_h(TE) = \frac{G(TE)}{G(TM)} \, x \, \frac{S(\alpha)}{S(\beta)} \, x \, V_h(TM).$$

Equation 3.2.5

The ratio $S(\alpha)/S(\beta)$ is known from eq. 3.2.3, so the ratio of the generation rates for TE and TM polarised light is derived from the measured photo-voltage signals using eq. 3.2.5. It is also valuable to plot the TE and TM photo-voltage signals on the same relative scale. Thus, the quantities

$$V_{h,cal}(TM) = \frac{S(\alpha)}{S(\beta)} \, x \, V_h(TM) \qquad (\boldsymbol{a})$$

&

$$V_{h,cal}(TE) = \frac{S(\beta)}{S(\alpha)} \, x \, V_h(TE) \qquad (\boldsymbol{b})$$

Equation 3.2.6

of eq. 3.2.6 (a) and (b), derived from eq. 3.2.5, represent the measured signal $V_{h,cal}(TM)$ (or $V_{h,cal}(TE)$) calibrated to the same spectral output of the source as the V_h(TE) (or $V_h(TM)$) signal. The generation rate ratio $G(TE)/G(TM)$ can then be derived from eq. 3.2.5 and 3.2.6(a) as follows

$$\frac{G(TE)}{G(TM)} = \frac{V_h(TE)}{V_{h,cal}(TM)}.$$

Equation 3.2.7

Having already connected the generation rate to the matrix element it is possible through eq. 3.2.7 to determine the relative response of the semiconductor device to different light

polarisations -TE and TM- by determining the ratio of the matrix elements $M_T(TE)/M_T(TM)$. These ratios are known ratios for bulk and QW materials (see chapter 1.6) and should be verified using this new experimental approach.

3.2.3 *Application to InGaP Quantum Well structures*

	Bulk		Quantum-Well	
polarization	C-HH	C-LH	C-HH	C-LH
TE	1/3	1/3	1/2	1/6
TM	1/3	1/3	0	2/3

Table 3.2.1 Magnitude of transition matrix element $|M_T|^2/|M|^2$ for different transitions and polarizations in bulk and quantum well (QW) structures . The values for the QW are only valid at the band-edge energy of the transitions and for small values of k-vector, due to band-mixing effects (table taken from [Coldren 1995]).

To test the validity of the methodology set out above, measurements on the tensile and compressive strained GaInP quantum well laser structures are carried out knowing that the lowest conduction band (cb)- valence band (vb) transitions are of different type for these two samples, being lh- and hh- type for the compressive- and tensile- strained structure respectively. It is expected the calibrated relative response –given by the ratio $G(TE)/G(TM)$ of eq.3.2.7- in each case to be determined by the ratio of the transition strengths underlined by the value numbers of table 3.2.1 (described earlier in figure 1.6.1).

Figure 3.2.5(a) (or (b)) shows the TE (or TM) photo-voltage spectra together with the calibrated TM (or TE), using eq. 3.2.6(a) (or (b)), to the same spectral response as that of the TE (or TM) spectra. Note that the individual spectra in figure 3.2.5 do not represent either the

true absorption spectra or the generation rate spectra because the signal magnitudes contain the variation in the spectral output of the system, $S(\lambda, \alpha \text{ or } \beta)$ and the photon flux, however their relative magnitudes have been corrected by eq. 3.2.6 such as their ratio at each wavelength should represent the ratio of the generation rates. For both samples the E-PVS signal in the vicinity of 2.3 eV corresponding to bulk waveguide material is the same for TE and TM polarisation, in agreement with the values of table 3.2.1. At the absorption edge of the quantum well the ordering of the TE and TM signals is reversed for the compressive and tensile strained samples as expected.

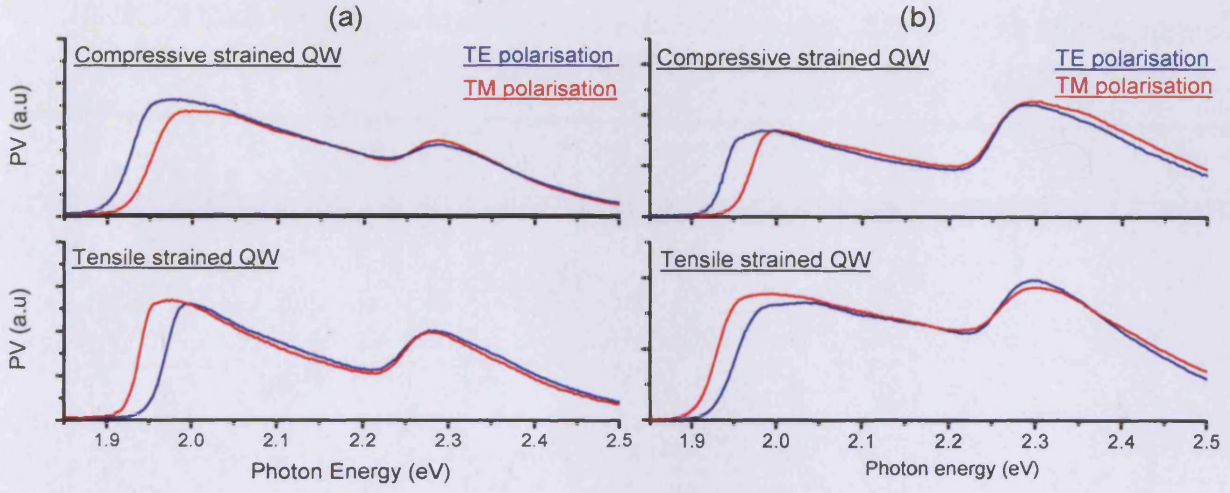

Figure 3.2.5 Photo-voltage absorption spectra for the compressive and tensile strained QW samples for a horizontal sample orientation, where in (a) the TM polarisation spectra are calibrated with respect to TE and in (b) the TE spectra are calibrated with respect to TM.

The ratio of the TE over TM_{cal} spectra is the generation rate ratio $G(TE)/G(TM)$, given by eq. 3.2.7 and plotted in figure 3.2.6. A TM signal originates only from the e^--lh^+ transition, and since for the compressive sample -figure 3.2.5(a)- the signal at lowest energy is obtained for TE polarisation this corresponds to the conduction band-heavy hole (cb-hh^+) transition (table 3.2.1) and the generation rate ratio is large, of the order of ten. Theoretically the table indicates that this ratio should be infinite, but due to the resolution of the monochromator and the fact that the light is focused onto the edge of the sample and not precisely normal to it, therefore there is a measured response at the cb-hh^+ transition with light of nominal TM polarisation, so this signal is not "zero". In the case of the tensile strained structure, figure

3.2.5(b) shows the lowest transition to be for TM polarisation and this is uniquely associated with the cb-lh$^+$ transition. The TE/TM ratio for the tensile strained QW in figure 3.2.6 has a minimum value of 0.24, which is close to the ratio of 0.25 predicted for the cb-lh$^+$ transition in table 3.2.1. At photon energies above both sub-band edges the signal is due to both cb-lh$^+$ and cb-hh$^+$ transitions and table 3.2.1 shows that the sums of the TE and TM absorption strengths are equal giving a generation rate ratio of unity as shown in figure 3.2.6. The contrast in the generation rate ratios for compressive and tensile strained samples is in agreement with the predictions of table 3.2.1.

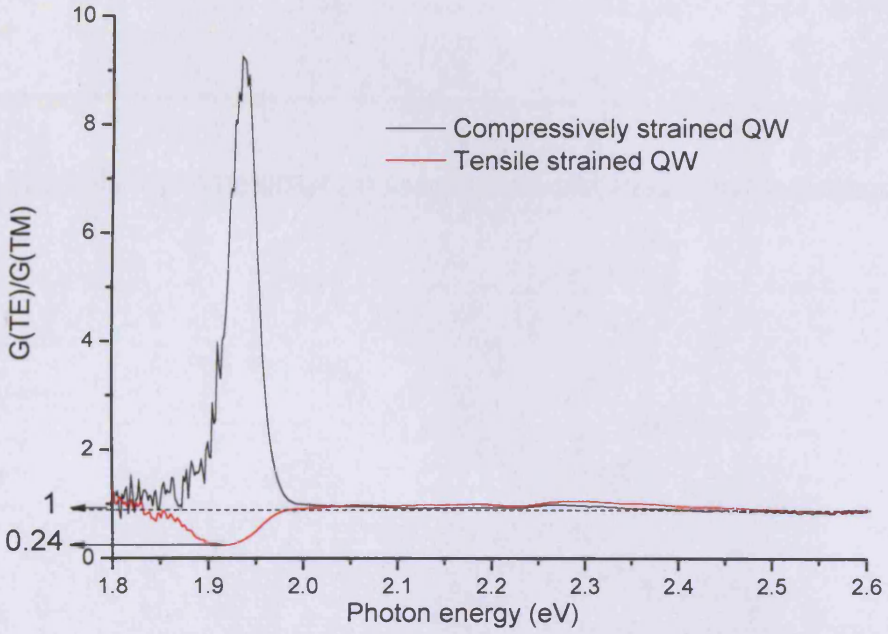

Figure 3.2.6 True TE/TM ratio for compressive (black line) and tensile (red line) strained InGaP QW.

Further confirmation of this new experimental approach is obtained by examining the behaviour of the geometry ratio $C(p)/C(h)$ and the system ratio $S(\alpha)/S(\beta)$ obtained from the experimental data using equations 3.2.4 and 3.2.3 respectively. These ratios are shown in figure 3.2.7. Plot (a) shows that the geometrical factor has a constant value of about 4. According to the definition of the geometrical coupling factor $C(p\ or\ h)$ the ratio $C(p)/C(h)$ should be independent of wavelength having a constant value. This value should be greater than one and this can be attributed to the vertical shaped aperture of the monochromator's slits where in the case of the perpendicular device orientation the area of the edge of the

device exposed to light is wider compared to that of horizontal device position. The system polarisation ratio $S(\alpha)/S(\beta)$ as expected does vary with wavelength and this is primarily due to the characteristics of the grating [Hutley 1982].

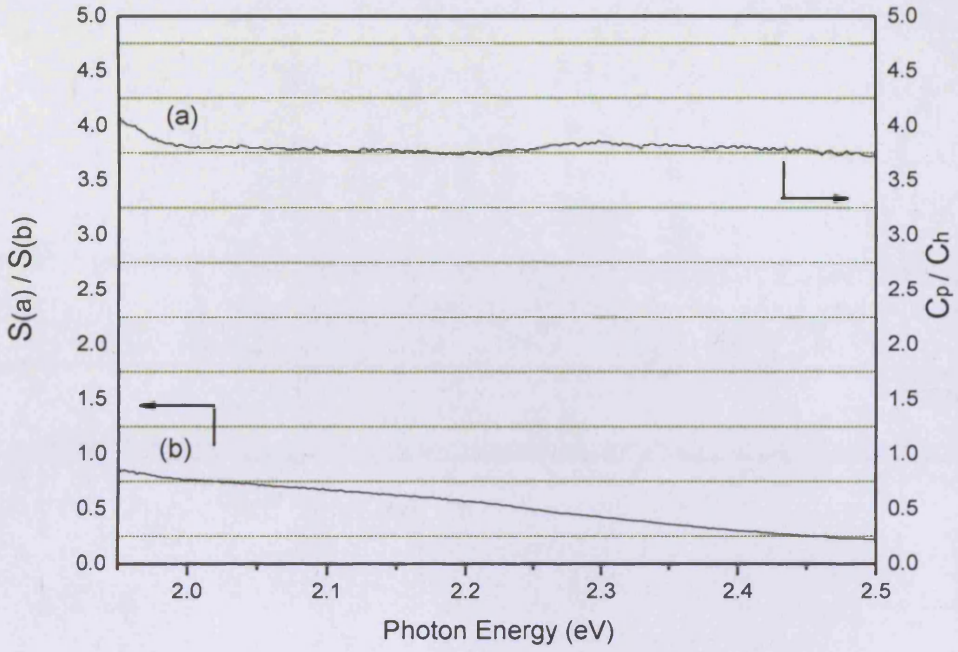

Figure 3.2.7 Plot of (a) geometry factor ratio and (b) polarization sensitivity ratio of the compressively strained GaInP QW.

3.2.4 *Discussion*

The TE/TM optical recombination rate ratio can be obtained using measurements of polarisation-resolved amplified spontaneous emission (ASE), photo- and electro-luminescence (PL and EL). By analysis of the ASE from the edge of a tensile-strained GaInP QW structure [Lewis 2002b] under electrical injection, a value of the TE/TM ratio at the band edge similar to that found here was obtained. In that case [Lewis 2002b] a particular methodology, requiring a specially prepared segmented contact sample, was used to convert the spontaneous emission rate measured in arbitrary units to the absolute values of the true spontaneous emission rate, without using a calibrated detector. More generally, the TE/TM ratio can be obtained if the relative response of the measurement system to different

polarisations is known. However, in this chapter a method to measure the more fundamental TE/TM optical generation rate ratio in a material close to equilibrium which is not modified by the presence of carriers and therefore directly reflects the transition matrix elements (which is not the case for the TE/TM optical recombination rate) is suggested. This method does not require a calibrated system and measures the optical response over a much wider wavelength range than can be obtained using the method of ref. [Lewis 2002b]. When this approach is applied to tensile and compressive strained QWs the fundamental TE/TM optical response derived experimentally shows an agreement with well known theoretical values of the ratio of the band-edge matrix elements. This method is of particular value for the study of QD and Quantum wire systems, where the strength of the interaction of TE and TM polarised light with QD energy transitions is difficult to predict.

An alternative method of the calibration technique proposed in paragraph 3.2.2 is by the use of an achromatic half-wave plate [optics.org 2006] which rotates the light polarisation by 90^0 for a wide range of light wavelength without changing the photon flux [Borri 2009]. The principle is the same as described in paragraph 3.2.2 however it has the advantage of keeping the device position fixed. This removes the geometrical coupling factor $C(p\ or\ h)$ from the measurements as described analytically in the technique of paragraph 3.2.2.

In the last section of this chapter the polarisation response of standard InAs/GaAs QD systems is identified by applying the above technique which is further used in chapter 4 to study the modified polarisation properties of the InAs/GaAs columnar-QD materials of higher aspect ratio compared to that of a standard aspect ratio QD.

3.3 Edge-Photo-Current Spectroscopy in quantum dot systems

3.3.1 *Polarisation response of InAs/GaAs Quantum Dot materials*

E-PCS measurements have been obtained for two different types of QD systems –grown separately by two research groups- with the aim of identifing their polarisation response using the method described in the previous section. The material structure of both QD systems is outlined in figure 3.3.1. The first structure (a) [Liu 2004a] consists of 5 layers of a DWELL QD layers and the other one (b) [Ridha 2007] is a standard 5-layer QD structure in which a 2nm InGaAs capping layer is deposited after the growth of each InAs QD layer. Although for both structures the InGaAs capping layer is of the same indium composition both the thickness of the InGaAs/GaAs layers and the GaAs spacer layer are different. In addition, the Al concentration and the thickness of the waveguide cladding material differ as well.

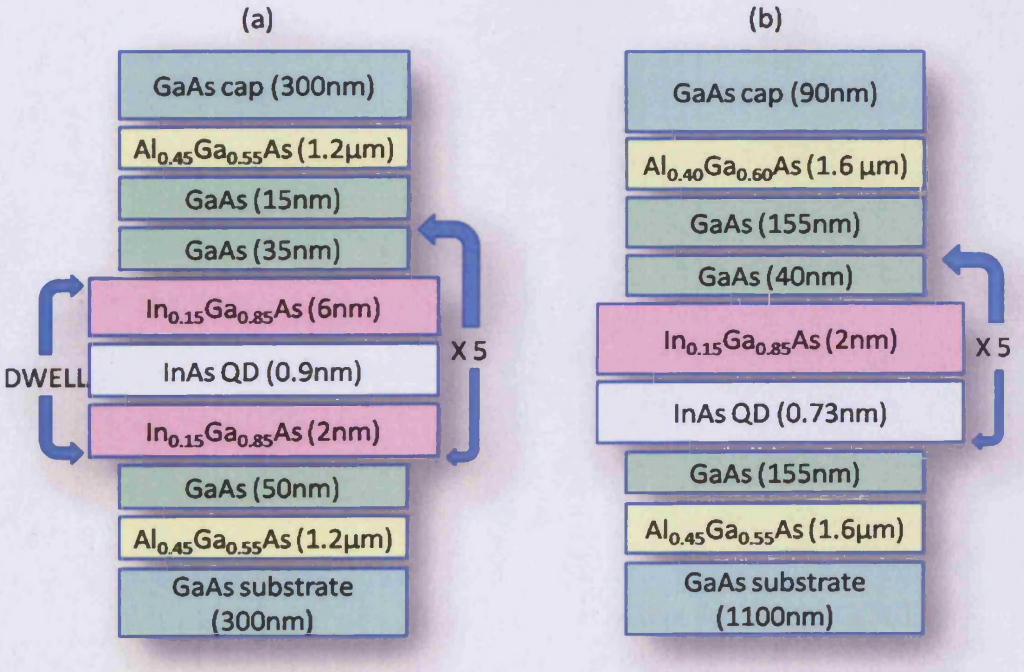

Figure 3.3.1 Material structure of a (a) 5-DWELL layers structure, where each DWELL is separated by a 35nm GaAs spacer and a (b) standard 5- QD layers structure, where each QD is separated by a 40nm GaAs spacer.

Before analysing and comparing the photo-current spectra of both samples it is worthy to mention the polarisation-dependent efficiency of the "long-wavelength range" grating (see appendix A) used for these measurements. Figure 3.3.2 shows polarised-selective E-PCS measurements for the DWELL laser diode. Apart from the two polarised spectra TE and TM, the figure shows the calibrated TM spectra with respect to TE (TM_{cal}) using the equation 3.2.6(a). For a photon energy around 1.24 eV there is a sudden drop in the signal amplitude which is more obvious in TE spectrum. This sharp signal valley is not associated with the response of the sample as is reproduced for the TM_{cal} spectrum. The polarisation-dependent nature of the efficiency drop associates this defect -occurring in particular photon energy- to a Wood's anomaly [Wood 1902] which is characteristic of the specific grating.

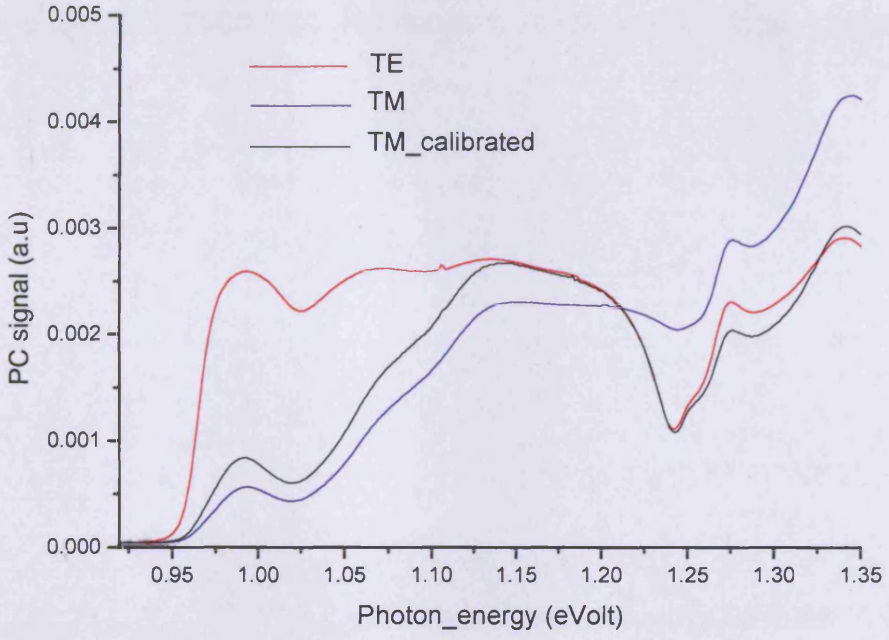

Figure 3.3.2 Polarisation-selective edge photo-current spectra of standard QD sample showing the Wood's anomaly at around 1.24eV.

Considering the low response of the grating for photon energies around the value 1.24 eV all the photo-current spectra are represented for photon energies less than 1.24 eV, which lies in the area of interest. Each orthogonal polarisation-selective spectrum for the rest of the thesis is calibrated according to the suggested method of the previous chapter and represented by the TE and TM_{cal} spectra or by the ratio of the carrier generation rates $G(TE)/G(TM)$ as defined in equation 3.2.7 (i.e the ratio TE/TM_{cal}). Thus, a direct polarisation response of each

studied structure is obtained excluding the polarisation-dependent response of the system within the measurements.

Following this concept in figure 3.3.3 the obtained $G(TE)/G(TM)$ ratio for both QD materials is presented. The ratio of the two polarisations has a maximum value close to the band-edge energy of the studied materials. Therefore, this peak is associated with the lowest QD e1-hh1 transition and further reduces for higher values of photon energy. There is also for both samples a second peak which can be associated with the first excited state e2-hh2 transition. The hh ground and first excited state energy difference is around 50meV and 45meV for the standard QD and DWELL QD sample respectively and depends on many parameters such as the width of the InAs and InGaAs capping layer. By variation of these parameters in ref. [Motyka 2006] an energy difference between the ground and the 1st excited state of 40 to 55 meV is reported.

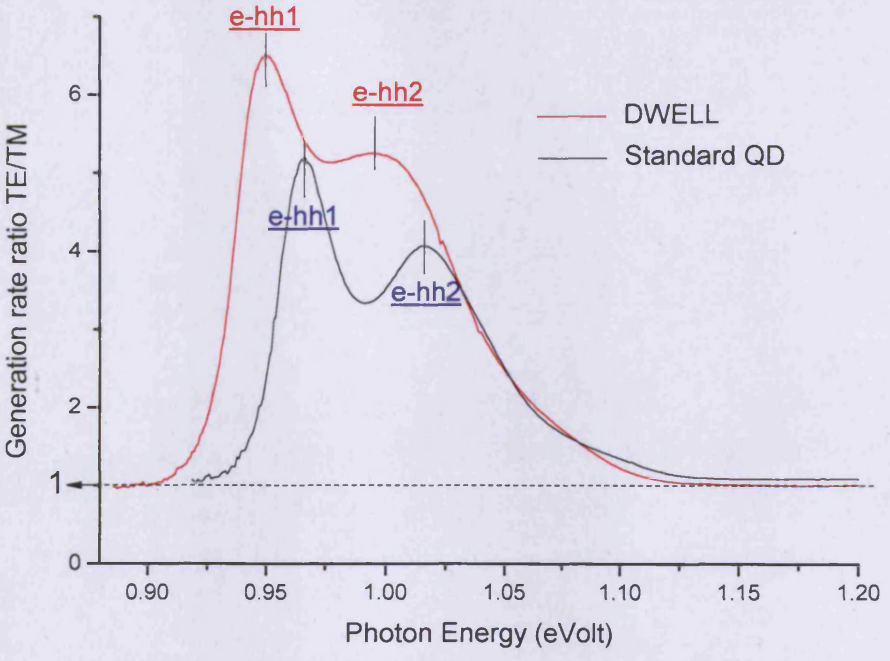

Figure 3.3.3 True TE over TM polarisation response of the DWELL and standard QD structure.

It follows that QD materials strongly absorb TE polarised light compared with TM and this is attributed to two main characteristics of QDs. The first is that these systems are

compressively strained due to large lattice constant of InAs QD material and the smaller lattice constant of the wetting layer material, being $In_{0.15}Ga_{0.85}As$ for the DWELL sample (figure 3.3.1(a)) and GaAs for the standard QD structure (figure 3.3.1(b)). A high degree of compressive strain in the active region moves the lh & hh energy states in the valence band further apart, where the hh- and lh- states move towards and away from the conduction band respectively [Coldren 1995]. TM polarised light interacts only with lh- sub-bands, therefore a shift of the lh- energy band away from the band-edge of the QD material reduces further the TM absorbed light. The lenticular [Mui 1995], conical [Marzin 1994] or squared based pyramidal with a truncated apex [Grundmann 1995] QD shape, having a greater base diameter compared to its height, is the second characteristic of the dot responsible for the low TM absorption. A typical dot size is of 20nm base and 4nm height with an aspect ratio of 0.2 [Sheng 2002]. Thus, the carriers are confined in a smaller area in the growth direction than in the plane normal to the growth direction, therefore the hole and electron interact stronger with light polarised to the growth plane, TE, rather than normal to it, TM, because of the strong quantisation in the growth direction relative to that in the growth plane. However, it is possible to engineer the shape of the dot by increasing its aspect ratio and to reduce the bi-axial strain distribution induced on the dot in order to enhance the coupling of TM polarised light with dot energy transitions. This is shown in the next chapter where the polarisation properties of different aspect ratio and *In* composition InAs/GaAs columnar-QD materials are studied.

3.3.2 *Photo-current signal origin*

There are two contributions of escape mechanisms of photo-generated carriers in QD systems resulting to the overall electrical signal in E-PCS, which are illustrated in the diagram of figure 3.3.4 for the simplest case of a QW-shaped confined potential. Photo-generated carriers can escape by tunneling which is a field-dependent mechanism and by thermal excitation which is temperature-dependent mechanism as described in ref. [Fry 2000a] by using normal-incident photo-current spectroscopy. In this section, by following the same concept, E-PCS with respect to temperature for a DWELL QD sample is applied, the thermal excitation mechanism is explained and useful conclusions for the nature of the photo-current

spectra are derived. Using the "short-wavelength range" grating (see appendix A) photo-current spectra are shown in figure 3.3.5 for a DWELL QD of the same type as that of figure 3.3.1(b). The difference between these two structures is in the growth temperature of the spacer layer [Liu 2004b].

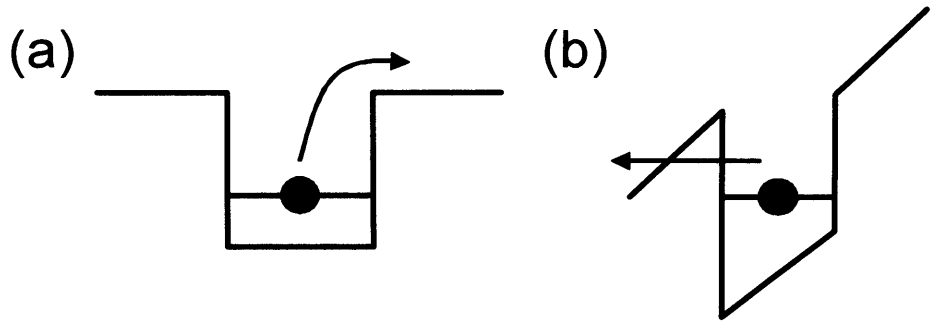

Figure 3.3.4 Diagram showing how carriers -in the simplest case of being confined in a well-shaped potential can escape into the barrier material by (a) thermal excitation or (b) tunnelling due to the presence of an external applied field.

Here, it should be mentioned that the spectra obtained in this and the next chapter contains the spectral output of the lamp and are not calibrated in amplitude by using a photo-detector of a known response. This however, does not affect the outcome of the analysis below, where the spectra are presented in order to indentify the different energy states without aiming to compare the signal amplitude between these states. In addition, for the studied wavelength range the spectral response of the lamp varies slowly with respect to wavelength (e.g manual-Bentham 200 Series) therefore this should not have an effect on the analysis of the next chapter where the relative change of the signal amplitude -with respect to applied reverse bias- for a single transition is presented. The maximum range of photon energy where the signal amplitude was measured is from 1.03 eV to 1.10 eV corresponding to a wavelength range where the response of the lamp is almost constant.

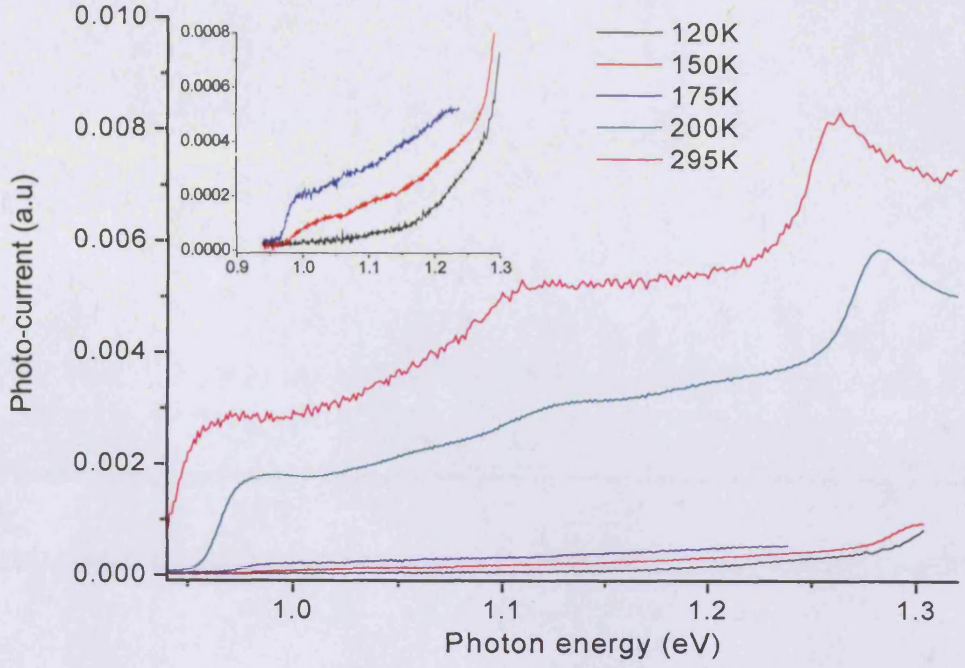

Figure 3.3.5 E-PCS with respect to temperature for a DWELL QD.

The spectra in figure 3.3.5 show a wavelength red-shift of the lowest energy photo-current peak amplitude with increasing temperature associated with the temperature-dependent band-edge energy of the semiconductor material. This is due to lattice constant variation of the constituent materials with respect to temperature therefore an energy shift is observed for all the features appearing in the spectra. The shift in higher photon energies close to 1.3 eV is associated with energy transitions in the WL. From 150 K to 200 K where values of sub-band edge can be determined, there is an energy shift around ~27 meV (from 0.991 eV to 0.964 eV). Figure 3.3.6 illustrates the band-gap energy shift of InGaAs with respect to temperature for different values of *In* concentration, having included strain in the model's calculations [Kopf 1997]. The experimentally determined band-gap energy values seem to agree more with the plot corresponding to an *In* concentration of 40%, which is typical value for a InAs/GaAs QD [Lemaitre 2004]. For a temperature range from 150 K to 200K the plot shows a band-gap shift of a few tens of meV supporting the experimentally determined sub-band edge shift value of ~27 meV.

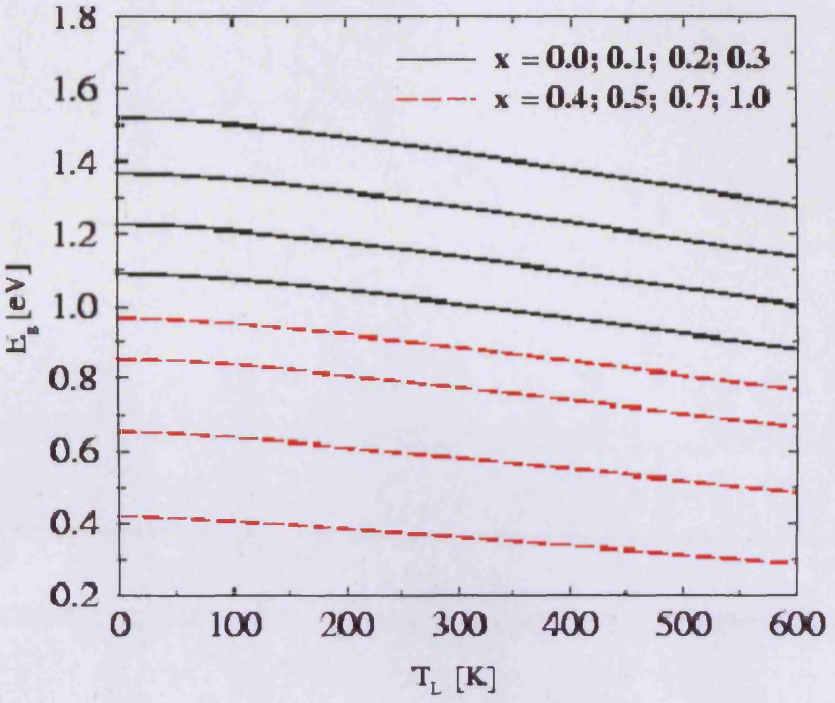

Figure 3.3.6 Temperature dependence of the bandgap in $In_xGa_{1-x}As$ with *In* content as parameter [Palankovski 2001].

In addition, the amplitude of the photo-current signal for both samples increases with elevated values of temperature. For the lower energy peak the increase of the amplitude with increasing temperature is due to thermal escape of carriers from QD energy states to the continuum of states in the WL. The thermally excited carriers are likely then to get swept away by the semiconductor internal field contributing to the detected electrical signal. Evidence of the thermal escape mechanism is that the signal at 120 K coming from the QD ground state is almost zero (inset – figure 3.3.5(a)) but not zero for excited energy states of QD or from WL states where carriers can still escape due to thermal excitation. This thermal activation for temperature higher than 120 K is also shown in ref [Fry 2000a], where at temperature of 5 K an absolute value of zero signal is observed in the photon energy part of the spectrum corresponding to transitions coming from QD energy states. A quantitative relationship between the photo-current signal amplitude and temperature is derived by relating the photo-current to photo-voltage (see section 1.4), which is written as $V_{OC} = \frac{kT}{q} ln\left(1 + \frac{I_P}{I_0}\right)$ (eq. 1.4.5).

Another characteristic of the temperature-dependent E-PCS is the rapid change of signal amplitude for a temperature range of 175 K to 200 K, which remains unclear at the present time. For higher temperature values the signal increases in a lower rate until it saturates close to room temperature, i.e 295 K. When values even higher than room temperature (RT) are reached the signal does not change in amplitude and becomes extremely noisy. The decrease of the SNR at high temperature can be attributed to the presence of many non photo-generated but thermally activated carriers screening the net signal originating from photo-generated carriers. The saturation of signal amplitude shows that at RT and under the presence of the semiconductor junction's "built-in" field E_0 all photo-generated carriers escape from the dots and contribute to the external detected photo-current signal. Therefore, it is assumed that the photo-current spectrum is absorption-like and represents the true absorption spectra of the dots [Fry 2000a].

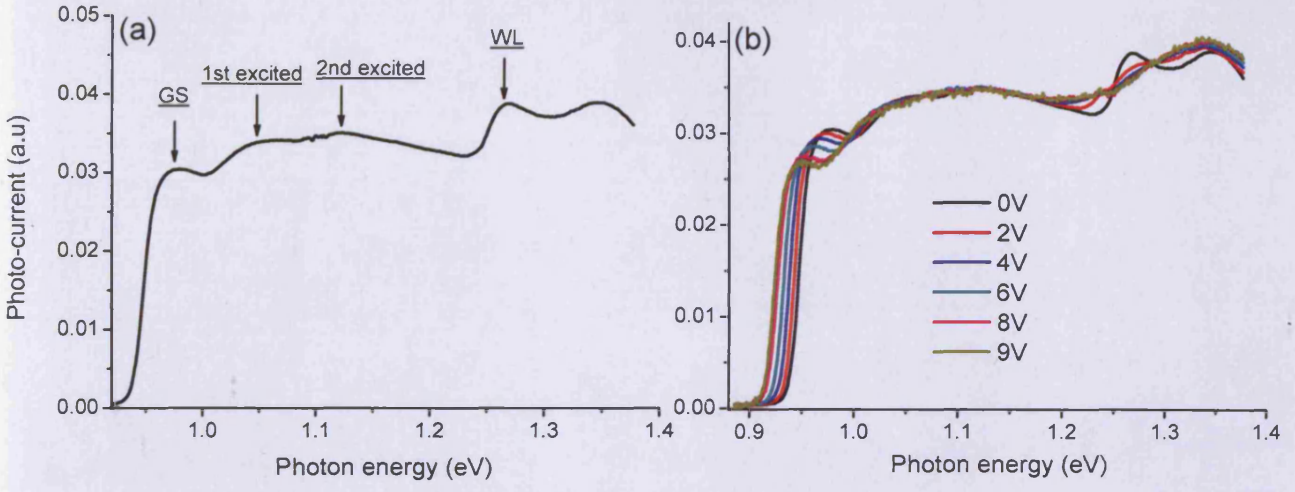

Figure 3.3.7 (a) E-PCS for zero bias, where the different energy transitions are indicated, and (b) with respect to reverse bias voltage for the DWELL QD.

This can be further confirmed by RT E-PCS measurements in figure 3.3.7, for the DWELL sample of figure 3.3.1(a), with respect to external applied reverse bias. Despite expectation to the contrary the photo-current signal amplitude -at high photon energy part of the spectrum- is not affected by the presence of an increased electric field and –at low photon energy- the

value of peak signal amplitude associated with the QD ground state drops with increasing reverse bias. By considering the fact that by reverse biasing the p-i-n junction the extraction efficiency of the photo-generated carriers is increased, it is expected an increase in the signal amplitude as well. However, the saturation of the signal amplitude in the higher photon energy part of the spectra with increasing electric field is an additional indication that at RT all the photo-generated carriers have thermally escaped and are contributing to the overall signal. Thus, the photo-current spectrum should represent the true absorption spectra and the drop in the signal amplitude corresponding to the dot ground state is associated only to the field-dependent oscillator strength of the ground state transition, which is discussed in details in the next chapter. This particular argument is important of the analysis of the QCSE in the next chapter, where the DWELL QD sample is used as a reference sample for the study of QCSE of columnar-QD materials with varied aspect ratio and *In* composition.

Photo-current signal corresponding to higher energy transitions does not seem to change in amplitude with applied field. However, this does not imply that the signal is saturated as for higher photon energy the signal is of higher amplitude. Saturation effects would cause a screening of the photo-absorption corresponding to different energy states and it would be impossible to identify them through the absorption spectra. Here, however, this is not the case because the different photo-absorption peaks in figure 3.3.7(a) are corresponding to different energy states in the dot and the WL. Furthermore in ref. [George 2007] [Sandall 2006], for different studied QD systems, the separation of the energy states as appeared in the edge photo-absorption spectra showed an agreement with this obtained by spontaneous emission, modal absorption measurements or with those theoretically estimated.

3.4 Summary

In this chapter, a new method to obtain the ratio of the fundamental TE/TM optical response of a quantum-confined system, which is controlled by the transition matrix elements, from the measurement of the polarisation dependence of the edge photo-voltage spectrum by correcting for polarisation dependent features of the experimental system is outlined.

I began in section 3.2 by illustrating the polarisation-dependent response of edge photo-absorption measurements by introducing a new experimental configuration, where the orientation of the device-polariser relative to the monochromator's output slit is changed by 90^0. This configuration is then used to describe a means to calibrate the relative polarisation response, which can be used for both E-PCS and E-PVS. Then, the method described here is verified by application to compressive and tensile strained InGaP QW structures and the results are in agreement with the known ratios of the transition matrix elements at the band edge.

Section 3.3 began by the application of this method to standard InAs/GaAs QDs, where it was shown that QD interacts strongly with TE but not with TM polarised light. I explained this by considering the shape of the dot, having low aspect ratio, and the compressive strain induced in the dot by the surrounding material. Furthermore, by applying temperature- and field-dependent photo-current spectroscopy, in a standard DWELL InAs/GaAs QD material, I explained the two main escape mechanisms of the photo-generated carriers, which are described by tunnelling and thermal excitation, and I showed that at room temperature the photo-current spectrum is absorption-like representing the true absorption spectra of the dots.

Chapter 4- Electro-optical properties of Columnar-Quantum Dots

4.1 Introduction

In this chapter the TE/TM optical response of a set of InAs/GaAs columnar-QD samples and the Quantum-Confined Stark Effect (QCSE) are studied and compared to those of a standard aspect ratio QD, presented in chapter 3. In addition, TM-dominant lasing emission from an extremely high-aspect ratio columnar-QD is shown.

In section 4.2, I start by briefly describing the characteristics, i.e shape and *In* composition, of the formed columnar-QDs. The studied samples form two groups; one of first generation columnar-QD comprising of two samples of aspect ratio up to 1.12:1 and two samples of different stack numbers with an aspect ratio of 3.51:1. The second generation are QRs of extremely high aspect ratio up to 10:1. By applying the method proposed in chapter 3 the TM polarised photo-current spectrum is calibrated with respect to TE and the dependence of the polarisation properties of the columnar-QD with respect to their aspect-ratio and the *In* compositional contrast between the QR and 2-D region surrounding the QR are studied and analysed.

In section 4.3, I present QCSE measurements by applying field-dependent photo-current spectroscopy. I start by expressing the external applied reverse bias in terms of internal electric field using a semiconductor simulator. Then, I briefly review the well known QCSE of standard aspect ratio QD materials, which is used as a reference to study the Stark-shift of higher aspect-ratio QD samples. There follows an analysis on the rod aspect ratio dependence of the band-edge shift of the photo-current spectra within the studied electric field range.

In the last section 4.4, I begin by showing polarisation-selective Amplified Spontaneous Emission (ASE) of a second generation QR. Then, I compare the emission spectra with the photo-absorption spectra and I discuss the dual polarisation property of QR lasing emission. Finally, I present threshold current density measurements with respect to temperature.

4.2 Edge Photo-Current Spectroscopy in Columnar Quantum Dot materials

In this section the polarisation properties of high aspect ratio self-assembled InAs/GaAs QD samples grown on (001)-oriented GaAs substrate by using Molecular Beam Epitaxy (MBE) are studied and compared to those of a conventional aspect-ratio QD [Liu 2004a], analysed extensively in the previous chapter. The columnar-QD materials were grown and processed by Dr. Lianhe Li and Philipp Ridha, respectively at Swiss Federal Institute of Technology Lausanne (EPFL).

4.2.1 *Sample growth and structural details*

The columnar-QDs are formed by first growing a 1.8 monolayer (ML) InAs QD seed layer in the standard Stranski-Krastanow (SK) mode, and then depositing a short period of InAs/GaAs superlattice (SL) on the GaAs substrate. Parameters during the growth, such as the temperature and the growth interruption (GI), determine the *In* uniformity, the volume of the QR and the *In* composition [Li 2007]. GI is the time interval between the growth of GaAs on InAs so as to form the SL layers. Apart from the growth conditions, the number of SL periods determines the aspect ratio and the *In* composition of the Quantum Rod (QR) formed structure, which consists of two parts; the QR area of high *In* composition itself and the 2-D layer surrounding the QR, having a lower *In* composition. The rod formation is confirmed by dark-field cross-sectional Transimission Electron Microscopy (TEM) image shown in figure 4.2.1(a), where the rod itself is indicated by the white dashed box. The lower *In* composition material around the rod forms the dark region and plays the same role as the Wetting Layer (WL) in a standard QD, acting as a carrier's "reservoir" injecting them into the QR. Thus, for

the rest of thesis this layer is called 2-D WL. The plot of the *In* concentration along the growth axis in figure 4.2.1(b) shows that there is a compositional fluctuation along the rod with the most *In* concentrates at the bottom and apex of the rod. Also, due to *In-Ga* intermixing during the growth *In* resides in the 2-D WL with uniform concentration. Thus, the whole structure can be considered as a high-aspect ratio of *In*-rich QD in an InGaAs QW. The characteristics of the QR materials such as the aspect ratio and the *In* compositional profile are derived by cross-sectional TEM images using the techniques of ref. [Patriarche 2004] and [Lemaitre 2004].

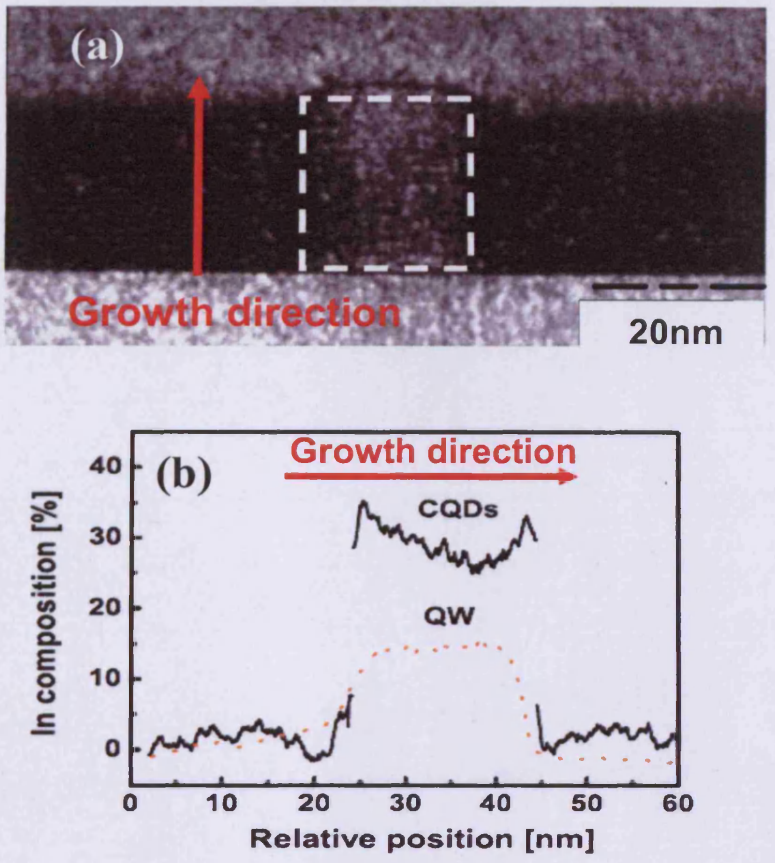

Figure 4.2.1 (a) Dark-field cross-sectional TEM image of a 16-period InAs/GaAs CQD and (b) a plot of indium profile in rod and 2-D WL area of the CQD along the growth axis by ref. [Ridha 2008a].

The studied columnar-QD samples form two groups summarised in table 4.2.1. The first group consists of a 1st generation columnar-QDs formed by depositing a 1.8 monolayer (ML)

InAs QD seed layer and then a period of GaAs (3ML)/InAs (0.62ML) superlattice (SL) [Ridha 2007]. The number of periods of InAs/GaAs SL is increased from 10 (P622) to 18 (P666) and finally to 30 for both P906 and P918 samples. The difference between the last two samples is in the number of stacks, i.e 1 and 3 for P906 and P918 respectively, which represents the number of repeated formed columnar-QDs in the growth direction, where each of the columnar-QD array, in the x-y plane (xyz- axes are indicated in figure 1.6.1-page 21), is separated from the next by a 100nm GaAs barrier material. The structural details were kindly provided by Philipp Ridha and are shown in appendix B.

Samples	Process number	InAs/GaAs SL periods	InAs/GaAs SL Monolayers	Number of stacks
1st generation Columnar Quantum Dots	P622	10	0.62 / 3	5
	P666	18	0.62 / 3	5
	P906	30	0.62 / 3	1
	P918	30	0.62 / 3	3
2nd generation Columnar Quantum Dots (QRods)	P990	35	0.95 / 6	3
	P968	30	0.95 / 6	1

Table 4.2.1 1st and 2nd generation self-assembled CQD and QR structures with varying the period and thickness of the InAs/GaAs SL as well as the number of stacks.

The growth conditions between the 30-periods InAs/GaAs columnar-QDs and the less periods samples are altered, thus the first samples show a higher *In* composition in the QR region together with a reduced rod diameter from 20nm (10- and 18-period CQD) to 10 nm [Ridha 2007]. Estimated values such as the aspect ratio and *In* composition of the columnar-QD samples are listed within table 4.2.1. The *In* composition along the rod as has already been mentioned (see figure 4.2.1b) is not uniform varies by approximately 10 to 15% from the average values listed within table 4.2.2.

Samples	Process number	Height/diameter (nm)	Aspect ratio	In composition	
				QR	2-D WL
1st generation Columnar Quantum Dots	P622	12.5 / 20	0.63	30	16
	P666	22.5 / 20	1.12	30	16
	P906	35.1 / 10	3.51	45	16
	P918	Expected to be similar to P906			
2nd generation Columnar Quantum Dots (QRods)	P990	75 / 10	7.5	51	12
	P968	70 / 7-10	7-10	44	12

Table 4.2.2 Aspect ratio and *In* composition of the 1st and 2nd generation self-assembled CQDs and QR structures.

Considering the increased number of periods from sample P622 to P906 it is obvious that the height of the rod is directly controlled by the number of the SL periods. However, the increased number of SL periods is responsible for the presence of additional defects, visible in Scanning Electron Microscopy (STM) images, which are responsible for low efficiency electroluminescence (EL) and higher laser threshold [Fiore 2008]. This is a possible reason for the extremely-low photo-current signal of sample P906, where defect states can reduce the extraction efficiency of photo-generated carriers in the case of E-PCS. However, this is not the case for the sample P918 with the same number of periods, where the level of photo-current signal is higher and this can be attributed to the fact that adding more stacks should cause an increase of photo-generated carriers when E-PCS is applied.

The second group of columnar-QD samples consists of two samples of 2nd generation columnar-QDs, where the issue of the low-efficiency 1st generation high aspect ratio columnar-QDs, due to the presence of many defect states is overcome mainly by changing the thickness of InAs/GaAs SL from 0.62/3 to 0.95/6 ML fabricating good-quality columnar-QDs of extremely high-aspect ratio with a value approximately up to 10:1 [Li 2008a][Li 2008b]. A TEM image of the 30-periods columnar-QD is illustrated in figure 4.2.2. Due to

the extremely high aspect ratio the samples of this group in this work are called QRs together with the 1st generation 30-periods columnar-QDs. The latest generation QRs exhibit a higher *In* contrast between the QR and the 2-D WL compared to samples of the 1st group, with lower *In* composition in the 2-D WL, and this is crucial for their unique polarisation properties, as it is shown later in this chapter. However, the *In* variation with respect to the mean value of table 4.2.2, is 5% along the QR and 2% in the 2-D WL. An evidence of the quality of the 2nd generation QR materials is that these structures are lasing at room temperature (RT) [Ridha 2008b]. In the last section of this chapter a RT TM-dominant lasing emission is illustrated for the 35-period sample (P990).

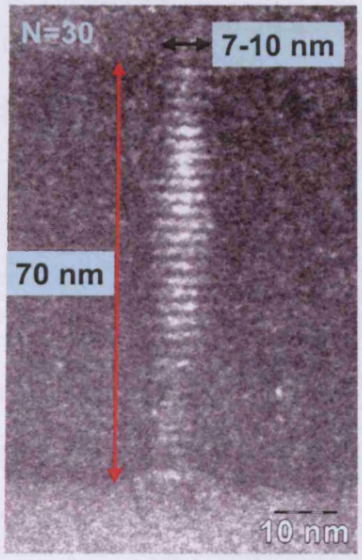

Firure 4.2.2 TEM image of 2nd generation QR sample of 30-periods InAs/GaAs SL (P968) with aspect ratio close to 10 (The TEM picture was kindly provided by Prof. Andrea Fiore).

Due to the elongated shape of the formed rod in the case of the 2nd generation columnar-QD there is an intermediate situation between 0-D and 1-D confinement [Li 2008a] [Sek 2008]. This is due to the fact that although the rod diameter is smaller than the exciton Bohr radius - which is approximately 10 to 20 nm in InAs/GaAs system [Sugawara 2000] and the carriers are strongly confined in the growth plane- the rod length is larger than the exciton Bohr radius resulting in a weak confinement along the growth direction.

4.2.2 *TE/TM optical response of Columnar-Quantum Dots*

The electronic states in a standard aspect ratio InAs/GaAs QD structure, which were analysed in the previous chapter, are quantised strongly in the growth direction due to the dot shape of low-aspect ratio and to the bi-axial compressive strain. Thus, there is a split of heavy-hole (hh) and light-hole (lh) states in valence band so that TE polarised light couples more strongly than TM with electronic states in a QD. However, theoretical investigations [Saito 2005] [Saito 2008] using an 8-band k·p model and experimental observations [Kita 2002] [Jayarel 2004] report that by increasing the height of the dot, the biaxial compressive strain is reduced and this causes an enhancement of the hh-lh mixing components of the hole states increasing the interaction of TM polarised light with e-h pairs because of the large lh-component of hole states. For a columnar-QD of aspect ratio $r_{asp.ratio} \geq 0.9$ the biaxial strain in the middle of the dot becomes negative [Saito 2008], therefore the lh- valence band moves towards the Conduction Band (CB) and ends up being closer to it than the hh-band.

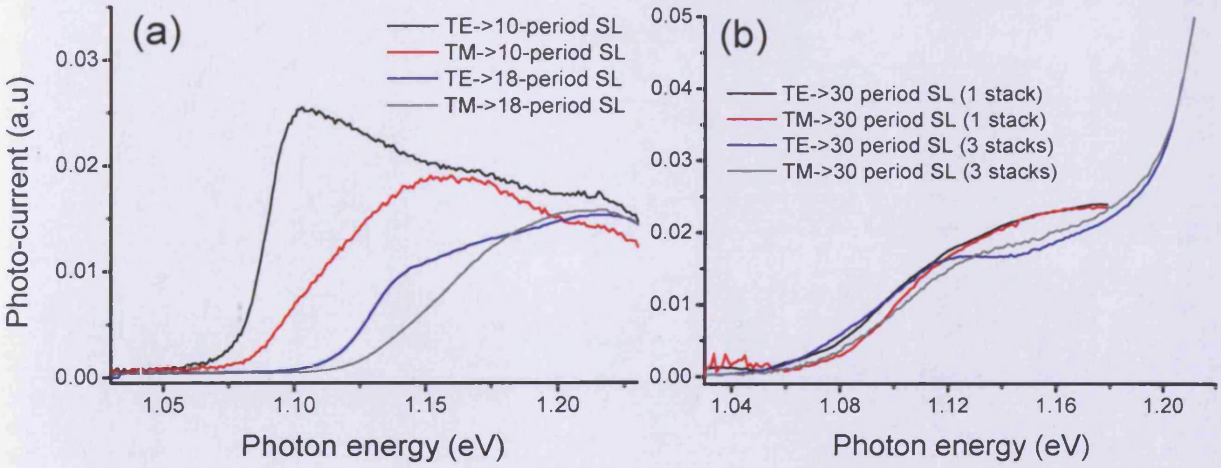

Figure 4.2.3 TE and TM_{cal} polarised photo-current spectra for the 1st generation (a) 10- and 18- period and (b) 30-period SL CQDs.

Polarisation-selective E-PCS measurements made by the author for the 1st generation columnar-QD samples, in figure 4.2.3(a), show that indeed by increasing the dot aspect ratio from 0.63:1 to 1.12:1, for the 10-period and 18-period SL columnar-QD respectively, in the low energy part of the spectra corresponding to photo-generated carriers originated from the QD states, the TM polarised photo-current is enhanced relative to TE (the TM spectra is calibrated with respect to TE using equation 3.2.6(a)). This confirms that by increases the dot aspect ratio there is an enhancement of the hh-lh mixing components of the hole states and this contribute to stronger absorption of TM polarised light as the lh-component increases. Then, in figure 4.2.3(b) for the 30-periods samples (P906 and P918) of aspect ratio 3.51:1 the amplitude of the photo-current spectra is similar for the two orthogonal polarisations. Polarisation-independent gain is of major importance for application in polarisation-independent Semiconductor Optical Amplifiers (SOA).

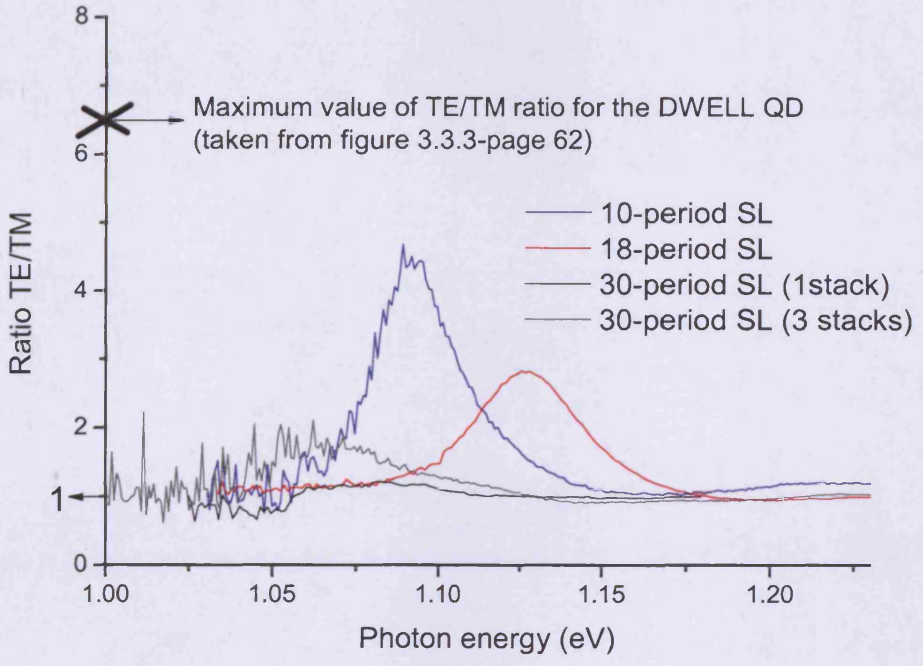

Figure 4.2.4 TE over $TM_{\_cal}$ ratio shows the polarisation response of 1st generation CQD structures.

To have a clearer picture, the ratio of the polarised-selected spectra is plotted in figure 4.2.4, where also the maximum ratio of TE/TM for the standard aspect ratio QD sample (obtained in section 3.3), is indicated. As it is expected the TE/TM ratio reduces by increasing the dot

aspect-ratio from a value of 6.5 for the QD DWELL sample to 4.5 and 3 for the columnar-QD of aspect ratio 0.63:1 and 1.12:1 respectively. However, this reduction for the 30-period columnar-QD samples is attributed both to the high aspect ratio and the higher contrast of *In* composition between the rod and the 2-D WL compared to that of columnar-QD of less number of periods (see table 4.2.2). The *In* compositional contrast is an important parameter defining the polarisation properties of the columnar-QD as it shown later in this section when the two 2nd generation QRs, of similar aspect ratio but different *In* composition in the QR region, are compared. In the case of similar aspect-ratios 30-period columnar-QD samples there is a noticeable difference in the TE/TM ratio. The sample of 1 stack (P906) shows a polarisation-independent photo-absorption response, where the ratio TE/TM is close to 1 (with 20% deviation around this value). In the case of the multi-stack sample (P918) the ratio reaches a value of 2. A possible reason for this difference between the two structures can be due to any unintentional difference in *In* composition between the columnar-QD of different stacks for the sample of 3-stacks (P918) caused during the growth. Another way in order to have a control over the biaxial-compressive strain coming from the 2-D WL has been proposed by the use of a highly tensile-strained barrier material, such as InGaAsP [Kawagushi 2006a]

The results of photo-current measurements for the 2nd generation QRs, for the two orthogonal polarisations, together with the TE over TM_{cal} ratio, are given in figure 4.2.5(a) and (b) respectively. The plots indicate that near the band edge the strength of TE-polarised photo-absorption is higher than that of TM for the sample of 30-periods SL QR, while for the 35-period sample the opposite is illustrated, where TM polarised photo-absorption is the dominant. For 35-periods SL QR sample of an aspect ratio of 7.5:1 (P990) the ratio of TE/TM near the band-edge is 0.14 and it reveals the dominant lh-component of hole states near the band edge. Contrary to 35-periods SL QR, the 30-period sample of aspect ratio 7 to 10:1 (P968) has a TE over TM ratio close to 2 in the low energy part of the spectra, thus indicating a dominant hh-component of hole states in the sub-band edge, although it is of similar or even higher aspect-ratio compared to sample P990.

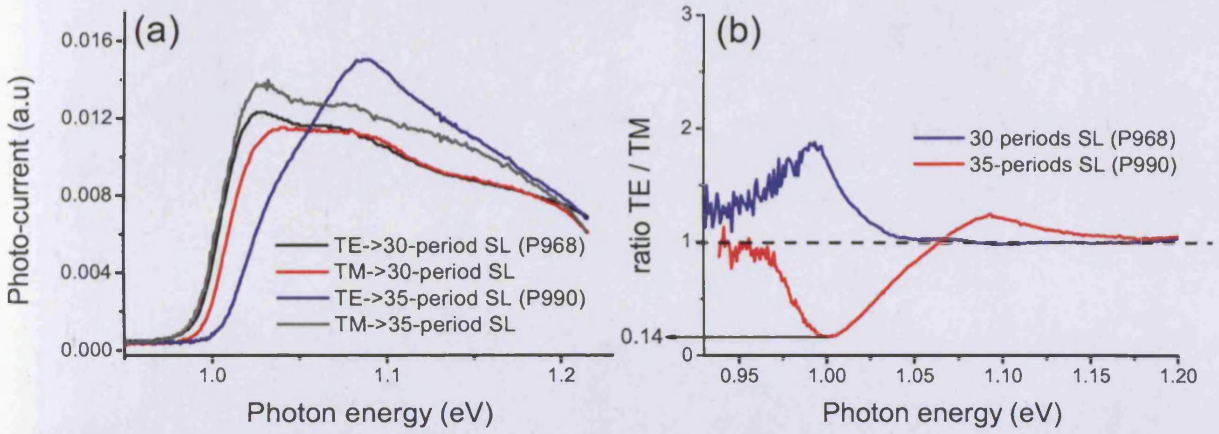

Figure 4.2.5 (a) TE and TM_{cal} polarised photo-current spectra for the 2nd generation CQDs and (b) the ratio TE over TM_{cal}.

Thus, the QR shape and aspect ratio is not the only parameter determining the polarisation properties of the columnar-QD, but the strain distribution is a prominent factor as well. The results on InAs columnar-QDs with highly tensile-strained InGaAsP barriers suggest that strain engineering is very important for controlling polarisation properties [Kawagushi 2006b]. Similar is the case for the columnar-QD materials studied here where the compressive strain is induced by the 2-D WL to the QR and is determined by the *In* compositional contrast.

A theoretical investigation of lh- and hh- VB, by using an eight-band k·p model calculation, for a fixed aspect ratio columnar-QD with a varied *In* compositional contrast is shown in ref [Ridha 2008b]. The impact of the *In* compositional contrast on the VB mixing of lh- and hh- energy bands confirm the TE/TM polarisation optical absorption response dependence on the *In* compositional contrast which is illustrated in figure 4.2.5 for the 30- and 35-period SL QR samples of similar aspect ratio. The eight-band k·p calculations showed that by decreasing the *In* composition in the 2-D WL, while keeping constant the *In* concentration in the QR, the lh- and hh- bands moving towards and away from the CB respectively, enhancing the lh- and hh- band mixing, therefore enhancing the coupling of TM polarised light with the energy transition in the QR. The opposite occurs when the *In* concentration is kept constant in the 2-D WL and decreases in the QR region, with lh- and hh- bands moving away and towards the CB respectively.

4.3 Field-dependent Edge Photo-Current Spectroscopy: Study of Quantum-Confined Stark Effect

4.3.1 *Introduction*

In this section the optical properties of columnar-QDs and QR materials of a varied aspect ratio and *In* compositional contrast are studied by applying field-dependent photo-current spectroscopy and new information about the wave-functions inside the QRs is obtained. To compare the Stark shift of different aspect ratio columnar-QDs the external applied reverse bias is expressed in terms of internal electric field by using a semiconductor simulator. Firstly, well known results for the standard aspect ratio QD sample are presented. This sample is used as a reference in order to analyse the Stark shift measurements of columnar-QD samples. The results are presented in two groups of samples; one consisting of the lowest aspect-ratio columnar-QD (P622 and P666) and the other one the high aspect ratio columnar-QD samples (1st generation-P906 and 2nd generation P968 and P990), where the samples of the latter group are called QRs in this thesis.

4.3.2 *Device simulations*

To compare the Quantum-Confined Stark Effect (QCSE) [Miller 1985] of the studied devices under reverse bias, the external applied potential (Volt) is expressed in terms of internal electric field (kV/cm) induced in the QR using the SimWin package [Winston 1999]. A p-i-n junction diagram under reverse bias is illustrated in figure 4.3.1, where the total electric field in i-region of the p-i-n junction, is the sum of junction's built-in field E_0 and the external applied field.

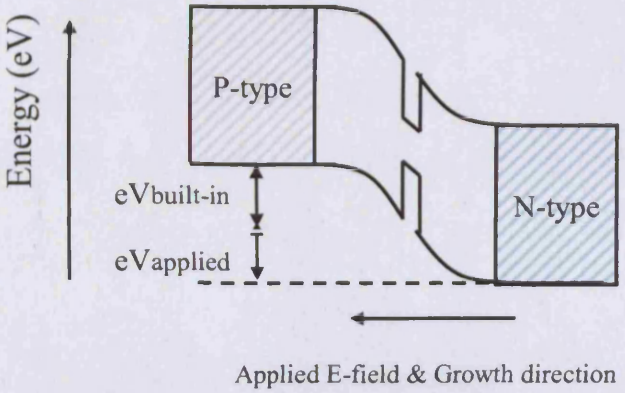

Figure 4.3.1 Diagram of a device p-i-n junction under reverse bias.

SimWin is one of many widely available 1-D simulators incorporating a self consistent Schrodinger – Poisson – Continuity equation solver in one dimension. Thus, it is assumed that all variables such as current, field and potential, etc vary parallel to the flow of current but are uniform in the direction perpendicular to the current. *In*-based alloy parameters are not included in the simulator's package, and therefore these are added according to ref. [Vurgaftman 2001]. The input values of doping-level were set according to values listed in the growth information tables of appendix B. Also, a value of p-type $3x10^{15}$ cm^{-3} background doping level was considered. In the case of forward bias the columnar-QDs current varies also in the direction perpendicular to the growth direction (current flows from the WL region into the QR). Thus, to simulate and obtain values of columnar-QD internal field with respect to externally applied reverse bias ideally a 2-D or 3-D simulator should be used. Due to the lack of such a commercial available package, suitable for columnar-QD structures, two 1-D simulations are performed; one simulates the QR region, where for the simulation purposes the structure is set to be a QW of width equal to the rod's height and of *In* composition equal to the mean value of rod *In* concentration according to values of table 4.2.2. The other one simulates the 2-D WL as a QW. Also, the value of *In* concentration in WL is taken from table 4.2.2. The real 2-D solution should tie somewhere between those two extremes. An example of this approach is shown in figure 4.3.2, where the electric field across the p-i-n junction is estimated for two bias values (0 and 4V).

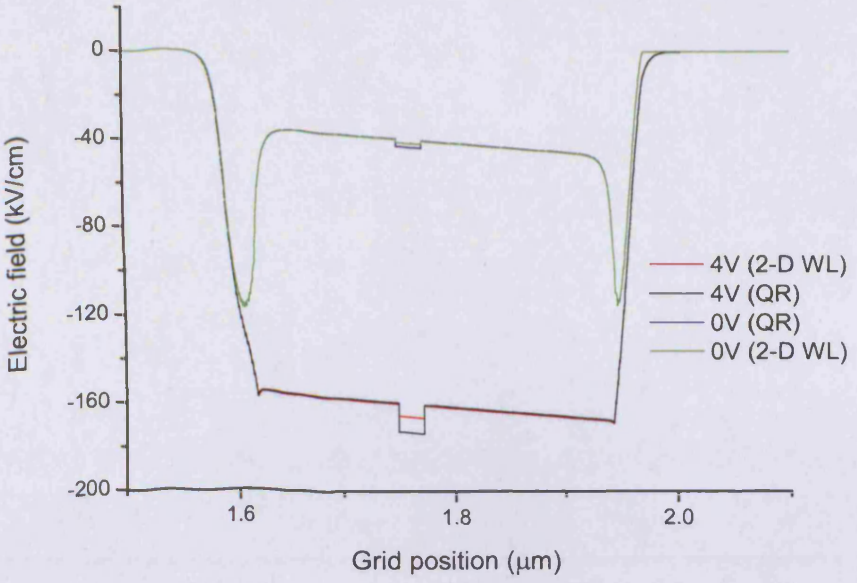

Figure 4.3.2 Calculation of the electric field across the active region of two simulated p-i-n junctions corresponding to the 2-D WL (0V-green, 4V-red) and rod region (0V-blue, 4V-black) of the 18-period CQD.

The field across the quantum-confined region of the columnar-QD can be considered to have a mean value between the values of internal field across the two simulated junctions. Therefore, in the estimation of the internal field of the columnar-QD semiconductor junctions -with respect to the externally applied reverse bias- an error is included, which is estimated by the extreme electric field values determined by the two performed simulations of the QR and 2-D WL regions of the columnar-QD structure. An example of simulated band diagrams, for the 2-D WL of the 18-period SL columnar-QD structure (P666) for the case of reverse, forward and zero bias, is illustrated in figure 4.3.3. Under no external applied field the semiconductor is in equilibrium with the Fermi-level lying in the middle of the conduction band (CB) and valence band (VB). By applying bias the quasi-Fermi levels for electrons (E_{f_e}) and holes (E_{f_h})) are separated and their relative position depends upon the direction of the applied field (i.e reverse or forward bias).

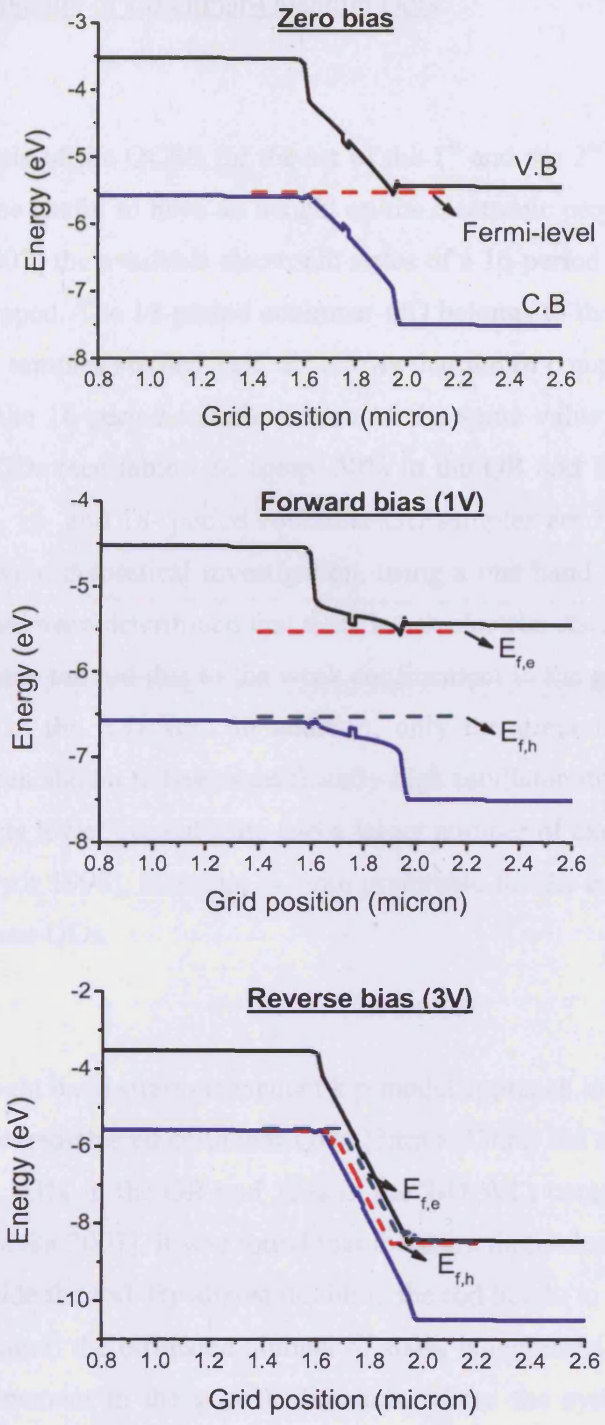

Figure 4.3.3 Energy band diagrams simulated for a 2-D WL InAs/GaAs CQD structure for forward, reverse and zero bias. In the case of non-equilibrium the position of electron and hole quasi-fermi levels are indicated.

4.3.3 Electronic structure of Columnar-Quantum Dots

Prior to any analysis of the QCSE for the set of the 1st and the 2nd generation columnar-QD samples it would be useful to have an insight on the electronic properties of these structures. In ref. [Motyka 2007] the available electronic states of a 16-period InAs/GaAs SL columnar-QD have been mapped. The 16-period columnar-QD belongs to the same family with that of 10- and 18-period samples studied here. It follows that the *In* compositional contrast and the rod diameter for the 16-period sample is also of the same value with this of 10- and 18-period columnar-QDs (see table - *In* comp. 30% in the QR and 16% in the 2-D WL). The heights of the 10-, 16- and 18- period columnar-QD samples are 12.5 nm, ~20 nm and 22.5 nm respectively. By a theoretical investigation, using a one band approximation for the 16-period sample, it has been determined that there is one electron state and up to three hh- or lh-states confined inside the rod due to the weak confinement in the growth plane, which is due to the *In*-content in the 2-D WL. In addition, only the ground state 1e-1hh and 1e-1lh transitions have been shown to have significantly high oscillator strength. However, an eight-band model predicts lower ground state and a larger number of excited states than any other approximation [Pryor 1998], therefore is more preferable for the estimation of the electronic structure in columnar-QDs.

By following an eight band strain-dependent k·p model approach in ref. [Krenner 2008], for a similar volume squared-shaped columnar-QD (23nm x 23nm) but of higher *In* compositional contrast (*In* comp. 43% in the QR and 10% in the 2-D WL) compared to that of 16-period columnar-QD [Motyka 2007], it was found that there are three-electron states and many hole states confined inside the rod. By almost doubling the rod height to 40nm (the diameter of the rod was kept the same) the estimated number of states is increased and this can be attributed to the weak confinement in the growth direction, where the system is in an intermediate situation between 0-D and 1-D confinement [Li 2008a]. Field-dependent PL measurements in ref. [Krenner 2008] for the 23nm in height quantum rod (or post) have shown an extremely high dipole moment value corresponding to an e-h separation 20.5nm which is equal to the nominal height of the post. The values of dipole moment are 40 times higher than those of standard QDs [Petroff 2007] and it was found that electrons can spread over the whole length

of the rod, whereas the holes are localised at the bottom and at the top, due to the fact that the highest *In* composition appears in these parts of the rod. The spread of the electron wave functions has been also confirmed by measurements of the lifetime constant (TC) in low-temperature time-resolved PL, where the TC is increasing with rod length [Li 2008a]. However, the field-dependent PL measurements can provide information about the Stark shift in a "low field regime" for field values maximum a few tens of kV/cm, as the PL emission is quenched at higher fields, whereas with in photo-current measurements the QCSE can be studied in a higher and wider range of electric field values as it is shown in ref. [Findeis 2001]. There the QCSE was studied for an InGaAs quantum dot material in both complementary regimes of photo-current (PC) and PL, which for the rest of this thesis are named as "PC-field regime" and "PL-field regime" respectively. In this thesis the CQSE is studied at the "PC-field regime" by applying field-dependent photo-current spectroscopy where the field varies from 40 kV/cm to 350 kV/cm. The results show some agreement with the large dipole moment values reported in ref. [Petroff 2007] [Krenner 2008].

4.3.4 *Results*

A] Standard aspect ratio Quantum Dot

The CQSE for a conventional shaped InGaAs QD material has been extensively studied in the literature [Fry 2000b] [Jin 2004]. Therefore an analytical investigation is out of the scope of this thesis. However, measurements showing the Stark-shift in a DWELL QD material (figure 4.3.4) are taken in order to have a comparison with those taken for higher aspect ratio columnar-QD materials. A brief introduction to the electronic properties of a standard shaped QD, which are obtained by studying the CQSE, follows as it appears in the literature.

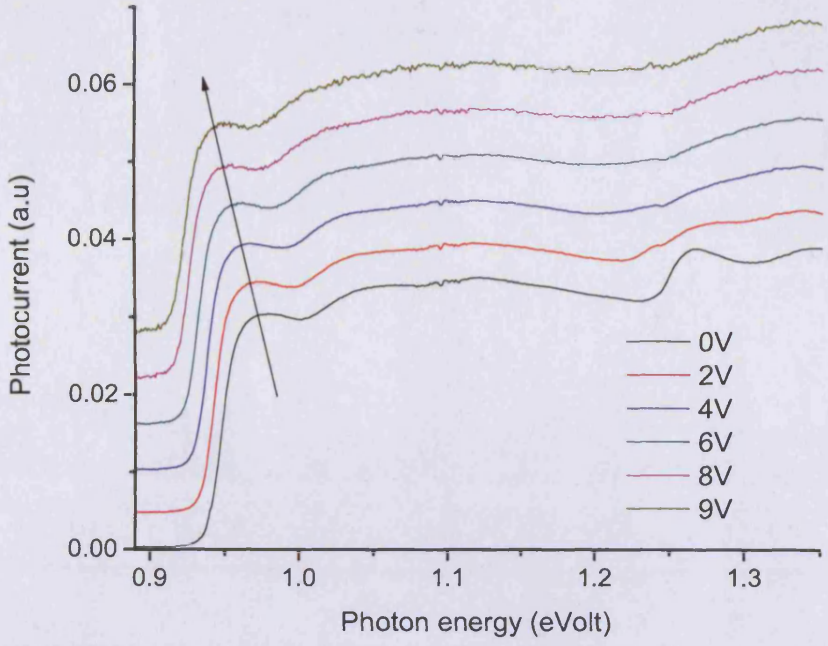

Figure 4.3.4 QCSE in the DWELL QD sample (shown earlier in figure 3.3.7(b)-page 68) for reverse bias values from 0 to 9 V corresponding to a field range from 50kV/cm to 320kV/cm. The zero level of each spectrum has been shifted in amplitude relative to that of 0 V spectrum in order the red-shift of the ground state peak amplitude -with respect to applied field- to be clearly illustrated.

The energy transitions (i.e ground and first excited state) are red-shifted and the Stark shift is not linear, being relatively smaller for lower fields. The transitions energy shift with respect to the internal electric field F, is described by the quadratic equation [Klingshirn 1997]:

$$E = E_0 + pF + \beta F^2$$

Equation 4.3.1

, where E_0 is the transition energy for zero electric field and the linear and quadratic terms of the equation consists the terms of dipole moment p and polarisability β respectively. The permanent dipole moment p is due to the initial spatial separation of electron and hole wave-functions along the growth axis, which is caused by the different confining potentials that these two carriers experience due to the difference in their effective masses. The polarisability β represents the extent to which an applied field can pull the electron-hole pair

apart, having an effect in the transition energy, and is found to be linked with the height of the dot [Barker 2000].

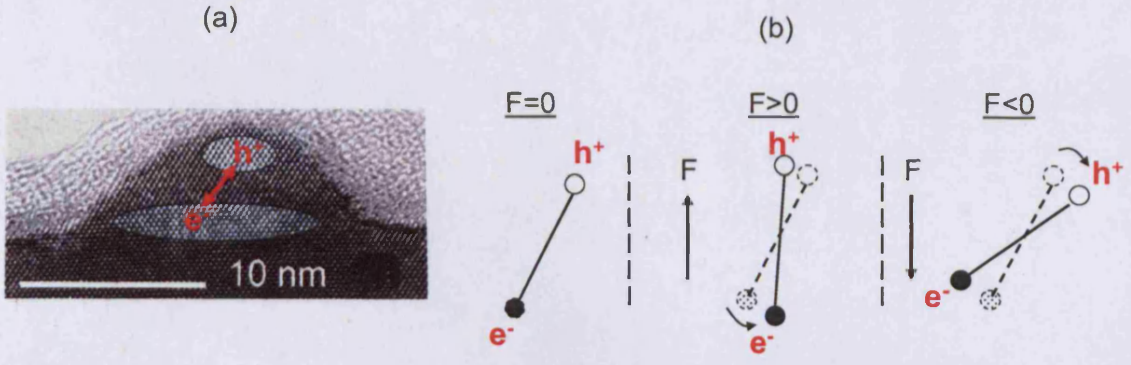

Figure 4.3.5 A simple diagram illustrating (a) the e-h dipole orientation (hole above electron) in a lens-shaped dot (figure taken from [Fry 2000b]) and (b) the effect that an applied field has on a dipole -in free space- due to the initial separation of the electron and hole mean positions. In the case of a dipole in a dot the effect of the quadratic term would need to be added (see eq. 4.3.1) to this picture, where in that case apart from the dipole rotation the dipole length is changing under the presence of the field.

In ref [Fry 2000b] it is shown that inside the dot the hole is localised at the apex while the electron wave-function spreads over the bottom of the dot (figure 4.3.5(a)). Considering this e-h dipole permanent orientation (i.e hole above the electron), the diagram in figure 4.3.5(b) illustrates the effect that an external applied field has in a dipole –in the free space- due to the initial mean spatial separation of the electron and hole wave functions, which determines the e-h wave functions overlap (i.e the dipole oscillator strength) and the transition energy. The diagram does not illustrate the effect of the quadratic term in the electron-hole separation as it depends on the characteristics of each dot material. This term is determined using a second-order perturbation theory [Barker 2000]. For a negative applied field the electron (or hole) is moved towards the apex (or base) of the dot and the e-h overlap increases with respect to the growth direction, whereas in the case of a positive applied field the e-h overlap decreases and the transition energy is reduced. The maximum transition energy of the e-h dipole is at the point where the maximum dipole oscillator strength is observed for a negative applied field [Fry 2000b]. Thus the permanent dipole moment is positive and the dipole orientation, i.e the hole above the electron, is attributed to the *In* compositional variation inside the QD, being

high and low at the apex and the base of the dot respectively. The hole of higher effective mass compared to the electron mass is more localised at the part of the dot with the highest *In* concentration.

B] Lowest-aspect ratio 1st generation Columnar-Quantum Dots

Photo-current measurements as a function of reverse bias for the 10- and 18-period InAs/GaAs SL columnar-QD samples, i.e P622 and P666 respectively, are illustrate here, where the amplitude of the Stark shift is compared with that of the DWELL QD sample of figure 4.3.4 in page 86. According to table 4.2.2 the 10-period and the 18-period columnar-QDs have the same diameter (20nm) and height of 12.5nm and 22.5nm respectively.

10-period InAs/GaAs SL columnar-QD

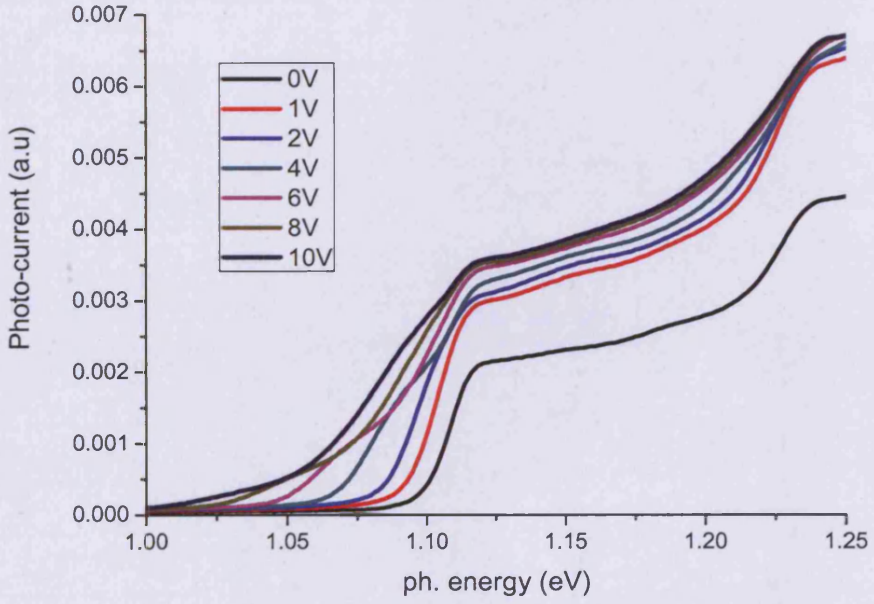

Figure 4.3.6 Field-dependent photo-current spectra for the 10-period CQD sample (P622) from 0V to 10V corresponding to a field range from 45 kV/cm to 340 kV/cm.

Figure 4.3.6 shows the red-shift of the photo-absorption spectra for the 10-period SL columnar-QD with respect to applied reverse bias. The sub-band edge shift is not clear for high values of reverse bias where a second peak in the low-energy part of the spectra appears, which red-shifts with bias.

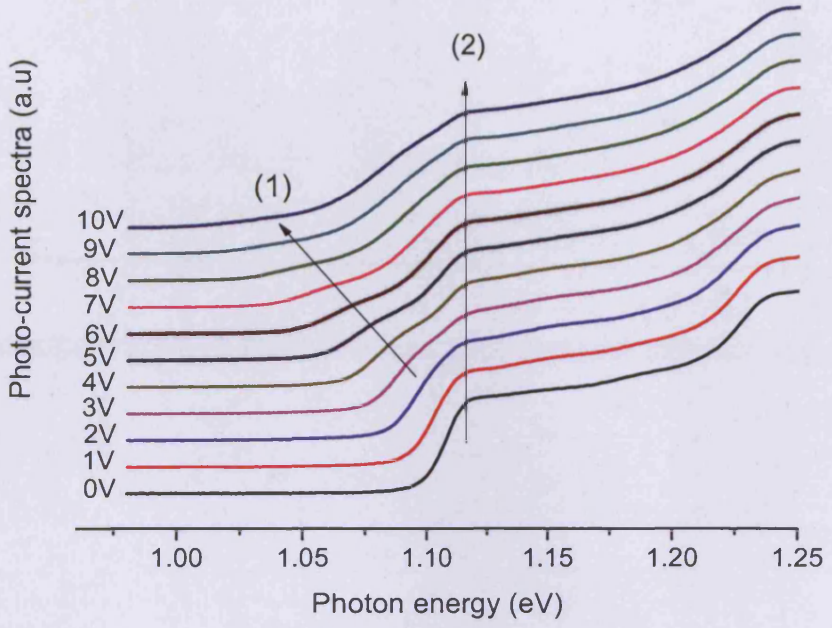

Figure 4.3.7 Field-dependent photo-current spectra where the signal amplitude –of the data showed in figure 4.3.6- is normalised and shifted to an extent so as to illustrate the Stark-shift of the 10-period CQD sample (P622).

This shift is illustrated clearly in figure 4.3.7 where the spectra of figure 4.3.6 have been relatively shifted in amplitude. According to the latest figure the evolution of the two different peaks with increasing reverse bias are represented by the arrows (1) and (2). For zero applied bias there is one peak at around 1.12eV which gets broader until a value of field around 125 kV/cm (corresponding to 2.5 V reverse bias). After this point and for a higher value of electric field is clear that there are two different peaks corresponding to two different transitions; one which is red-shifted in energy with the presence of electric field and one which is not affected. The first transition corresponds to a heavy hole ground state transition because there is no similar shift of the band-edge of the TM photo-current spectra within the range of the applied field and the latter transition corresponds to an excited transition,

according to the analysis below, where in order to investigate these transitions and study the QCSE the shift of transitions energy and change of the relative photo-induced signal amplitude with respect to electric field is analysed.

In figure 4.3.8 the normalised peak signal intensity corresponding to each transition (indicated by the arrows (1) and (2) in figure 4.3.7) is plotted with respect to electric field and is compared with that of the ground state peak signal DWELL QD sample (as it is shown in figure 3.3.7(b) of chapter 3-page 68).

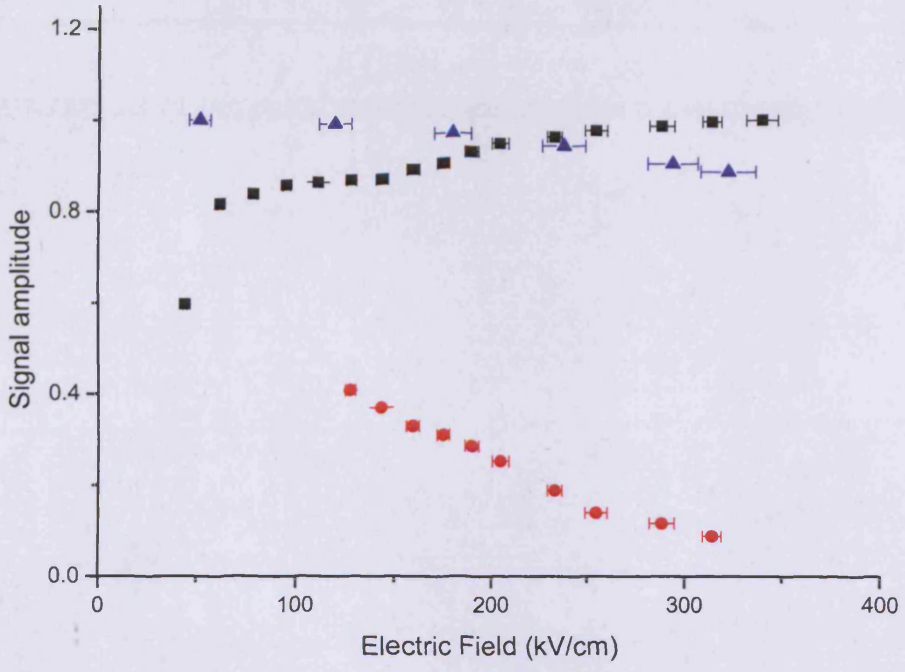

Figure 4.3.8 Normalised peak signal amplitude with respect to electric field for the ground state of standard aspect ratio QD (blue triangles) and the ground state transitions, (1) (red circles) and (2) (black squares) of the 10-period CQD material.

The attention should be focused on the relative change of signal amplitude with increasing electric field because the absolute photo-current signal amplitude for different structures is not exactly comparable as the signal magnitude contains their system response. This includes

the extraction efficiency of the photo-generated carriers, where different samples have different confinement potentials. The photo-current signal amplitude for each sample is expected to change with an increasing value of applied field in two possible ways: (1) increase due to higher extraction efficiency of carriers in the p-i-n junction and (2) decrease (or increase) as the applied field moves the of the e-h pair of the dipole away (or closer) to each other with respect to the dot growth direction. For the standard aspect ratio QD sample there is a drop of the signal peak amplitude –corresponding to ground state transition- with increasing field (see figure 3.3.7(b)) and this can be explained by the fact that by increasing the value of field, the e-h pair wave-functions move further apart and the spatial overlap is reduced with respect to the growth direction (see the picture in figure 4.3.5(b)). The drop of the signal amplitude for the range of applied reverse bias values is 15% and is associated directly with the ground state e-h dipole transition oscillator strength as the photo-current signal for the DWELL QD is absorption-like according to section 3.3. This drop in the oscillator strength also agrees well with a drop in amplitude by 20 to 25%, for similar values of field, reported in ref. [Fry 2000b].

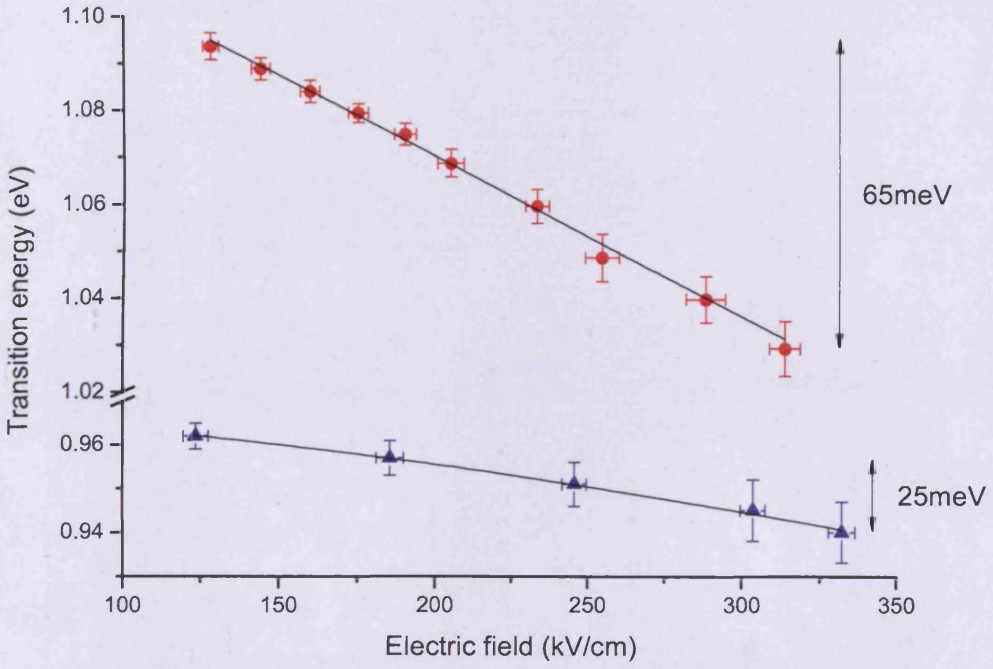

Figure 4.3.9 Energy shift of the ground state peak for the 10-period CQD sample-P622 (red circle) and DWEEL QD sample (blue triangle) with respect to a electric field.

For the case of the 10-period columnar-QD in figure 4.3.7, although there is a small increase in signal amplitude of the peak value which is not affected in terms of energy by the change of electric field and is represented by the arrow (2), the signal amplitude for the lowest energy transition is (arrow (1)) drops dramatically and loses almost 85% of the zero bias peak value. The difference between the signal intensity of these two peaks is significant and it shows that the wave functions overlap of the ground state transition (arrow (1)) decreases rapidly -with increasing field- for a dot of increased volume, which is also followed by a large energy shift illustrated in figure 4.3.9 for reverse bias values higher than 2.5 V. It follows that the oscillator strength reduces rapidly, for a range of field values from 130 kV/cm to 320 kV/cm, and the energy shift ΔE of the ground state transition, in this region, is almost linear represented by the equation $\Delta E \approx pF$. For a field range from 130 kV/cm to 320 kV/cm this shift is 65 meV and is much higher than this of the standard aspect ratio QD which is less than 20 meV. The strong energy shift should be described by a dipole where the electron is weakly confined inside the rod and a hole localised at the one end, i.e at the apex of the rod. In this field-regime, corresponding to a reverse bias range from 2.5 V to 9 V, the polarisability β can be considered to have a very small value, i.e $\beta \approx 0$, and the field can increase the e-h separation in a much greater extent than that in a standard aspect ratio QD due to the increased dot volume. It follows that a large red-shift in the transition energy due to the very high dipole moment is taken place, and this shift is accompanied by a rapid reduction of the oscillator strength. Thus, a value for the dipole moment p, for the ground state e-h pair, can be determined by fitting a linear equation to the data of figure 4.3.9. The slope of the graph gives a value $(5.4\pm0.4)\times10^{-28}$ Cb·m, corresponding to a large electron-hole separation of 3.4+/-0.2 nm which is much higher than the values of 0.4 nm [Fry 2000b], 0.5 nm [Findeis 2001] and 0.62 nm [Hsu 2001] given in the literature for a dipole separation in standard aspect ratio QD. It is also higher than that of ring-shaped QDs, where there was reported a separation up to 2.5 nm [Warburton 2002], investigated in "PL-field regime". However, the e-h separation of the dipole (3.4 nm) is 3-4 times less than the height of the columnar-QD (12.5 nm) and this can be attributed to the fluctuation of *In* composition along the rod as it is shown in figure 4.2.1(b)-page 72. Local potentials can confine the e-h pair in a smaller volume than that of the total volume of the rod.

In the case of the excited state transition, indicated by the arrow (2)-figure 4.3.7, this does not change in energy with respect to the electric field, i.e $\Delta E \approx E_0$. This is an indication that both

electron and hole wavefunctions are localised in the same spatial position inside the dot, i.e at the base of the dot, which has been demonstrated by calculated wavefunctions for a similar columnar-QD system using an 8 band-k·p model [Krenner 2008]. In this case the application of an electric field along the growth direction does not have an effect on changing the electron position inside the dot, due to the direction of the applied field under reverse bias, or the position of the hole which is strongly confined at the bottom of the dot due to the high local *In* concentration. This behaviour where there are transitions which shift weakly or very strongly in energy as a function of field due their spatial position -as it is studied in "PC-field regime" above- has been also observed in "PL-field regime" [Krenner 2008].

18-period InAs/GaAs SL columnar-QD

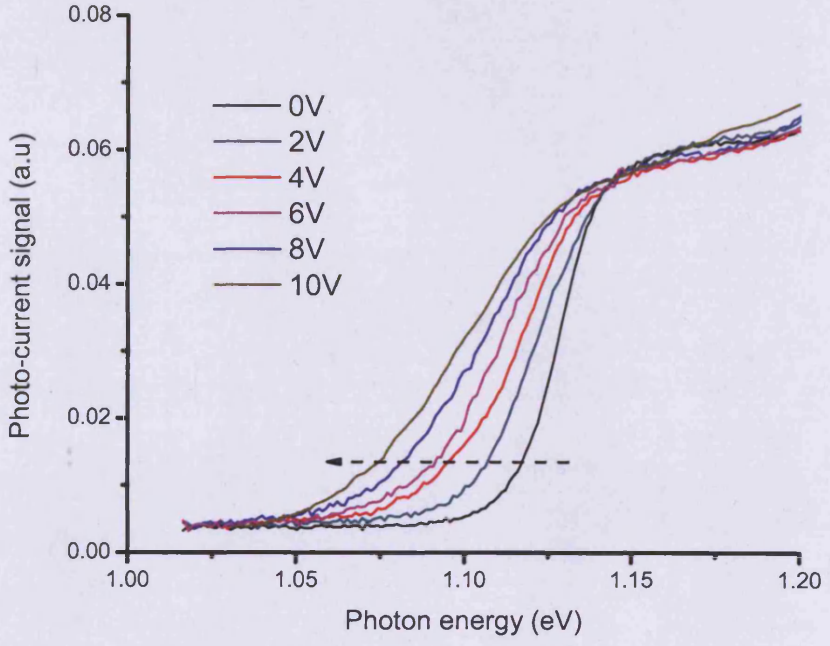

Figure 4.3.10 Field-dependent photo-current spectra for the 18-period CQD sample (P666) from 0V to 10V corresponding to a field range from 43 kV/cm to 330kV/cm.

Figure 4.3.10 shows the red-shift of the photo-absorption spectra with applied reverse bias for the 18-period columnar-QD sample (rod height 22.5nm). The amplitude of the Stark-shift is

similar to that of lower height 10-period columnar-QD structure for the same range of electric field. From figure 4.3.10 two mean characteristics of the photo-current spectra, which are useful for the explanation of the Stark shift in the "PC-field regime", can be derived. These are the follows:

(1) There is not any apparent peak signal amplitude shifting with applied field, like in the case of the 10-period columnar-QD, where an almost linear shift of the peak -corresponding to ground state transition-, within an applied field range from 130 kV/cm to 320 kV/cm, was illustrated (figure 4.3.9).

(2) The absorption-like tail of the spectrum gets broader with increasing value of reverse bias as is indicated by the dashed arrow on the plot.

According to an earlier discussion in section 4.3.3 it is expected, by almost doubling the rod height from 12.5 nm to 22.5 nm, that more states will be confined inside the rod and dipoles with higher values of dipole moment will exist due the increased rod volume. However, an increase of the dipole moment should enhance the amplitude of the Stark shift with applied field (i.e this can be explained by the simple case where $\Delta E \approx pF$), but at the same time the value of the oscillator strength, i.e determined by the overlap of the wave functions, is expected to exhibit a even more rapid decrease or increase with applied field, depending on which direction the field moves the e-h wave functions, than that in the case of the 10-period columnar-QD. Thus, transitions where their wave functions showing strong overlap (or weak overlap) for a given value of electric field can exhibit a very rapid decrease (or increase) of their overlap by even a small change of the field. Therefore, the characteristic (1) of the photo-current spectra, mentioned above, is due to two effects taking place at the same time; first there are more states contributing to the overall photo-current signal and second each transition's oscillator strength changes (increases or decreases) rapidly with respect to electric field, therefore the shift in energy for a specific transition cannot be resolved in the "PC-field regime". The red-shift of the photo-absorption spectra with applied field in figure 4.3.10 is due to an overall effect, where photo-generated carriers corresponding to different transitions -which these transitions experience a rapid change in their oscillator strength with respect to field- contribute to the photo-current signal amplitude for a given field value. The characteristic (2) of the photo-current spectra, where a broadening of the absorption tail is observed, confirms further both of these effects mentioned above. However, in the case of the "PL-field regime", where the field along the rod is changing by only a few kV/cm, the

gradual increase (e-h dipole moves close to each other with respect to the growth direction) or decrease (e-h dipole moves away from each other) in the ground state e-h wave function's overlap can be mapped from the shift of the PL spectra, therefore giant e-h dipoles have been reported [Petroff 2007], where the e-h separation is related directly to the nominal rod height.

C] Quantum Rods

To study the CQSE in high-aspect ratio columnar-QDs, i.e QRs, field-dependent photo-current measurements for the 1st generation 30-period QR consisting 1-stack of columnar-QDs and for both 2nd generation QR samples (see table 4.2.1 and 4.2.2 for further details) are obtained. In figure 4.3.11, the photo-current spectra with respect to external applied field for the 1st generation and the 2nd generation 30-period QR sample (rod heights: 1st gen: 35.1nm and 2nd gen: 70nm) are shown.

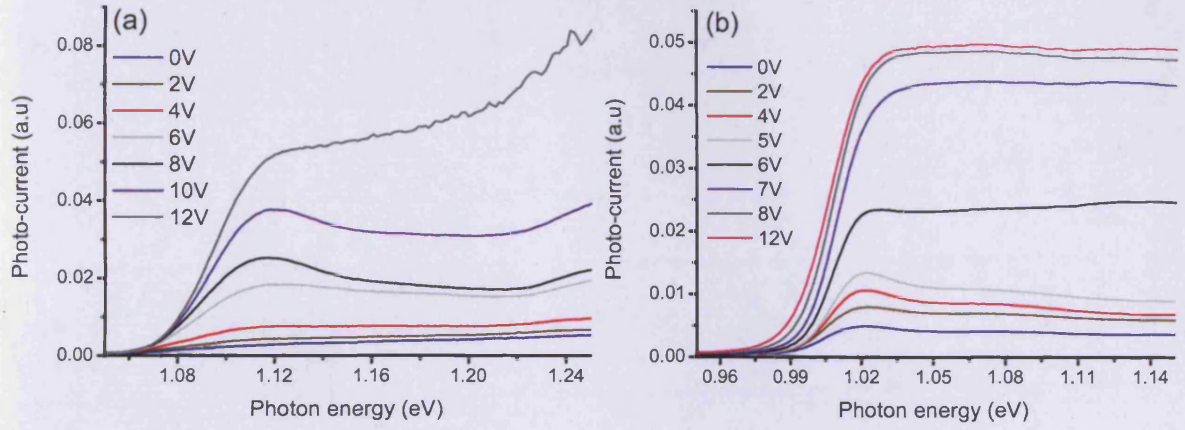

Figure 4.3.11 Photo-current spectra for the (a) 30-period 1st generation QR (P906) and (b) 35-period 2nd generation QR with respect to reverse bias.

For both of the samples there is an enhancement of the excitonic absorption feature in the low part of the energy spectra with increased values of reverse bias. The strongest photo-absorption peak appears at 8V and 4V for the 1st and 2nd generation QR respectively. For higher values of bias the peak gets smoother. Excitons absorb light of lower energy than that of the semiconductor band edge. Thus, any estimation of the band-edge energy shift of the absorption spectra with respect to applied field is not possible due to the field dependent strength of the excitonic absorption. However, the exciton absorption strength is expected to

decrease with increased temperature, where in this case the exciton can obtain the necessary energy to ionise.

In figure 4.3.12 photo-current measurements with respect to temperature -for temperature greater that room temperature- are illustrated for the 2nd generation QR (P968) under a reverse bias value of 4V, i.e where the excitonic absorption strength is maximum. For temperature higher than 360K the excitonic peak is less pronounced and at 420K is not apparent at all.

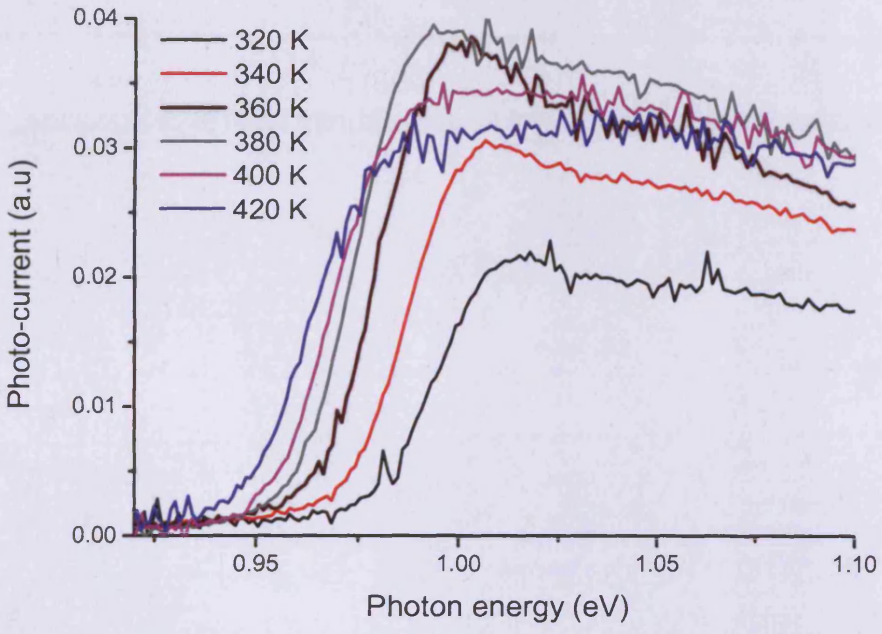

Figure 4.3.12 Photo-current spectra for the 2nd generation of 30-period InAs/GaAs QR (P968) under 4V of reverse bias for a temperature range of 320 to 420K.

In order to investigate the shift of the photo-current spectra field-dependent measurements are obtained at 420K (figure 4.3.13(a)), where the spectra band edge is not screened by the exciton photo-absorption. In figure 4.3.13 (b) the spectra are normalised in amplitude for a photon energy around 1.02eV corresponding to a region where the photo-current signal appears to be flat.

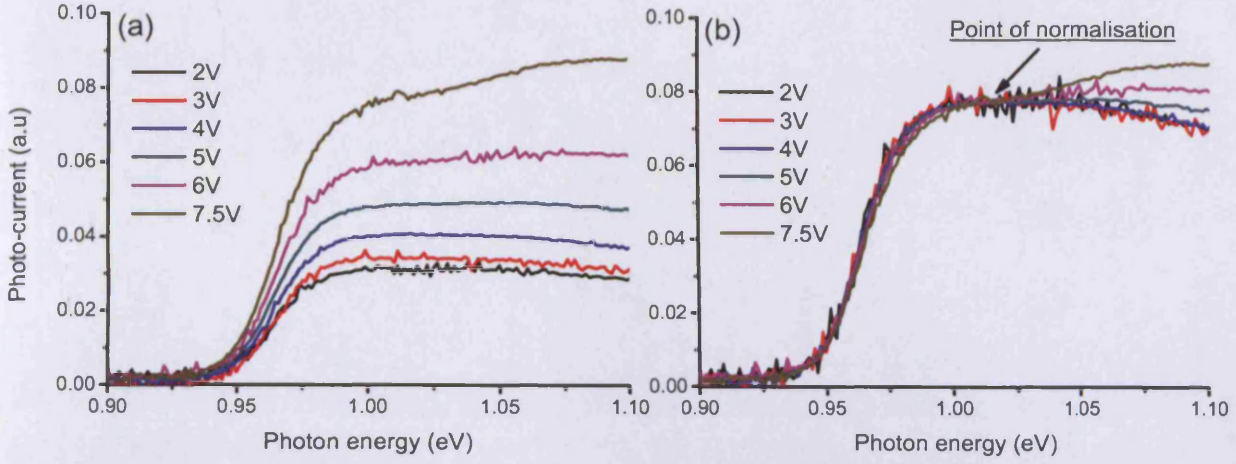

Figure 4.3.13 (a) Photo-current spectra for the QR P968 with respect to reverse bias at 420K, where in (b) have been normalised in amplitude in order to investigate the Stark-shift.

Given that the estimation of the absorption edge shift of the spectra with respect to applied field have an associated error which is due to the choice of the point where the spectra are normalised and to the SNR there is no observable shift of the cut-off wavelength as illustrated in figure 4.3.13(b). In the case of the QR samples the signal amplitude of the photo-absorption tail is associated with photo-generated carriers coming from an increased number of closely spaced energy states, compare to that of lower aspect ratio 10- and 18-period columnar-QDs, due to the intermediate situation between 0-D and 1-D confinement. At the same time due to the elongated-shape of the dot in the growth direction the spatial separation of e-h pairs, determining their transition oscillator strength, can change very rapidly with applied field as the electrons are spread out over the whole dot volume. Following the same analysis for the edge shift of the photo-absorption spectra with applied reverse bias for the 18-period columnar-QD in page 94 the overall observed energy shift can then be smaller than the shift in energy of any individual transition. However, in the case of the extremely high aspect ratio 30-period QR, due the high number of energy transitions, there is no observable shift of the band edge in the studied field regime.

4.3.5 *Discussion*

The dramatic enhancement of the electro-optic effect which is observed by changing the dot shape from that of the DWELL QD to that of the lowest aspect ratio columnar-QD samples (aspect ratio 0.62:1 and 1.125:1), is promising for the fabrication of optical modulation/switching devices in optical telecommunication. However, there are limitations in further enhancement of the Stark-shift amplitude by increasing the height of the dot, as it is shown in the "PC-field regime", which can be summarised to the two following basic parameters, with the second to be a combination of two effects taken place at the same time:

(1) *The fluctuation of In composition along the rod* where local potentials can confine the e-h pair in a smaller volume than that of the total volume of the rod as is observed in the case of the lowest aspect ratio 10-period SL columnar-QD. For the field values 130 to 315 kV/cm, where there is an almost linear energy shift of the ground state with respect to the electric field, a dipole of e-h separation (3.4 nm) of a value 3-4 times less than this of the columnar-QD height (12.5 nm), derived. An additional confirmation for the strong local potentials exhibit along the rod is the presence of e-h pairs that are strongly localised inside the dot as it is found that their transition energy does not change with a variation of the electric field value.

(2) *The appearance of additional states & the rapid change of the transitions oscillator strength with the applied field, which both are due to the dot elongation in the growth direction.* By almost doubling the dot height to a value of 22.5 nm the amplitude of the Stark-shift remains to similar levels with that of 12.5 nm height dot. The induced Stark red-shift of the photo-absorption spectra shown in figure 4.3.9 -page 91- is an outcome of contribution of photo-generated carriers corresponding to different energy transitions, where the carrier's wavefunctions overlap change rapidly with the electric field, in the case of the "PC-field regime". By further increasing the dot height- fabricating QRs- the confinement along the growth direction becomes even weaker and many additional energy transitions, confirmed by calculations of the electronic states within 3-D approach in the eight-band k·p approximation [Li, 2008(b)], contribute to the photo-current spectrum. For the extremely high aspect ratio 30-period QR, there is no observable shift of the spectra band edge with applied field.

In this section also it was shown that by increasing the QD height - fabricating high-aspect ratio columnar-QDs- can be either obtained polarisation-insensitive devices for a possible application in SOA or devices where light of TM polarisation is absorbed stronger than that of TE near the band-edge. A TM-dominant emission property for the latter device is reported in details in the following section.

4.4 Laser characteristics of extremely high aspect ratio Columnar Quantum Dot

4.4.1 Light polarisation and wave-guiding

The Amplified Spontaneous Emission (ASE) spectra at room temperature (20 ^{0}C) for the extremely high aspect-ratio 35-period SL QR for both TE and TM light polarisations are illustrated in figure 4.4.1.

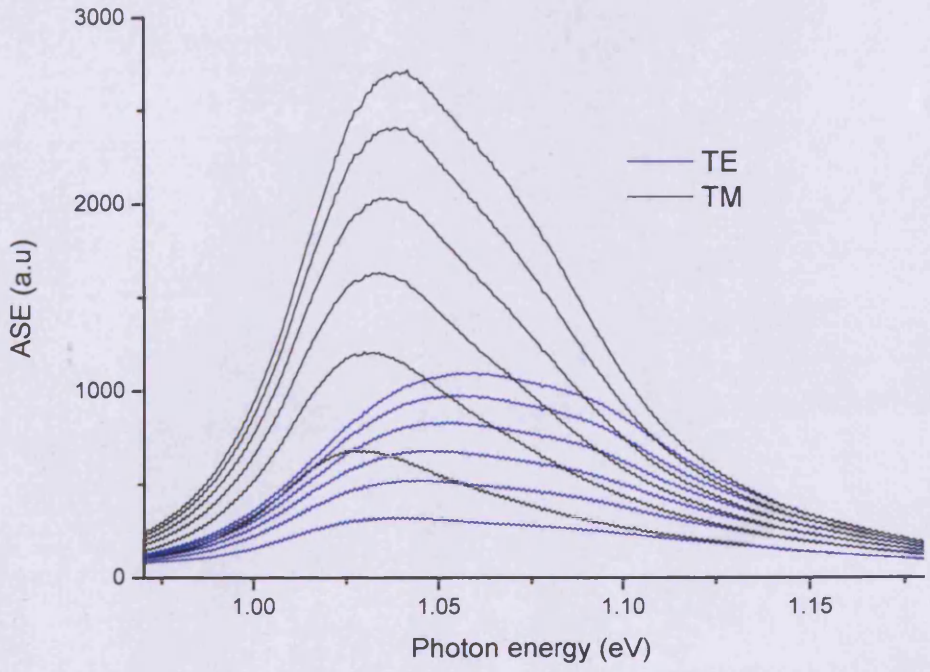

Figure 4.4.1 Amplified Spontaneous Emission (ASE) spectra for the 35-period InAs/GaAs SL QR for both TE and TM polarisations at drive current densities from 111 to 667 A/cm^2.

As it is expected from edge photo-current measurements in earlier section of this chapter, in figure 4.2.5(a), the plot shows that at the low energy part of the spectrum the dominant light emission of the QR is of TM polarised light where the emission is due to e-lh transition.

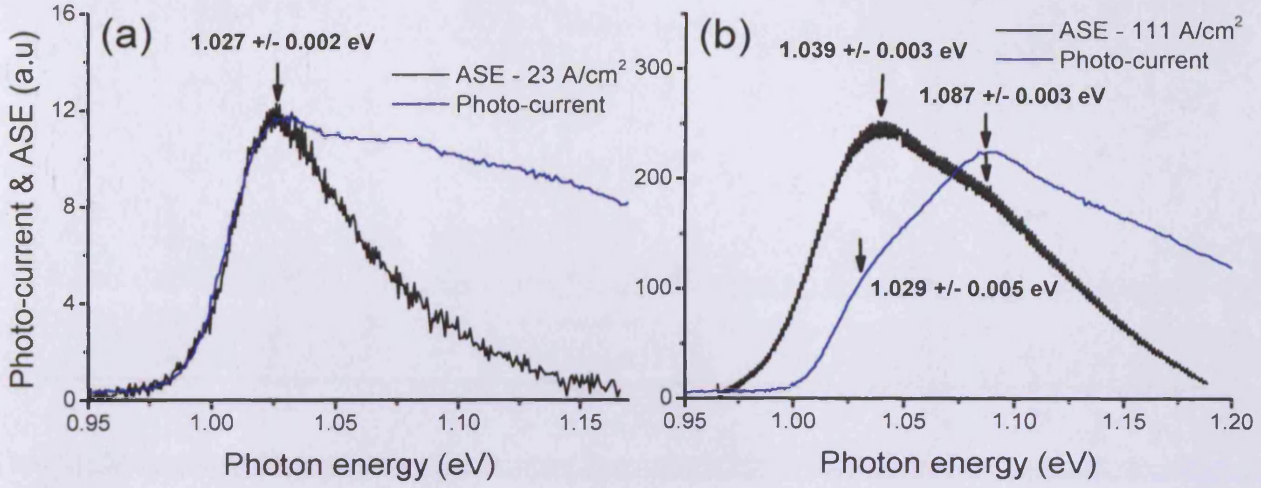

Figure 4.4.2 Comparison of ASE and photo-current measurements for (a) TM and (b) TE polarisation.

In order to verify the different peak intensity values appearing in the polarised-selected ASE spectra, figure 4.4.2 demonstrates a comparison between the E-PVS and ASE measurements for the two polarisations TE (figure 4.4.2(a)) and TM (figure 4.4.2(b)), where the photo-current signal amplitude is normalised to the same level with that of ASE spectrum. Figure 4.4.2(a) represents data taken for TM polarisation where the peak value of very low current density ASE spectra coincides with this of photo-current for photon energy at around 1.027 eV. For the case of TE polarisation -in figure 4.4.2(b)- in order to identify the different energy state transitions, in comparison with this of photo-current absorption, an ASE spectrum of higher drive current density than this of TM (figure 4.4.2(a)) is shown. The first peak in low energy part of the ASE spectrum -at 1.039 eV- is associated with the peak value of photo-current spectrum at 1.029 eV and represents an e-lh transition as can be seen both in TE and TM photo-absorption spectra. However, an approximately 10meV energy blue-shift of the ASE peak value with respect to this of photo-current spectrum is due to band filling. This must be so, since as the current density increases electrons and holes occupy higher energy states of the bands, and therefore recombine emitting light of higher photon energy.

There is also a second peak in ASE spectrum approximately 48meV apart from the first and this peak value agrees well with this of photo-current spectrum. At that particular photon energy this peak is also obvious in the TM ASE spectrum of similar current density value with that of TE (not shown here). This is further confirmed by the calibrated polarisation-selective photo-current measurements (figure 4.2.5(a) – page 77) where the TE and TM photo-current at this photon energy are almost of the same amplitude as well. This suggests that there is a lh-hh band-mixing effect for higher energy states than that of the ground state. Both photo-current and ASE measurements demonstrate that the ground state transition is of e-lh type, with an estimation of transition matrix element ratio $M_T(TE)/M_T(TM)$ equal to 0.14 close to band-edge photon energy (see figure 4.2.6(b)-page 77). This is followed by a laser emission at TM polarisation as shown in figure 4.4.3 at room temperature (20^0 C) and at a wavelength of 1194nm (1.038eV). However, there is an obvious TE polarisation lasing emission just at threshold, having the same threshold current density and peak emission wavelength value with this of TM (see later figure 4.4.4(b)). The dual polarisation property of lasing emission, corresponding to the same threshold current density for both polarisations, cannot be explained from the ASE and photo-current spectra, which show a lh-type ground state in the valence band. Therefore, it would be expected that TM lasing only would occur due to the lh-like ground state.

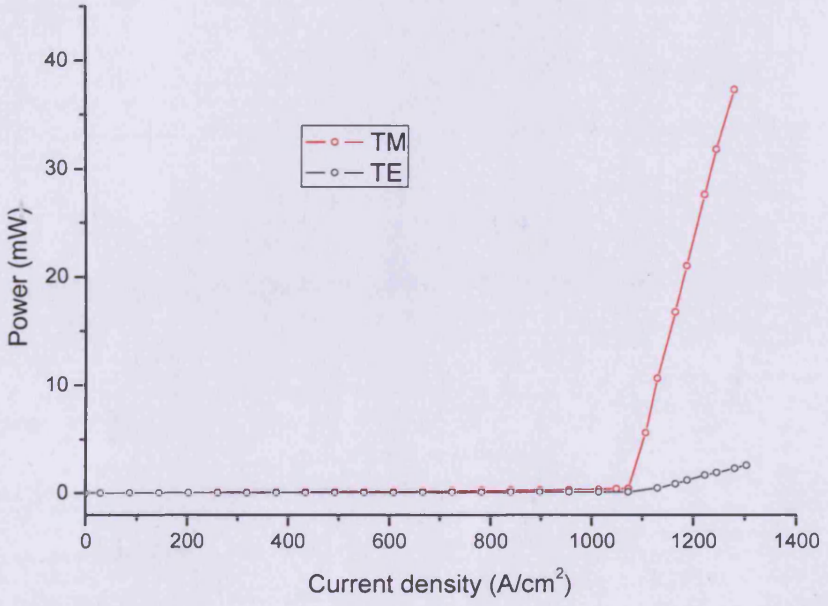

Figure 4.4.3 Room temperature TM-dominant lasing emission from the 35-period InAs/GaAs SL QR with a threshold current density of 1.07 kA/cm^2.

In order to investigate the polarisation properties of the 35-period columnar-QD sample the near field emission and the light spectrum are captured just above threshold for laser devices of two different ridge widths, 11 and 23 μm. The results are summarised in figure 4.4.4.

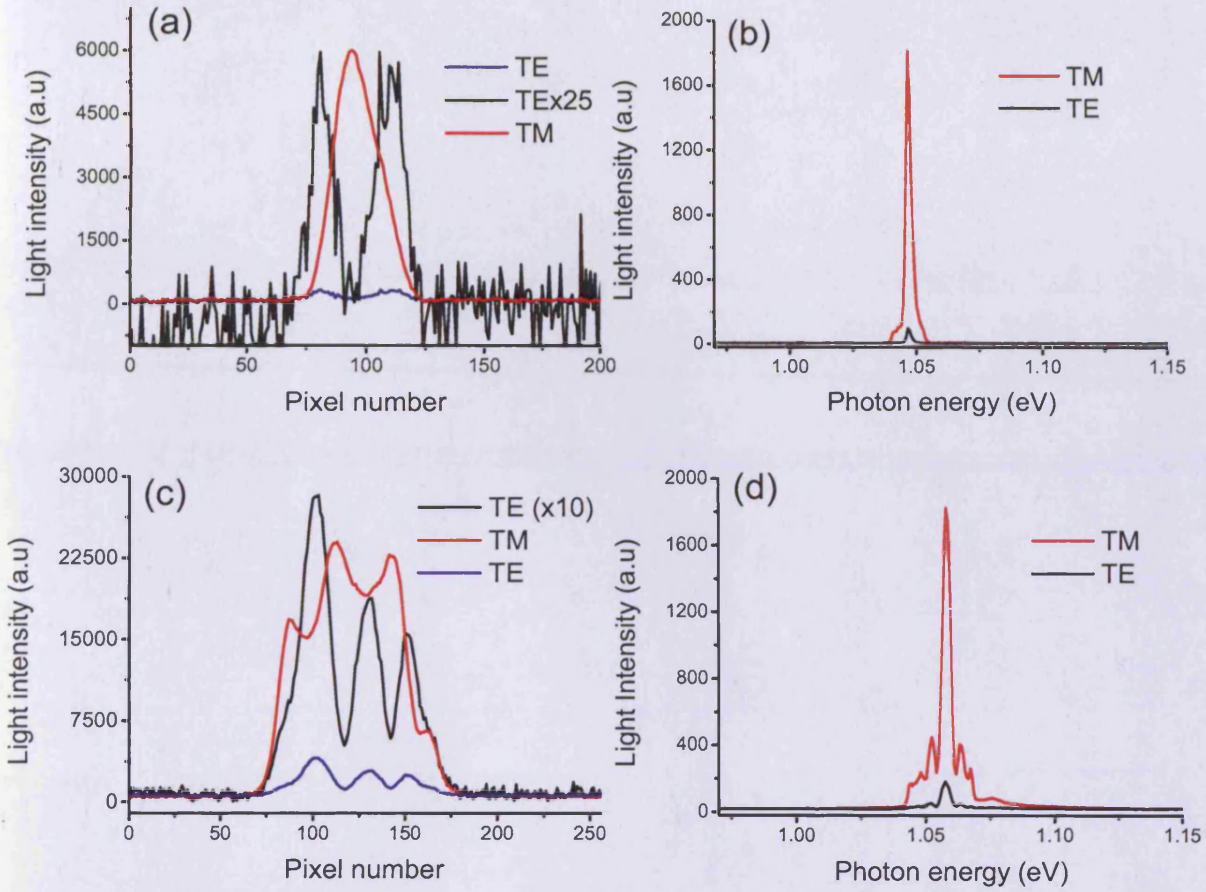

Figure 4.4.4 Near field emission along the laser diode x-direction (a) & (c) and emission spectra (b) & (d) -just above threshold- for two 35-period InAs/GaAs SL QRs RW devices of 11 μm and 23 μm ridge width respectively. The emission characteristics are taken at different temperatures (230 K and 260 K for 23 μm- and 11 μm-RW respectively).

The near field emission for the two RW laser diodes of 11μm and 23μm show that there is a spatial separation between the maximum light intensity peak values of the two orthogonal polarisations TE and TM. Plot (a), which refers to the 11μm-RW, shows that at the point – across the facet- where the maximum light intensity of TM polarised light appears, there is no

TE polarised light coming from the RW. On the contrary, the light emission of the latter polarisation appears near to and around the TM-maximum, where the level of TM-polarised light is low. For the case of the 23 μm-RW similar light emission behaviour is illustrated in plot (c), where the RW device lase in different spots across the facet, with light intensity to peak between TE and TM polarisation with a spatially alternative way across the facet. However, it is noticed, both from the near field (a) and (c) and from the lasing spectra (b) and (d), that as the ridge width decreases the total TM/TE light intensity ratio -above threshold- decreases. This polarisation-dependent near field emission pattern as well as the variation of relative overall TM/TE light intensity with respect to the ridge width indicates that this characteristic emission should be due to the 2-D ridge wave-guiding property of the laser diode, where components of both polarisations (TE and TM) can exist at the same time in a single mode, contributing both to the lasing mode above threshold. However, it should be noted that the lasing emission in both polarisations requires the material to provide TE as well as TM optical gain, where this should be the case for the 35-period sample.

In a similar ridge waveguide optical fiber structure [Kaiser 1973], designed for single mode operation, it was shown that there can exist two different polarisations in a single mode, i.e there are two fundamental modes E_{00}^{x} and E_{00}^{y} corresponding to polarisation in the x and y direction respectively. The TE-TM coupling leads to a leakage of power from the ridge [Adams 1981] and the degree of leakage depends on the ridge height, determined by the etching depth, and the ridge width [Ogusu 1979]. Therefore, in the case of the 35-period QR RW laser diodes it should be expected by decreasing further the ridge width to reduce the TE light intensity with respect to TM, without being able to cancel it, paying as well a penalty in the output light power.

During the laser measurements an increase of the threshold current density and an apparent filamentation in the near field emission was observed when measurements were repeated several times. Especially at high temperatures, where the devices were driven harder to reach the threshold current density, the degradation was occurring even faster. Therefore, only at low temperature the devices were driven to a current density up to 7 or 8 times the threshold current density to monitor the laser action at high current densities. Figure 4.4.5 shows

spectra for a current value of almost 1.5 times the threshold current, where a two-state lasing occurs with TM-dominant polarisation emission for both states. Two lasing states have been reported for a standard QD [Markus 2003] or for a QD incorporating tunnel injenction [George 2007] with an energy separation between the two-states of 65 or 80 meV respectively. In the case of the 35-period QR this separation is around 18meV. Multi-wavelength laser characteristics of columnar-shaped InAs/GaAs QD lasers have also been reported elsewhere, with a separation of the lasing spectral lines between 16 to 19 meV [Sugawara 1999b]. This is attributed to the fact that dots of different size, and therefore of different energies, start to lase independently –in order in which the required threshold gain has been obtained- due to their spatial localisation.

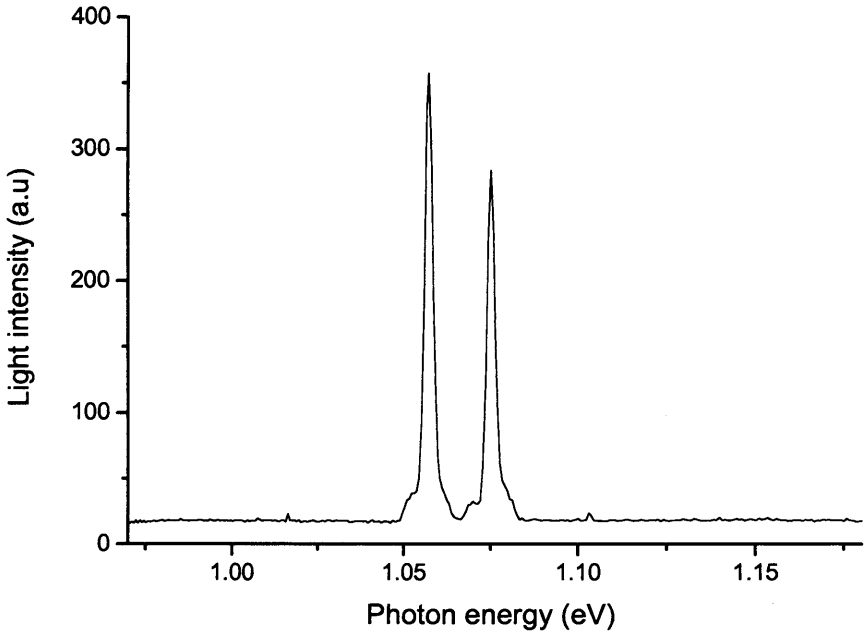

Figure 4.4.5 TM-dominant two states lasing emission at 230K for a laser device of length of 3mm for a current density of 0.38 kA/cm^2.

4.4.2 Threshold current measurements versus temperature

The threshold current density values as a function of temperature for a range from 200 K to 300 K are illustrated in figure 4.4.6, where a noticeable increase of threshold current density at elevated temperatures occurs. This is a general characteristic that has been observed in QW and QD structures due to the increase of thermally activated leakage current and to the increase of the spontaneous emission originating from higher sub-bands in QWs. Gain saturation in QDs has also been observed due to escape of carriers in the wetting layer at high temperatures [Matthews 2002]. This can be a possible reason for the abrupt increase of threshold current density for temperatures higher than 260K.

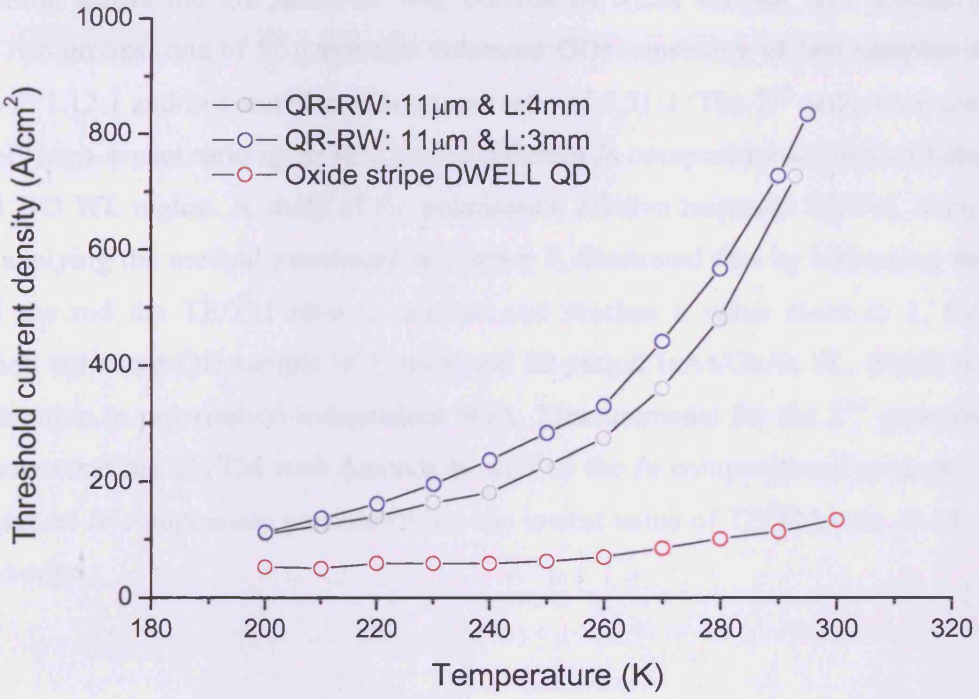

Figure 4.4.6 Temperature-dependent threshold current density for a 35-period InAs/GaAs SL QR (P990), ridge width 11 μm and diode length of 3mm (blue circle) and 4mm (gray circle), and an oxide stripe DWELL QD as appear in ref. [Scandall 2006]

4.5 Summary

In this chapter, I have outlined the dependence of the TE/TM optical response of InAs/GaAs columnar-QDs to the QD aspect ratio and the *In* compositional contrast between the QR and the 2-D WL region. Also, an analytical study of the QCSE has shown that the direction and amplitude of the Stark-shift is aspect-ratio dependent. A dominant TM polarised laser light emission was observed from the 35-period InAs/GaAs SL QR.

In Section 4.2, I started by describing briefly the geometry characteristics of the columnar-QD materials studied in this chapter and I gave details such as the aspect ratio and the *In* composition across the QR and 2-D WL, derived by TEM images. The studied samples formed two groups; one of 1st generation columnar-QDs consisting of two samples of aspect ratio up to 1.12:1 and two samples of an aspect ratio of 3.51:1. The 2nd generation are QRs of extremely high-aspect ratio up to 10:1 and of different *In* compositional contrast between the QR and 2-D WL region. A study of the polarisation relative response TE/TM, using E-PCS and by applying the method introduced in chapter 3, illustrated that by increasing the aspect ratio of the rod the TE/TM ratio is reduced and reaches a value close to 1, for the 1st generation columnar-QD sample of 1 stack and 30-period InAs/GaAs SL, which is desired for application in polarisation-independent SOA. Measurements for the 2nd generation QRs have shown that the TE/TM ratio depends as well on the *In* compositional contrast. The QR of the highest *In* composition contrast shown the lowest value of TE/TM ratio -0.14- close to the band-edge.

In section 4.3, I began by expressing the external applied reverse bias in terms of internal electric field, using a semiconductor simulator, in order to compare the QCSE of the varied aspect-ratio columnar-QDs. I first introduced the much studied Stark shift in an InAs/GaAs QD system -where the energy shift is described by the quadratic equation $E = E_0 + pF + \beta F^2$ [Fry 2000a]- by presenting field-dependent edge photo-current measurements for the standard aspect ratio QD sample.

By studying dots of different heights and aspect ratio, the amplitude and of the absorption spectra band-edge shift with respect to electric field is found to be related with the dot aspect ratio. For the case of the lower aspect-ratio 1st generation columnar-QD samples (asp. ratio 0.63:1 and 1.12:1), a dramatic enhancement of the electro-optic effect was observed, which is promising for the use of these material in optical telecommunication (i.e optical modulators/switches). In addition the limitations concerning the further enhancement of the electro-optic effect by fabricating even higher aspect ratio columnar-QDs were analysed and discussed here. The two main parameters contribute to the quenching of the large Stark-shift - as it is studied in "PC-field regime"- are: (1) the fluctuation of *In* composition along the rod, where the e-h dipoles can confine in smaller volume than that of the total volume of the rod due to the presence of local potentials along the rod and (2) the appearance of additional states & the rapid change of the transitions oscillator strength with the applied field, which both are due to the dot elongation in the growth direction. In the latter parameter the Stark-shift of the photo-absorption spectra is an overall effect of photo-generated carriers corresponding to different transitions, where their oscillator strength changes rapidly with field. By further increasing the dot height- by fabricating extremely high aspect ratio QRs, there is no any observable shift of the band-edge as illustrated for the QR of aspect ratio 10:1.

In section 4.4, ASE spectra for the extremely high aspect-ratio 35-period InAs/GaAs columnar-QD sample shows emission from both TE and TM polarisations, with TM to be the dominant. The different emission peaks as appears in polarised ASE spectra agrees well with those of edge photo-current spectra. I then, demonstrate a TM-dominant laser emission at room temperature (20^0C) with a threshold current density of 1.07 kA/cm^2. The dual polarisation emission above threshold was also analysed and attributed to the ridge waveguide properties, where the nominal TM mode consists of a small TE component, and to the fact that the studied material provides optical gain in both polarisations. By increasing further the current density a two-state lasing with a small separation of 18meV is observed. Threshold current density measurements with respect to temperature show an abrupt increase of the threshold current density above 260K.

Chapter 5 - Summary and future work

5.1 Motivation recap, background and Summary

In this thesis I have produced results with the aim to examine the optoelectronic properties of InAs/GaAs columnar-QDs and compare them with those of a standard aspect ratio QD. Each section begins with a motivation recap with the experimental investigation and results analysis obtained in this work summarised in the following bullet points.

5.1.1 Polarisation response of Columnar-Quantum Dots

Motivation/Background

In general, PL [Sugawara 1999] or EL [Ridha 2008a] measurements have been taken for different columnar-QD systems in order to identify the polarisation properties of these materials for possible application in polarisation-insensitive Semiconductor Optical Amplifiers (SOAs). For the columnar-QD materials studied here prior to their fabrication the polarisation properties has been modelled and theoretically investigated by using eight-band k·p model calculations [Ridha 2008b] with aim to predict the TE/TM optical response dependence on dots aspect ratio and *In* compositional contrast between the rod and the 2-D WL region. However, polarisation sensitive photon emission measurements do not provide information on the relative TE/TM optical absorption strengths which itself determines the gain in an amplifier. Here in order to study the polarisation properties of these novel materials a new –more fundamental- approach was proposed, which allow obtaining the TE/TM optical generation ratio for a wide wavelength range including that close to the band edge, which is of the most importance.

In this thesis:

► For the investigation of the polarisation properties of columnar-QDs, with aim to compare them with this of a standard shape QD, a novel experimental technique in chapter 3 was

suggested by using edge photo-absorption spectroscopy. This technique requires a new experimental configuration, where the orientation of the device-polariser relative to the monochromator's output slit is changed by 90^0, providing a mean to calibrate the relative TE/TM optical response –for both E-PVS and E-PCS- and measure the fundamental TE/TM optical generation rate ratio.

► The suggested method is verified by application to different type of strained InGaP QW. The TE/TM photo-voltage signal spectra ratios for the tensile and compressive strained QW samples were found to be 0.24 and 10 respectively, agreeing well with the theoretical predicted TE/TM transition matrix elements ratio values. For the case of the compressive strained QW sample this ratio theoretically should be infinity. This deviation was mainly attributed to the fact that the light is focused onto the edge of the sample and not precisely normal to it.

► By applying the method above to a group of columnar-QD samples and a standard aspect ratio QD, which was used as a reference sample, the dependence of TE/TM optical response of columnar-QDs to the dot's aspect ratio and the *In* composition contrast, which determine the biaxial strain induced into the rod, was shown and explained. The studied samples were divided into two groups of columnar-QDs defined by the generation type; the 1^{st} generation is of high aspect ratio up to 3.51:1 and the 2^{nd} generation of extremely high aspect ratio up to 10:1 and of different *In* compositional contrast with this of 1^{st} generation. The two main outcomes explaining the dependence of the fundamental TE/TM optical response of columnar-QDs are outlined as follows:

- ***The TE/TM ratio decreases with an increase in dot height.*** The TE/TM ratio near the band edge for the columnar-QD is reduced approximately from 6.5 for the standard aspect ratio QD, to 4.5 and 3 for a columnar-QD of aspect ratio 0.63:1 and 1.12:1, respectively. The two columnar-QDs have the same diameter value (different height) and similar values of *In* compositional contrast.

- ***The TE/TM ratio decreases with an increase in In compositional contrast.*** The values of TE/TM ratio near the band-edge of the extremely high aspect ratio QRs, but of similar aspect ratio, were found to be 2 (aspect ratio 7-10:1) and 0.14 (aspect ratio 7.5:1). The difference in the relative TE/TM optical response is due to the *In*

composition in the QR area being 51% and 44% for the sample of lowest and highest TE/TM ratio respectively.

► For the two 1st generation samples of 3.51:1 aspect ratio the amplitude of the photo-current spectra is similar for the two orthogonal polarisations and this has potential application in polarisation-insensitive SOAs. Although these two samples were grown to have similar characteristics (only the number of QD stacks is different) the 1 stack sample showed a TE/TM ratio close to 1 while the 3 stack columnar-QD reached a value of 2 close to the band edge. The cause of this deviation is not clear at the moment, however the most likely cause is a difference in *In* composition between the two samples due to unintentional growth differences.

5.1.2 Quantum-Confined Stark Effect in Columnar-Quantum Dots

Motivation/Background

The QCSE in a standard aspect ratio InAs/GaAs QD material has been studied by normal-incident photo-current spectroscopy [Fry 2000b] and the energy shift caused by the application of an external electric field parallel to the semiconductor growth direction, is described by the equation $E = E_0 + pF + \beta F^2$. The field-dependent photo-current measurements showed a permanent dipole orientation with a positive dipole moment, i.e the hole is localised above the electron inside the dot [Fry 2000b]. By increasing the dot height field-dependent low-temperature PL measurements for a Quantum Posts (or Quantum rods) of high aspect ratio, where the post length was varied from 10 nm to 60 nm, have shown that values of dipole moment 40 times higher than those of QDs of standard shape can be found [Petroff 2007], corresponding to extremely high values of e-h separation inside the post [Krenner 2008]. These enhanced electro-optic properties which are desired for application in electro-optical modulation and optical switching are studied here in a higher and wider range of applied field, i.e in the "PC-field regime", in order to have a complete picture of the QCSE in these materials. This leads to new information about the Stark shift amplitude and direction which is found to be closely linked to the aspect ratio of the columnar-QD samples studied here.

Results taken in this thesis are summarised as follows:

► By using temperature- and field-dependent edge-photocurrent spectroscopy the two main escape mechanisms, i.e tunnelling and thermal excitation, of the photo-generated carriers from the dot states of a standard DWELL sample has been discussed in chapter 3. It is shown that at room temperature the photo-current spectrum is absorption-like representing the dot's true absorption spectra, therefore the 15% decrease in signal amplitude –corresponding to ground state- for a internal electric field range from approximately 50 to 320 kV/cm is associated with the reduction of the e-h pair oscillator strength. The above results are then used as a reference in chapter 4 for the study of QCSE in dot of higher aspect ratio, i.e columnar-QDs and QRs.

► From the characteristics of the Stark shift analysis of the 1st and 2nd generation columnar-QD samples the results can be summarised in the two following categories:

- ***Lowest aspect-ratio 1st generation Columnar-QDs.*** For the 10- and 18-period InAs/GaAs SL columnar-QDs, having a height of 12.5 and 22.5nm and an aspect ratio of 0.63 and 1.12 respectively, an enhancement of the electro-optic was observed. In the case of the lowest aspect ratio 10-period columnar-QD, transitions that are shifted very weakly or very strongly with applied field were indicated. For the latter case, a large and linear red-shift of the ground state transition, i.e 65 meV compared to that of 20 meV for the DWELL QD in a field range from 130 kV/cm to 320 kV/cm, was observed which was accompanied by a rapid reduction of the oscillator strength with field. Thus, in this field range, a high value of positive dipole moment value was derived corresponding to an e-h separation of 3.4+/-0.2 nm inside the rod, which is almost 7 times higher than that of a standard aspect ratio QD and 3-4 times less than that of the rod height. The deviation between the e-h separation and the rod height was attributed to the local *In* compositional fluctuation along the rod, which confines the carriers in a volume less than that of the total volume of the rod. In the case of higher aspect ratio columnar-QDs the Stark-shift is of the same amplitude (18-period CQD) or of smaller amplitude (2nd generation QRs-see below) and this explained as an outcome of two effects taking place at the same time; (1) there are more states contributing to the overall photo-current spectra and (2) these transitions experience a very rapid change in

their oscillation strength -in the studied field range regime, i.e "PC-field regime",- as the rod volume increases.

• ***High aspect ratio Columnar-QDs, i.e Quantum Rods.*** By further increasing the dot height- fabricating QRs- the confinement along the growth direction becomes even weaker and many additional energy transitions, confirmed by calculations of the electronic states within 3-D approach in the eight-band k·p approximation [Li, 2008(b)], contribute to the photo-current spectrum. For the extremely high aspect ratio 2nd generation 30-period QR, there is no observable shift of the spectra band edge with applied field in the "PC-field regime".

5.1.3 Laser characteristics of extremely high aspect ratio Columnar-Quantum Dot.

Motivation/Background

Control over the polarisation for columnar-QD systems grown by different approaches has been reported [Kita 2002] [Li 2008a], with evidence of net TM optical gain [Kita 2006] [Yasuoka 2008b]. However, until now a TM lasing emission from any InGaAs material has not been reported. By using the proposed method of calibrating the relative TE over TM photo-absorption response in chapter 3, it was observed for the extremely high aspect ratio 35-period InAs/GaAs columnar-QD sample a TM-dominant photo-absorption, i.e the TE/TM ratio of the photo-current spectra near the band edge was 0.14. Thus, the emission properties of these samples are studied here and show a TM-dominant amplified spontaneous and lasing emission, which agrees well with the TM-dominant photo-absorption strength.

Here,

► A TM-dominant laser emission at room temperature (20^0 C) with emission wavelength at 1.194 μm and a threshold current density of 1.07 kA/cm^2 is observed. The light emission above threshold and at both orthogonal polarisations was analysed by obtaining the near field emission from laser diodes of different ridge widths. The presence of both polarisations in lasing emission was attributed to the ridge waveguide properties, where for the nominal TM mode a small TE component can exist at the same time, contributing both to the lasing mode above threshold for a material structure that provides both TE and TM optical gain.

Temperature-dependent threshold current density measurements for a temperature range from 200K to 295K show that there is an abrupt increase in threshold current density above 260K, which requires further investigation.

5.2 Overall summary

In this thesis the fundamental TE/TM optical response of a set of InAs/GaAs columnar-QD was analysed by proposing a new method in order to measure the relative TE/TM optical generation rate ratio using edge photo-current spectroscopy. The dependence of polarisation response on the dot aspect ratio and the *In* compositional contrast between the rod and the 2-D WL regions was identified. By applying photo-current spectroscopy, the dependence of the amplitude of the band edge shift of the spectra, with respect to electric field, on the columnar-QD aspect ratio was analysed and information about the wave function's behaviour under the presence of electric field was obtained. Finally, TM-dominant lasing emission was observed in the case of extremely high aspect ratio columnar-QD.

5.3 Future work

In this thesis the optoelectronic properties of a set of columnar-QD materials grown by a new approach were analysed. However, due to the novelty of these structures and their interesting properties shown here there is a lot of spaces for further research as a few questions have arisen.

From the study of QCSE in lowest aspect ratio columnar-QD samples it was possible to extract information about the amplitude of the Stark-shift and how the *In* variation along the rod influences the e-h dipole under the presence of an electric field. However, there is no information about the orientation of the dipole in the case of zero field because there is no data taken for negative or positive –in a regime less than the junction's "built-in" field-values of electric field. An interesting contribution in this work would be the growth of such material structures with inverted p-i-n regions, i.e two identical in growth columnar-QDs of

n-i-p and p-i-n junctions, which allow measurements of the Stark shift to taken both for negative and positive values of internal field. A further investigation of the aspect ratio dependence of the dipole orientation could lead to fabrication of columnar-QDs with maximum overlap of electron and hole wave functions for optimum laser performance.

Optical gain measurements for the lowest aspect ratio columnar-QD of TE-dominant gain have already been reported by our collaborators [Ridha 2008b] and an investigation of TM-dominant gain has recently been reported in ref. [Yasouka 2008b], without a demonstration of TM lasing. Therefore, gain measurements for the extremely high-aspect ratio sample (lasing in TM) would be an interesting addition to this work as it would provide us with an insight to TE-TM gain relation and how this related to the dual-polarisation emission property of the laser structure. In addition, gain measurements using the segmented contact method [Blood 2003] could answer to the question about the non-radiative mechanisms responsible for the abrupt increase of threshold current density above 260K. However, gain measurements weren't possible here as the devices showed a fast degradation during the laser measurements. Nevertheless, these novel materials have shown good laser properties, i.e lasing in room temperature [Li 2008] [Li 2008b], although they are very new materials. Therefore, there is a potential for further improvement in the future which can be realised with a combination of improvement in growth technique and the understanding of the radiative mechanisms responsible for the temperature-sensitive threshold current density. For application as laser sources in optical telecommunication it would be also interesting to know if this novel material can be modified to cover emission wavelengths of 1.3 or 1.55μm. Theoretically, as the dot size increases the emission wavelength red-shifts [Coleman 2008], therefore by controlling the shape and *In* composition in columnar-QD it should be possible to tune the emission wavelength to desired values.

Finally, to use these columnar-QD materials as polarisation-insensitive SOA there are a few requirements that should be further studied, such as the level of material gain, the carrier dynamics and the level of noise figure.

Appendix A- Diffraction grating theory and monochromator set-up

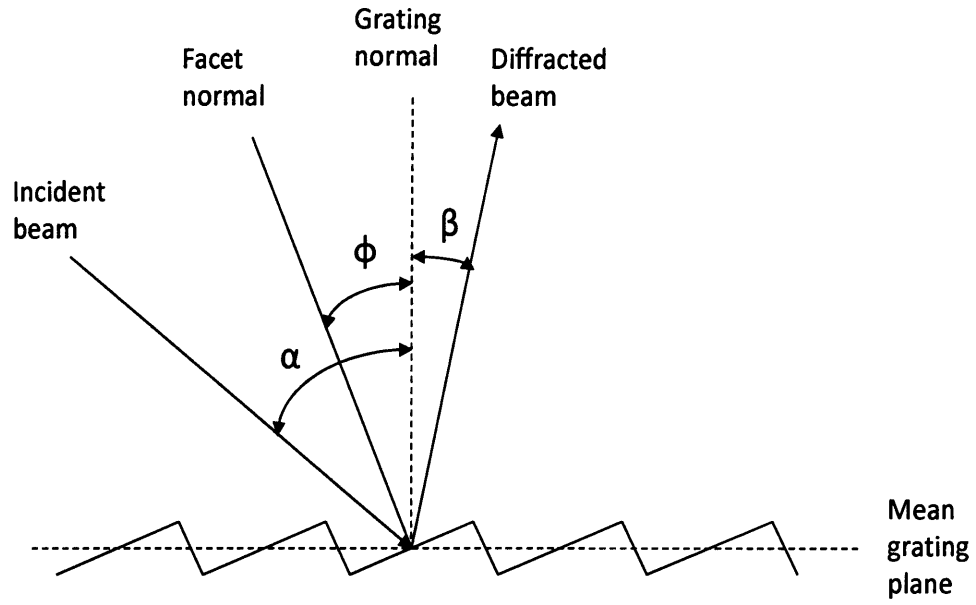

Figure A.1: Light ray picture of a blazed grating

The principal idea behind a diffraction grating is to disperse the incoming light in a way such as to spatially separate each of the incident light wavelengths. The wavelength selection then can be possible by setting an output slit aperture. Because of the spatial wavelength separation the width of the aperture determines the resolution of the output wavelength. A typical diffraction grating in a monochromator consists of a number of small parallel grooves ruled on the surface of an appropriate material and then coated by a high reflected material such as aluminium. Thus in a blazed diffraction grating each of the grooves is inclined at an angle operating as small mirrors reflecting the incident light at a specific angle.

According to figure A.1 the light is incident and diffracted at an angle α and β, respectively, with respect to the grating normal. Each blazed grating is characterised by a groove facet angle φ,

equal to the angle between the facet and the grating normal. The general grating equation is given by

$$d\{sin\alpha - \sin\beta\} = m\lambda$$

Equation A.1

, where d is the pitch of the grooves, m is the order of the diffraction and λ corresponds to the light wavelength.

The blaze condition, corresponding to "blaze wavelength" λ_{blaze} for which the grating is most efficient, is satisfied when the light incidence angle is equal to the angle of reflection, where both of the angles are with respect to the facet normal. This is expressed in terms of an equation as

$$\alpha - \varphi = \beta + \varphi$$

or

$$\beta = \alpha - 2\varphi$$

Equation A.2

Then the general grating equation is given as [Hutley 1982],

$$d\{sin\alpha - \sin(\alpha - 2\varphi)\} = m\lambda_{blaze}$$

Equation A.2

, where the angle of diffraction β is substituted by using equation A.1. The manufacturers can alter the "blaze wavelength", thus "tune" the efficiency of a grating such as different designed gratings operate more efficiently in the desired wavelength ranges. However, the efficiency of the grating can drop dramatically for a specific value of grating angle, first observed by Wood [Wood 1902], and is called Wood's anomaly. This drop in the efficiency it is polarisation dependent and has extensively explained later by Hessel [Hessel 1962].

In this thesis edge photo-absorption spectroscopy is applied for both QW red emitting laser diodes (emission wavelength around 633nm) and GaAs/InAs QD systems emitting at infrared up to 1.3μm. Thus, for the measurements of QW and QD laser devices two different grating systems are used. The first grating contains 1200 grooves per mm, having a "blaze wavelength" at 750nm to obtain measurements for the QW structures. This grating system was also used for early stage measurements of QD materials. The operating wavelength range of this grating is from 400 to 1300nm and in this thesis is called "short-wavelength range" grating. The "long-wavelength range" grating has 830 grooves per mm and a "blaze wavelength" at 1200nm and is optimum for a wavelength range from 1.1 to 1.8μm.

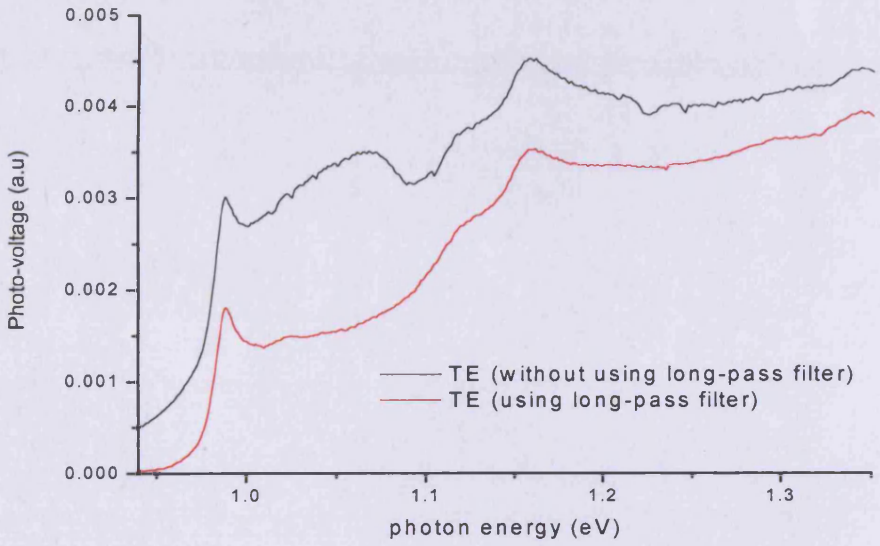

Figure A.2 TE polarised E-PVS of InGaAsN QW structure with or without using long-pass filter.

Together with the "long-wavelength range" grating for each spectroscopic measurement obtained in this wavelength range a 715nm long pass filter -100% efficient to "cut" light wavelengths shorter than 680nm- is used to block light of second order diffraction up to 1360nm (~0.91eV). Usually, in conventional monochromators the first order diffraction of light is used as a monochromator's output wavelength with higher order diffraction wavelengths (eq. A.2) getting blocked by the set-up. However, the monochromator used in the experiment described above

allows some higher diffraction order light wavelengths to get through. Evidence of that is shown in figure A.2, where TE polarised E-PVS measurements are obtained from InGaNAs QW structures. Although, the spectra are similar at the photon energy range 1.1 to 1.35eV, at low energy part of the spectrum there are obvious enhanced absorption features for the spectrum obtained without the use of long-pass filter. These features are associated with absorption coming from second order diffraction of light wavelengths corresponding to the visible range.

Appendix B – Growth details

1st generation Columnar-QDs:

P622 (columnar QDs with 5 QD stacks and 10 multilayers)

top				
air				
GaAs	40 nm	p-doped	p=2e19	
GaAs	22 nm	p=2e19		
AlGaAs grading	28 nm	p=2e18		
AlGaAs	1200 nm	p=1e18	(70% Al and 30% GaAs)	
AlGaAs	300 nm	p=5e17	(70% Al and 30% GaAs)	
AlGaAs grading	28 nm	p=5e17		
GaAs	131.5 nm	undoped		
GaAs	40 nm	undoped		
InAs QD	0.55 nm	undoped		5 times (= 5QD stacks)
As		undoped		
GaAs QD	0.85 nm	undoped		10 times (= 10 multilayers)
As		undoped		
InAs QD	0.21 nm	undoped		
GaAs	171.5 nm	undoped		
AlGaAs grading	28 nm	n=5e17		
AlGaAs	300 nm	n=5e17	(70% Al and 30% GaAs)	
AlGaAs	1200 nm	n=1e18	(70% Al and 30% GaAs)	
AlGaAs grading	28 nm	n=1e18		
GaAs (buffer)	720 nm	n-doped	n=2e18	
bottom				

P666 (columnar QDs with 5 QD stacks and 18 multilayers)

top				
air				
GaAs	40 nm	p-doped	p=2e19	
GaAs	22 nm	p=2e19		
AlGaAs grading	28 nm	p=2e18		
AlGaAs	1200 nm	p=1e18	(70% Al and 30% GaAs)	
AlGaAs	300 nm	p=5e17	(70% Al and 30% GaAs)	
AlGaAs grading	28 nm	p=5e17		
GaAs	131.5 nm	undoped		
GaAs	40 nm	undoped		
As		undoped		
InAs QD	0.55 nm	undoped		5 times (= 5QD stacks)
As		undoped		
GaAs QD	0.85 nm	undoped		18 times (= 18 multilayers)
As		undoped		
InAs QD	0.19 nm	undoped		
GaAs	171.5 nm	undoped		
AlGaAs grading	28 nm	n=5e17		
AlGaAs	300 nm	n=5e17	(70% Al and 30% GaAs)	
AlGaAs	1200 nm	n=1e18	(70% Al and 30% GaAs)	
AlGaAs grading	28 nm	n=1e18		
GaAs (buffer)	720 nm	n-doped	n=2e18	
bottom				

P906 (columnar QDs with 1 QD stacks and 30 multilayers)

top			
air			
GaAs	40 nm	p-doped	p=2e19
GaAs	22 nm	p=2e19	
AlGaAs grading	16 nm	p=2e18	
AlGaAs	1200 nm	p=1e18	(40% Al and 60% GaAs)
AlGaAs	300 nm	p=5e17	(40% Al and 60% GaAs)
AlGaAs grading	16 nm	p=5e17	
GaAs	130.5 nm	undoped	
InAs QD	0.55 nm	undoped	1 columnar QD (CQD) stack
As		undoped	
GaAs QD	0.85 nm	undoped	30 times (= 30 multilayers)
As		undoped	
InAs QD	0.19 nm	undoped	
GaAs	130.2 nm	undoped	
AlGaAs grading	16 nm	n=5e17	
AlGaAs	300 nm	n=5e17	(40% Al and 60% GaAs)
AlGaAs	1200 nm	n=1e18	(40% Al and 60% GaAs)
AlGaAs grading	16 nm	n=1e18	
GaAs (buffer)	820 nm	n-doped	n=2e18
bottom			

P918 (columnar QDs with 3 QD stacks and 30 multilayers)

top			
air			
GaAs	40 nm	p-doped	p=2e19
GaAs	22 nm	p=2e19	
AlGaAs grading	16 nm	p=2e18	
AlGaAs	1200 nm	p=1e18	(40% Al and 60% GaAs)
AlGaAs	300 nm	p=5e17	(40% Al and 60% GaAs)
AlGaAs grading	16 nm	p=5e17	
GaAs	130.5 nm	undoped	
InAs QD	0.55 nm	undoped	
As		undoped	3rd CQD stack
GaAs QD	0.85 nm	undoped	
As		undoped	30 times (= 30 multilayers)
InAs QD	0.19 nm	undoped	
GaAs	100 nm	undoped	
InAs QD	0.55 nm	undoped	
As		undoped	2nd CQD stack
GaAs QD	0.85 nm	undoped	
As		undoped	30 times (= 30 multilayers)
InAs QD	0.19 nm	undoped	
GaAs	100 nm	undoped	
InAs QD	0.55 nm	undoped	
As		undoped	1st CQD stack
GaAs QD	0.85 nm	undoped	
As		undoped	30 times (= 30 multilayers)
InAs QD	0.19 nm	undoped	
GaAs	130.2 nm	undoped	
AlGaAs grading	16 nm	n=5e17	
AlGaAs	300 nm	n=5e17	(40% Al and 60% GaAs)
AlGaAs	1200 nm	n=1e18	(40% Al and 60% GaAs)
AlGaAs grading	16 nm	n=1e18	
GaAs (buffer)	820 nm	n-doped	n=2e18
bottom			

2nd generation Columnar-QDs:

P968 (columnar QDs with 1 QD stacks and 30 multilayers)

top			
air			
GaAs	40 nm	p-doped	p=2e19
GaAs	22 nm	p=2e19	
AlGaAs grading	16 nm	p=2e18	
AlGaAs	1200 nm	p=1e18	(40% Al and 60% GaAs)
AlGaAs	300 nm	p=5e17	(40% Al and 60% GaAs)
AlGaAs grading	16 nm	p=5e17	
GaAs	180.5 nm	undoped	
			1 columnar QD (CQD) stack
As		undoped	
InAs QD	0.29 nm	undoped	30 times (= 30 multilayers)
As		undoped	
GaAs QD	1.7 nm	undoped	
InAs QD	0.55 nm	undoped	
GaAs	180.2 nm	undoped	
AlGaAs grading	16 nm	n=5e17	
AlGaAs	300 nm	n=5e17	(40% Al and 60% GaAs)
AlGaAs	1200 nm	n=1e18	(40% Al and 60% GaAs)
AlGaAs grading	16 nm	n=1e18	
GaAs (buffer)	800 nm	n-doped	n=2e18
bottom			

P990 (columnar QDs with 3 QD stacks and 35 multilayers)

top			
air			
GaAs	40 nm	p-doped	p=2e19
GaAs	22 nm	p=2e19	
AlGaAs grading	16 nm	p=2e18	
AlGaAs	1200 nm	p=1e18	(40% Al and 60% GaAs)
AlGaAs	300 nm	p=5e17	(40% Al and 60% GaAs)
AlGaAs grading	16 nm	p=5e17	
GaAs	130.5 nm	undoped	
InAs QD	0.29 nm	undoped	
As		undoped	3rd CQD stack
GaAs QD	1.7 nm	undoped	
As		undoped	35 times (= 35 multilayers)
InAs QD	0.55 nm	undoped	
GaAs	180 nm	undoped	
InAs QD	0.29 nm	undoped	
As		undoped	2nd CQD stack
GaAs QD	1.7 nm	undoped	
As		undoped	35 times (= 35 multilayers)
InAs QD	0.55 nm	undoped	
GaAs	180 nm	undoped	
InAs QD	0.29 nm	undoped	
As		undoped	1st CQD stack
GaAs QD	1.7 nm	undoped	
As		undoped	35 times (= 35 multilayers)
InAs QD	0.55 nm	undoped	
GaAs	130.2 nm	undoped	
AlGaAs grading	16 nm	n=5e17	
AlGaAs	300 nm	n=5e17	(40% Al and 60% GaAs)
AlGaAs	1200 nm	n=1e18	(40% Al and 60% GaAs)
AlGaAs grading	16 nm	n=1e18	
GaAs (buffer)	820 nm	n-doped	n=2e18
bottom			

References

[Adams 1981] M.J. Adams, *"An introduction to optical waveguides"*, New York, Wiley (1981).

[Adams 1986] A.R. Adams, *"Band-structure engineering for low-threshold high-efficiency semiconductor lasers", Electronics Letters* **22**(5), 249 (1986).

[Agrawal 1993] G.P. Agrawal and N.K. Dutta, *"Semiconductor Lasers"*, Van Nostrand Rienhold, New York (1993).

[Aizawa 1991] T. Aizawa, K. Shimomura, S. Arai and Y. Suematsu, *"Observation of field-induced refractive index variation in quantum box structure"*, IEEE Photonics Technology Letters, **3**(10), 907 (1991).

[Alferov 1970] Zh.I. Alferov, V.M. Adreev, E.L. Portnoi and M.K. Trukan, *"AlAs-GaAs heterojunction injection lasers with a low temperature threshold"*, Soviet Physics Semiconductors **3**(9), 1107 (1970).

[Akiyama 2005] T. Akiyama, M. Ekawa, M. Sugawara, K. Kawaguchi, H. Sudo, A. Kuramata, H. Ebe and Y. Arakawa, *"An ultrawide-band semiconductor optical amplifier having an extremely high penalty-free output power of 23 dBm achieved with quantum dots"*, IEEE Photonics Technology Letters **17**(8), 1614 (2005).

[Arakawa 1982] Y. Arakawa and H. Sakaki, *"Multidimensional quantum well laser and temperature dependence of its threshold current"*, Applied Physics Letters **40**(11), 939 (1982).

[Asryan 2001] L.V. Arsyan and S. Luryi, *"Tunneling-injection quantum-dot laser:ultrahigh temperature stability"*, IEEE Journal of Quantum Electronics, **37**(7), 905 (2001).

[Bastard 1988] G. Bastard, *"Wave mechanics applied to semiconductor heterostructures"*, Halsted Press, New York (1988).

[Barker 2000] J.A. Barker and E.P. O'Reilly, *"Theoretical analysis of electron-hole alignment in InAs-GaAs quantum dots"*, Physical Review B **61**(20), 13840 (2000).

[Berg 2003] T.W. Berg and J. Mork, *"Quantum dot amplifiers with high output power and low noise"*, Applied Physics Letters **82**(18), 3083 (2003).

[Bertolotti 2004] M. Bertolli, *"The history of the laser"*, Published by Institute of Physics (2004).

[Bimberg 1999] D. Bimberg, M. Grundmann and N.N. Ledentsov, *"Quantum dot heterostructures"*, Wiley, New York (1999).

[Blood 1985] P. Blood, *"Measurement of optical absorption in epitaxial semiconductor layers by a photovoltage method"*, Journal of Applied Physics **58**(6), 2288 (1985).

[Borri 2000] P. Borri, W. Langbein, J.M. Hvam, F. Heinrichsdorff, M.-H. Chao and D. Bimberg, *"Ultrafast gain dynamics in InAs-InGaAs quantum-dot amplifiers"*, IEEE Photonics Technology Letters **12**(6), 594 (2000).

[Borri 2009] Proposed by Paola Borri during personal communication (2009).

[Casey 1978] H.C. Casey and M.B. Panish, *"Heterostructures lasers, Part A"*, Academic Press, New York (1978).

[Cho 1971] A.Y. Cho, *"Growth of periodic structures by the molecular beam method"*, Applied Physics Letters **19**(11), 467 (1971).

[Coldren 1995] L.A. Coldren and S.W. Corzine, *"Diode Lasers and Photonic Integrated Circuits"*, New York, Wiley (1995).

[Coleman 2008] J.J. Coleman, *"Quantum Dots: Materials, physics and devices"*, Short course in LEOS' 08, Newport Beach, USA (2008).

[Damilano 1999] B. Damilano, N. Grandjean, S. Dalmasso, and J. Massies, *"Room-temperature blue-green emission from InGaN/GaN quantum dots made by strain-induced islanding growth"*, Applied Physics Letters **75**(24), 3751 (1999).

[Davies 1978] D.A Davies *"Waves, Atoms and Solids"*, New York, Longman (1978).

[Dingle 1974] R. Dingle, W. Wiegmann and C.H. Henry, *"Quantum states of confined carriers in very thin $Al_xGa_{1-x}As$-GaAs- $Al_xGa_{1-x}As$ heterostructures"*, Physical Review Letters **33**(14), 827 (1974).

[Dingle 1976] R. Dingle and C.H. Henry, *"Quantum effects in heterostructure lasers"*, US Patent 3982207 (1976).

[Einstein 1917] A. Einstein, *"On the quantum theory of radiation"*, Physics Z **18**, 121 (1917).

[Findeis 2001] F. Findeis, M. Baier, E. Beham, A. Zrenner, and G. Abstreiter, *"Photocurrent and photoluminescence of a single self-assembled quantum dot in electric fields"*, Applied Physics Letters **78**(19), 2958 (2001).

[Fiore 2008] Personal communication (2008).

[Fonseca 1998] L.R.C. Fonseca, J.L. Jimenez and J.P. Leburton *"Electronic coupling in InAs/GaAs self-assembled stacked double-quantum-dot systems"*, Physical Review B **58**(15), 9955 (1998).

[Fox 2001] M. Fox, *"Optical properties of solids"*, Oxford University Press, New York (2001).

[Fry 2000a] P.W. Fry, I.E. Itskevich, S.R. Parnell, J.J. Finley, L.R. Wilson, K.L. Shumacher, D.J. Mobray, M.S. Skolnick, M. Al-Khafaji, A.G. Cullis, M. Hopkinson, J.C. Clark and G. Hill, *"Photocurrent spectroscopy of InAs/GaAs self-assembled quantum dots"*, Physical Review B **62**(24), 16784 (2000).

[Fry 2000b] P.W. Fry, I.E. Itskevich, D.J. Mowbray, M.S. Skolnick, J.J. Finley, J.A. Barker, E.P. O'Reilly, L.R. Wilson, I.A. Larkin, P.A Maksym, M. Hopkinson, M. Al-Khafaji, J.P.R. David, A.G. Cullis, G. Hill and J.C. Clark, *"Inverted Electron-Hole Alignement in InAs-GaAs Self-Assembled Quantum Dots"*, Physical Review Letters **84**(4), 733 (2000).

[George 2007] A. George, thesis, *"Carrier distributions in long wavelength quantum dot laser diodes"*, Cardiff University, Wales (2007).

[Grundmann 1995] M. Grundmann, O. Stier, and D. Bimberg, *"InAs/GaAs pyramidal quantum dots: Strain distribution, optical phonons and electronic structure"*, Physical

Review B **52**(16), 11969 (1995).

[Grundmann 2000] M. Grundmann, *"The present status of quantum dot lasers"*, Physica E **5**, 167 (2000).

[Hall 1962] R.N. Hall, G.E. Fenner, J.D. Kingsley, T.J. Soltys and R.O. Carlson, *"Coherent light emission from GaAs junctions"*, Physical Review Letters **9**(9), 366 (1962).

[He 2007] J. He, H.J. Krenner, C. Pryor, J.P. Zhang, Y. Wu, D.G. Allen, C.M. Morris, M.S. Sherwin and P.M. Petroff, *"Growth, structural, and optical properties of self-assembled (In,Ga)As quantum posts on GaAs"*, Nano Letters **7**(3), 802 (2007).

[Hecht 1999] J. Hecht, *"Understanding fiber optics"*, Prentice Hall, New York (1999).

[Heinrichsdorff 1997] F. Heinrichsdorff, M.H. Mao, N. Kirstaedter, A. Krost, D. Bimberg, A.O. Kosogov and P. Werner, *"Room temperature continuous-wave lasing from stacked InAs/GaAs quantum dots grown by metalorganic chemical vapor deposition"*, Applied Physics Letters **71**(1), 22 (1997).

[Hessel 1965] A. Hessel and A.A. Oliner, *"A new theory of Wood's anomalies on optical gratings"*, Applied Optics, **4**(10), 1275 (1965).

[Hook 1991] J.R. Hook and H.E. Hall, *"Solid state physics"*, Wiley, Chichester, New York (1991).

[Hsu 2001] T.M. Hsu, W.H. Chang, C.C. Huang, N.T. Yeh and J.I. Chyi, *"Quantum-confined Stark shift in electroreflectance of InAs/$In_xGa_{1-x}As$ self-assembled quantum dot"*, Applied physics Letters **78**(12), 1760 (2001).

[Huffaker 1998] D.L. Huffaker, G. Park, Z. Zou, O.B. Shchekin and D.G. Deppe, *"1.3μm room-temperature GaAs-based quantum-dot laser"*, Applied Physics Letters, **73**(18), 2564 (1998).

[Hutley 1982] M.C. Hutley, *"Diffraction gratings"*, London, Academic Press (1982).

[Jayavel 2004] P. Jayavel, H. Tanaka, T. Kita, O. Wada, H. Ebe, M. Sugawara, J. Tatebayashi, Y. Arakawa, Y. Nakata and T. Akiyama, *"Control of optical polarization anisotropy in edge emitting luminescence of InAs/GaAs self-assembled quantum dot"*,

Applied Physics Letter **84**(11), 1820 (2004).

[Jin 2004] Peng Jin, C.M. Li, Z.Y. Zhang, F.Q. Liu, Y.H. Chen, X.L. Ye, B. Xu and Z.G. Wang, *"Quantum-confined Stark effect and built-in dipole moment in self-assembled InAs/GaAs quantum dots"*, Applied Physics Letters **85**(14), 2791 (2004).

[Joma 1992] M. Joma, H. Horikawa, C.Q. Xu, K. Yamada, Y. Katoh, and T. Kamijoh, *"Polarization insensitive semiconductor laser amplifiers with tensile strained InGaAsP/InGaAsP multiple quantum well structure"*, Applied Physics Letters **62**(2), 121 (1993).

[Kaiser 1973] P. Kaiser, E.A.J. Marcatili and S.E. Miller, *"A new optical fiber"*, Bell System Technical Journal **52**, 265 (1973).

[Kapon 1989] E. Kapon, D.M. Hwang and R. Bhat, *"Stimulated emission in semiconductor quantum wire heterostructures"*, Physical Review Letters **63**(4), 430 (1989).

[Kawagushi 2006a] K. Kawagushi, M. Ekawa, N. Yasuoka, T. Akiyama, H. Ebe, M. Sugawara, and Y. Arakawa *"1.3-1.6μm broadband polarisation-independent luminescence by columnar InAs quantum dots on InP(001)"*, Physical status solidi (c) **3**(11), 3646 (2006).

[Kawagushi 2006b] K. Kawagushi, N. Yasuoka, M. Ekawa, H. Ebe, T. Akiyama, M. Sugawara, and Y. Arakawa, *"Controlling polarisation of 1.55-μm columnar InAs quantum dots with highly tensile-strained InGaAsP barriers on InP(001)"*, Japanese Journal of Applied Physics Part 2 **45**, L1244 (2006).

[Keldysh 1958] L.V. Keldysh, *"The effect of a strong electric field on the optical properties of insulating crystals"*, Soviet Physics JETP **34**, 788 (1958).

[Kita 2002] T. Kita, O. Wada, H. Ebe, Y. Nakata and M. Sugawara, "*Polarization-independent photoluminescence from columnar InAs/GaAs self-assembled quantum dots*", Japanese Journal of Applied Physics Part 2 **41**, n.10B, pp. L1143 (2002).

[Kita 2006] T. Kita, N. Tamura, O. Wada, M. Sugawara, Y. Nakata, H. Ebe and Y. Akawara, "*Artificial control of optical gain polarization by stacking quantum dot layers*", Applied Physics Letters **88**(21), 211106 (2006).

[Kittel 1996] C. Kittel, *"Introduction to solid state physics"*, 7th edition, Wiley, New York (1996).

[Klingshirn 1997] C.F Klingshirn, *"Semiconductor Optics"*, Springer, New York (1997).

[Komori 1991] K. Komori, S. Arai and Y. Suematsu, *"Noise in semiconductor laser amplifiers with quantum box structure"*, IEEE Photonics Technology Letters **3**(1), 39 (1991).

[Koonath 2002] P. Koonath, K. Sangin, W.J. Cho and A. Gopinath, *"Polarization-insensitive quantum-well semiconductor optical amplifiers"*, IEEE Journal of Quantum Electronics, **38**(9), 1282 (2002).

[Kopf 1997] C. Köpf, H. Kosina, and S. Selberherr, *"Physical Models for Strained and Relaxed GaInAs Alloys: Band Structure and Low-Field Transport"*, *Solid-State Electronics* **41**(8), 1139 (1997).

[Krenner 2008] H.J. Krenner, C. Pryor, J. He, J.P. Zhang, Y. Wu, C.M. Morris, M.S. Sherwin and P.M. Petroff, "*Growth and optical properties of self-assembled InGaAs Quantum Posts*", Physica E **40**, n.6,1785 (2008).

[Ledentsov 1996a] N.N. Ledentsov, J. Bohrer, D. Bimberg, I.V. Kochnev, M.V. Maximov, P.S. Ko'pev, Zh.I Alferov, A.O. Kosogov, S.S. Ruvimov, P. Werner, and U. Gosele, *"Formation of coherent superdots using metal-organic chemical vapor deposition"*, Applied Physics Letters **69**(8), 1095 (1996).

[Ledentsov 1996b] N.N. Ledentsov, V.A. Shchukin, M. Grundmann, N. Kirstaedter, J. Bohrer, O. Schmidt, D. Bimberg, V.M. Ustinov, A.Yu. Erogov, A.E. Zhukov, P.S. Ko'pev, S.V. Zaitsev, N.Yu. Gordeev, Zh.I. Alferov, A.I. Borovkov, A.O. Kosogov, S.S. Ruvimov, P. Werner, U. Gosele and J. Heydenreich, *"Direct formation of vertically coupled quantum dots in Stranski-Krastanov growth"*, Physical Review B **54**(12), 8743 (1996).

[Ledentsov 2002] N.N. Ledentsov, "Long-wavelength quantum-dot lasers on GaAs substrates: from media to device concepts", IEEE Selected Topics in Quantum Electronics **8**(5), 1015 (2002).

[Lemaitre 2004] A. Lamaitre, G. Patriarche and F. Glas, "*Composition profiling of InAs/GaAs quantum dots*", Applied Physics Letters **85**(17), 3717 (2004).

[Lester 1999] L.F. Lester, A. Stintz, H. Li, T.C. Newell, E.A. Pease, B.A. Fuchs and K.J. Malloy, *"Optical characteristics of 1.24-μm InAs quantum-dot laser diodes"*, IEEE Photonics Technology Letters **11**(8), 931 (1999).

[Lewis 2002a] G.M. Lewis, *"Study of spontaneous emission and gain from strained $(Al_yGa_{1-y})_xIn_{1-x}P$ quantum well laser diodes"*, Thesis, Cardiff (2002).

[Lewis 2002b] G.M. Lewis, P.M. Smowton, P. Blood, G. Jones and S. Bland, *"Measurement of transverse electric and transverse magnetic spontaneous emission and gain in tensile strained GaInP laser diodes"*, Applied Physics Letters **80**(19), 3488 (2002).

[Li 2007] L.H. Li, G. Patriarche, M. Rossetti and A. Fiore, *"Growth and characterization of InAs columnar quantum dots on GaAs substrate"*, Journal of Applied Physics **102**, 033502 (2007).

[Li 2008a] L.H. Li, G. Patriarche, N. Chauvin, P. Ridha, M. Rossetti, J. Andrzejewski, G. Sek, J. Misiewicz and A. Fiore, *"Controlling the Aspect Aatio of Quantum Dots: From Columnar Dots to Quantum Rods"*, IEEE Journal of Selected Topics In Quantum Electronics, **14**(4), 1204 (2008).

[Li 2008b] L.H. Li, P. Ridha, G. Patriarche, N. Chauvin and A. Fiore, *"Shape-engineered epitaxial InGaAs quantum rods for laser applications"*, Applied Physics Letters **92**(12), 121102 (2008).

[Liang 2002] J.P. Liang, S.D. Wang, Y.S. Huang, C.W. Tien, Y.M. Chang, C.W. Chen, N.Y. Li, D.Y. Lin and F.H. Pollak, *"Polarized edge-incident photovoltage spectroscopy and reflectance characterization of a GaAs/GaAlAs vertical-cavity surface-emitting laser structure"*, Applied Physics Letters **80**(4), 752 (2002).

[Liu 2004a] H.Y. Liu, I.R. Sellers, M. Gutierrez, K.M. Groom, W.M. Soong, M. Hopkinson, J.P.R. David, R. Beanland, T.J. Badcock, D.J. Mowbray and M.S. Skolnick, *"Influences of the spacer layer growth temperature on multilayer InAs/GaAs quantum dot structures"*, Journal of Applied Physics **96**(4), 1988 (2004).

[Liu 2004b] H.Y. Liu, I.R. Sellers, T.J. Badcock, D.J. Mowbray, M.S. Skolnick, K.M. Groom, M. Gutierrez, M. Hopkinson, J.S. Ng, J.P.R. David and R. Beanland, *"Improved*

performance of 1.3 μm multilayer InAs quantum-dot lasers using a high-growth-temperature GaAs spacer layer", Applied Physics Letters **85**(5), 704 (2004).

[Loudon 1983] R. Loudon, *"The quantum theory of light"*, 2nd edition, Oxford University Press, New York (1983).

[Ludowise 1985] M.J. Ludowise, *"Metalorganic chemical vapor deposition of III-V semiconductors"*, Journal of Applied Physics **58**(8), R31 (1985).

[Magari 1991] K. Magari, M. Okamoto and Y. Noguchi, *"1.55 μm polarisation-insensitive high-gain tensile-strained-barrier MQW optical amplifier"*, IEEE Transactions Photonics Technology Letters **3**(11), 998 (1991).

[Maiman 1960] T.H. Maiman, *"Stimulated optical radiation in Ruby"*, Nature **187**, n.4776, 493 (1960).

[Markus 2003] A. Markus, J.X. Chen, C. Paranthoen, A. Fiore, C. Platz and O. Gauthier-Lafaye, *"Simultaneous two-state lasing in quantum-dot lasers"*, Applied Physics Letters **82**(12), 1818 (2003).

[Marzin 1994] J.A.Y. Marzin and G. Bastard, *"Calculation of the energy level in InAs/GaAs quantum dots"*, Solid State Communication **92**(5), 437 (1994).

[Matthews 2002] D.R. Matthews, H.D. Summers, P.M. Smowton and M. Hopkinson, *"Experimental investigation of the effect of the wetting-layer states on the gain-current characteristic of quantum-dot lasers"*, Applied Physics Letters **81**(26), 4904 (2002).

[Micic 1996] O.I. Micic, J. Sprague, Z. Lu, and A.J. Nozik, *"Highly efficient band-edge emission from InP quantum dots"*, Applied Physics Letters **68**(22), 3150 (1996).

[Miller 1984a] D.A.B. Miller, D.S. Chemla, T.C. Damen, A.C. Gossard, W. Wiegmann, T.H. Wood and C.A. Burrus, *"Band-edge electroabsorprtion in quantum well structures: The Quantum-Confined Stark Effect"*, Physical Review Letters **53**(22), 2173 (1984).

[Miller 1984b] D.A.B. Miller, D.S. Chemla, T.C. Damen, A.C. Gossard, W. Wiegmann, T.H. Wood and C.A. Burrus, *"Novel hybrid optically bistable switch: The quantum well self-electro-optic effect device"*, Applied Physics Letters **45**(1), 13 (1984).

[Miller 1985] D.A.B. Miller, D.S. Chemla, T.C. Damen, A.C. Gossard, W. Wiegmann, T.H. Wood and C.A. Burrus *"Electric field dependence of optical absorption near the band gap of quantum-well structures"*, Physical Review B **32**(2), 1043 (1985).

[Miller 2004] Alan Miller's MSc lectures in *"Semiconductor devices"*, St. Andrews University, 2004.

[Mogensen 1997a] P.C. Mogensen, S.A. Hall, P.M. Smowton, U. Bangert, P. Blood, P. Dawson, *"The effect of high compressive strain on the operation of AlGaInP quantum-well lasers"*, IEEE Journal of Quantum Electronics **34**(9), 1652 (1998).

[Mogensen 1997b] P.C. Mogensen, *"Strain limits in (AlyGa1-y)xIn1-xP quantum well laser diodes"*, Thesis, Cardiff University (1997).

[Moreau 2007] G. Moreau, A. Martinez, D.-Y. Cong, K. Merghem, A. Miard, A. Lemaitre, P. Voisin, A. Ramdane, I. Krestnikov, A.R. Kovsh, M. Fischer and J. Koeth, *"Enhanced In(Ga)As/GaAs quantum dot based electro-optic modulation at 1.55μm"*, Applied Physics Letters **91**(9), 091118 (2007).

[Motyka 2006] M. Motyka, R. Kudrawiec, G. Sek, J. Misiewicz, I.L. Krestnikov, S. Mikhrin and A. Kovsh, *"Room temperature contactless electroreflectance characterization of InGaAs/InAs/GaAs quantum dot wafers"*, Semiconductor Science and Technology **21**(10), 1402 (2006).

[Motyka 2007] M. Motyka, G. Sek, K. Ryczko, J. Andrzejewski, J. Misiewicz, L.H. Li, A. Fiore and G. Patriarche, *"Optical and electronics properties of GaAs-based structures with columnar quantum dots"*, Applied Physics Letter **90**(18), 181933 (2007).

[Mui 1995] D.S.L. Mui, D. Leonard, L.A. Coldren and P.M. Petrof, *"Surface migration induced self-aligned InAs islands grown by molecular beam epitaxy"*, Applied Physics Letters **66**(13), 1620 (1995).

[Mukai 1998] K. Mukai, Y. Nakata, H. Shoji, M. Sugawara, K. Ohtsubo, N. Yokoyama and H. Ishikawa, *"Lasing with low threshold current and high output power from columnar-shaped InAs/GaAs quantum dots"*, Electronics Letters **34**(16), 1588 (1998).

[Mukai 1999] K. Mukai and M. Sugawara, *"Suppression of temperature sensitivity of interband emission energy in 1.3-μm-region by an InGaAs overgrowth on self-assembled InGaAs/GaAs quantum dots"*, Applied Physics Letters **74**(26), 3963 (1999).

[Nakamura 2003] Y. Nakamura, H. Nakamura, S. Ohkouchi, N. Ikeda, Y. Sugimoto and K. Asakawa, *"Selective formation of high-density and high-uniformity InAs/GaAs quantum dots for ultra-small and ultra-fast all-optical switches"*, Compound Semiconductors, Institute of Physics Conference Series, **174**, 133 (2003).

[Nakata 1997] Y. Nakata, Y. Sugiyama, T. Futatsugi and N. Yokoyama, *"Self-assembled structures of closely stacked InAs islands grown on GaAs by molecular beam epitaxy"*, Journal of Crystal Growth **175/176**(2), 713 (1997).

[Nakata 2000] Y. Nakata, K. Mukai, M. Sugawara, K. Ohtsubo, H. Ishikawa and N. Yokoyama, *"Molecular beam epitaxial growth of InAs self-assembled quantum dots with light-emission at 1.3μm"*, Journal of Crystal Growth **208**(1-4), 93 (2000).

[Neamen 1997] D.A. Neamen, *"Semiconductor Physics and Devices: Basic Principles"*, 2nd edition, New York, Irwin McGraw-Hill (1997).

[Ogusu 1979] K. Ogusu, S. Kawakami and S. Nishida, *"Optical strip waveguide: An analysis"*, Applied Optics **18**, 908; correction in Applied Optics **18**, 3725.

[Ohishi 1991] Y. Ohishi, T. Kanamori, T. Kitagawa, S. Takahashi, E. Snitzer and G.H. Siger Jr., *"Pr^{3+} -doped fluoride fiber amplifier operating at 1.31 μm"*, Optics Letters **16**, n.22, 1747 (1991).

[Optics.org 2006] http://optics.org/cws/article/research/24354

[Orton 1990] J.W. Orton and P. Blood, *"The electrical characterization of semiconductors: Measurement of minority carrier properties"*, Academic Press, San Diego (1990).

[Palankovski 2001] V. Palankovski, Thesis, *"Simulation of Heterojunction Bipolar Transistors"*, TU Wien, Austria (2001).

(http://www.iue.tuwien.ac.at/phd/palankovski/node37.html)

[Patriarche 2004] G. Patriarche, L. Largeau, J.C. Harmand and D. Gollub, *"Morphology and composition of highly strained InGaAs and InGaAsN layers grown on GaAs substrate"*, Applied Physics Letter **84**(2), 203 (2004).

[Petroff 2007] P.M. Petroff, H.J. Krenner, J. He, C. Pryor, C. Morris and M.S. Sherwin, *"Optical properties of quantum dots and quantum posts"*, IEEE LEOS Annual Meeting Conference proceedings, art. n. 4382258, p.29 (2007).

[Qasaimeh 1998] O. Qasaimeh, K. Kamath, P. Bhattacharya and J. Phillips, *"Linear and quadratic electro-optic coefficients of self-organized $In_{0.4}Ga_{0.6}As/GaAs$ quantum dots"*, Applied Physics Letters **72**(11), 1275 (1998).

[Reif 1965] F. Reif, *"Funtamentals of statistical and thermal physics"*, McGraw-Hill, New York (1965).

[Ridha 2007] P. Ridha, L.H. Li, A. Fiore, G. Patriarche, M. Mexis and P.M. Smowton, *"Polarization dependence study of electroluminescence and absorption from InAs/GaAs columnar quantum dots"*, Applied Physics Letters **91**(19), 191123 (2007).

[Ridha 2008a] P. Ridha, L.H. Li, M. Rossetti, G. Patriarche and A. Fiore, *"Polarization dependence of electroluminescence from closely-stacked and columnar quantum dots"*, Optical and Quantum Electronics **40**(2-4), 239 (2008).

[Ridha 2008b] P. Ridha, thesis, *"Polarization properties of semiconductor quantum dot and dash lasers"*, EPFL, Switzerland (2008).

[Pryor 1998] C. Pryor, *"Eight-band calculations of strained InAs/GaAs quantum dots compared with one-, four- and six-band approximations"*, Physical Review B **57**(12), 7190 (1998).

[Saito 2005] T. Saito, T. Nakaoka, T. Kakitsuka, Y. Yoshikuni and Y. Arakawa, *"Strain distribution and electronics states in stacked InAs/GaAs quantum dots with dot spacing 0-6nm"*, Physica E **26**(1-4), 217 (2005).

[Saito 2008] T. Saito, H. Ebe, Y. Arakawa, T. Kakitsuka and M. Siguwara, *"Optical polarization in columnar InAs/GaAs quantum dot: 8-band k·p calculations"*, Physical

Review B **77**(19), 195318 (2008).

[Sandall 2006] I.C. Sandall, Thesis, *"The characterisation of In(Ga)As dot lasers"*, Cardiff University, Wales (2006).

[Sek 2008] G. Sek, P. Podemski, J. Msiewicz, L.H. Li and G. Patriarche, *"Photoluminescence from a single InGaAs epitaxial quantum rod"*, Applied Physics Letters **92**(2), 021901 (2008).

[Sheng 2002] W. Sheng and J.P. Leburton, *"Interband transition distributions in the optical spectra of InAs/GaAs self-assembled quantum dots"*, Applied Physics Letters **80**(15), 2755 (2002).

[Shoji 1997] H. Shoji, Y. Nakata, K. Mukai, Y. Sugiyama, M. Sugawara, N. Yokoyama and H. Ishikawa, *"Lasing characteristics of self-formed quantum-dot lasers with multistacked dot layer"*, IEEE Journal of Selected Topics in Quantum Electronics **3**(2), 188 (2000).

[Siegman 1986] A.E. Siegman, *"Lasers"*, Oxford University Press (1986).

[Smowton 1996] P.M. Smowton, P. Blood, P.C. Mogensen and D.P. Bour, *"Role of sublinear gain-current relationship in compressive and tensile strained 630 nm GaInP lasers"*, International Journal of Optoelectronics **10**, 383 (1996).

[Solomon 1996a] G.S. Solomon, J.A. Trezza, A.F. Marshall and J.S. Harris, Jr., *"Vertically aligned and electronically coupled growth induced InAs islands in GaAs"*, Physical Review Letter **76**(6), 952 (1996).

[Solomon 1996b] G.S. Solomon, M.C. Larson and J.S. Harris, Jr., *"Electroluminescence in vertically aligned quantum dot multilayer light-emitting diodes fabricating by growth-induced islanding"*, Applied Physics Letters **69**(13), 1897 (1996).

[Sopanen 2000] M. Sopanen, H.P. Xin and C.W. Tu, *"Self-assembled GaInNAs quantum dots for 1.3 and 1.55μm emission on GaAs"*, Applied Physics Letters **76**(8), 994 (2000).

[Sugawara 1999a] M. Sugawara, *"Self-assembled quantum dots InGaAs/GaAs quantum dots"*, Semiconductor and semimetals, vol. **60**, Academic Press, New York (1999).

[Sugawara 1999b] M. Sugawara, K. Mukai and Y. Nakata *"Light emission spectra of columnar-shaped self-assembled InGaAs/GaAs quantum-dot lasers: Effect of homogeneous broadening of the optical gain on lasing characteristics"*, Applied Physics Letters **74**(11), 1561 (1999).

[Sugawara 2000] M. Sugawara, K. Mukai, Y. Nakata, K. Otsubo and H. Ishilkawa, *"Performance and physics of quantum-dot lasers with self-assembled columnar-shaped and 1.3-μm emitting InGaAs quantum dots"*, IEEE Journal of Selected Topics in Quantum Electronics **6**(3), 462 (2000).

[Tatebayashi 2007] J. Tatebayashi, R.B. Laghumavarapu, N. Nuntawong and D.L. Huffaker, *"Measurement of electro-optic coefficients of 1.3μm self-assembled InAs/GaAs quantum dots"*, Electronics Letters, **43**(7), 410 (2007).

[Temkin 1987] H. Temkin, D. Gershoni and M.B. Panish, *"InGaAsP/InP quantum well modulators grown by gas source molecular beam epitaxy"*, Applied Physics Letter **50**(25), 1776 (1987).

[Ustinov 2003] V.M. Ustinov, A.E. Zhukov, A.Y. Egorov, N.A. Maleev, *"Quantum Dot Lasers"*, Oxford , Oxford University Press (2003).

[Verma 2008] V.B. Verma and J.J. Coleman, *"High density patterned quantum dot arrays fabricated by electron beam lithography and wet chemichal etching"*, Applied Physics Letters **93**(11), 111117 (2008).

[Vurgaftman 2001] I. Vurgaftman, J.R. Meyer and L.R. Ram-Mohan, *"Band parameters for III-V compound semiconductors and their alloys"*, Journal of Applied Physics **89**(11), 5815 (2001).

[Warburton 2002] R.J. Warburton, C. Schulhauser, D. Haft, C. Schäflein, K. Karrai, J.M. Garcia, W. Schoenfeld and P.M. Petroff, *"Giant permanent dipole moments of excitons in semiconductor nanostructures"*, Physical Review B **65**(11), 113303 (2002).

[Wilson 1998] J. Wilson and J. Hawkes, *"Optoelectronics an Introduction"*, 3rd edition, Prentice Hall (1998).

[Winston 1999] W. Winston, http://ece-www.colorado.edu/~bart/ecen6355/simwindows/ (1999).

[Wood 1902] R.W. Wood, *"On a remarkable case of uneven distribution of light in a diffraction grating spectrum"*, Phylosophical Magazine **4**, 396 (1902).

[Wood 1984] T.H Wood, C.A. Burrus, D.A.B. Miller, D.S. Chemia, T.C. Damen, A.C. Gossard and W. Wiegmann, *"High-speed optical modulation with GaAs/GaAlAs quantum wells in a p-i-n diode structure"*, Applied Physics Letters **44**(1), 16 (1984).

[Wood 1988] T.H. Wood, *"Multiple quantum well waveguide modulators"*, Journal of Lightwave Technology **6**(6), 743 (1988).

[Xie 1995] Q. Xie, A. Madhukar, P. Chen and N.P. Kobayashi, *"Vertically Self-Organised InAs Quantum Box Islands on GaAs (100)"*, Physical Review Letters **75**(13), 2542 (1995).

[Yablonovitch 1986] E. Yablonovitch and E.O. Kane *"Reduction of lasing threshold current density by the lowering of valence and effective mass"*, Journal of Lightwave Technology **4**(5), 504 (1986).

[Yamada 1998] M. Yamada, A. Mori, K. Kobayashi, H. Ono, T. Kanamori, K. Oikawa, Y. Nishida and Y. Ohishi, *"Gain-flattened tellurite-based EDFA with a flat amplification bandwidth of 76nm"*, IEEE Photonics Technology Letters **10**(9), 1244 (1998).

[Yamamoto 1985] H. Yamamoto, M. Asada and Y. Suematsu, *"Electric-field-induced refractive index variation in quantum-well structure"*, Electronics Letters **21**(13), 579 (1985).

[Yasuoka 2008a] N. Yasuoka, K. Kawaguchi, H. Ebe, T. Akiyama, M. Ekawa, K. Morito, M. Sugawara, and Y. Arakawa, *"Quantum dot semiconductor optical amplifiers with polarization-independent gains in 1.5-μm wavelength bands"*, IEEE Photonics Technology Letters **20**(23), 1908 (2008).

[Yasuoka 2008b] N. Yasuoka, K. Kawagushi, H. Ebe, T. Akiyama, M. Ekawa, S. Tanaka, K. Morito, A. Uetake, M. Sugawara and Y. Arakawa, *"Demonstration of transverse-magnetic dominant gain in quantum dot semiconductor optical amplifiers"*, Applied Physics Letters **92**(10), 101108 (2008).

[Yu 1999] P. Yu, W. Langbein, K. Leosson, J.M. Hvam, N.N. Ledentsov, D. Bimberg, V.M. Ustinov, A.Yu. Egorov, A.E. Zhukov, A.F. Tsatsul'nikov and Yu.G. Musikhin, *"Optical anisotropy in vertically coupled dots"*, Physical Review B **60**(24), 16680 (1999).

[Zeghbroeck, 2007] B.Van Zeghbroeck "Principles of semiconductor devices", http://ece-www.colorado.edu/~bart/book/ (2007).

[Zory 1993] P.S. Zory, *"Quantum Well Lasers"*, Academic Press, San Diego (1993).

Publications List

Journals

M. Mexis, P. Blood, P.M. Smowton, *"Polarization response of quantum confined structures using edge-photovoltage spectroscopy"*, Semiconductor Science and Technology **22**, 1298 (2007) (Institute of Physics selected article).

P. Ridha, A. Fiore, G. Patriache, M. Mexis and P.M. Smowton, *"Polarization dependence study of electroluminescence and absorption from InAs/GaAs columnar quantum dots"*, Applied Physics Letters **91**, 191123 (2007).

P. Ridha, L.H. Li, M. Mexis, P.M. Smowton, J. Andrzejewski, G. Sek, J. Misiewicz, E.P. O'Reilly, G. Patriarche, M. Bozkurt, P.M. Koenraad and A. Fiore. *"Polarization properties of columnar quantum dots: Effects of the aspect ratio and the compositional contrast"*, Accepted for publication in Journal of Quantum Electronics (2009).

L.H. Li, M. Mexis, P. Ridha, M. Bozkurt, G. Patriarche, P.M. Smowton, P. Blood, P.M. Koenraad and A. Fiore. *"Control of polarization and dipole moment in semiconductor quantum dots"*, To be submitted to Applied Physics Letters (2009).

International Conference Proceedings

D.S. Naidu, M. Mexis, A. Sobiesierski, P. M. Smowton, H.D Summers, D. J. Mowbray, H.Y. Liu, M. Hopkinson, *"Role of the device structure on the performance of quantum dot lasers. IEEE LEOS Annual Meeting Conference proceedings"*, Vols 1 and 2, p. 435-436, Lake Buena Vista, Florida, USA, 2007.

M. Mexis, P. M. Smowton, P. Blood, P. Ridha, L.H. Li, A. Fiore and G. Patriarche, *"Dipole orientation in a Quantum Rod"*, IEEE LEOS Annual Meeting Conference, art. No. 4688724, pp. 527-528, Newport Beach, California, USA, 2008.

P. Ridha, L.H. Li, A. Fiore, G. Patriarhce, M. Mexis, P. M. Smowton, J. Andrzejewski, G. Sek and J. Misiewicz, *"Towards Polarisation Insensitive Semiconductor Optical Ampifiers*

using InAs/GaAs columnar quantum dots". IEEE Conference on Lasers and Electro-Optics (CLEO), art. no. 4551555 (2 pages), San Jose, California, USA, 2008.

L.H. Li, P. Ridha, M. Mexis, P.M. Smowton, G. Patriarche, J. Andrzejewski, G. Sek, J. Misiewicz, M. Bozkurt, P.M. Koenraad and A. Fiore, *"TM Lasing with InAs Quantum Rods"*. Accepted in Proceedings of the International Society for Optical (SPIE), Novel In-Plane Semiconductor Lasers VIII, San Jose, California, USA, 2009.

Presented work in other conferences in UK

"Polarization response of columnar quantum dot system using edge-photovoltage spectroscopy", Semiconductor and Integrated OptoElectronics (SIOE) Conference, 31 April - 2 May, Cardiff, Wales, UK, 2008.

"Calibration in polarization dependent edge-photovoltage spectroscopy", Semiconductor and Integrated OptoElectronics (SIOE) Conference, 3-4 April, Cardiff, Wales, UK, 2007.